Catalytic Reforming of Biogas for Syngas Production

McKenzie Primerano Kohn

Submitted in partial fulfillment of the
requirements for the degree of
Doctor of Philosophy
in the Graduate School of Arts and Sciences

COLUMBIA UNIVERSITY

2012

ABSTRACT

Catalytic Reforming of Biogas for Syngas Production

McKenzie Primerano Kohn

Biogas is a mixture of methane and carbon dioxide produced from the anaerobic microbial digestion of biomass. It is an inexpensive, local source of energy but is usually wasted because the CO_2 content dilutes the quality of the fuel. Dry and auto-thermal reforming are catalytic methods that convert both the CH_4 and CO_2 into H_2 and CO, or syngas, a valuable product that can be used to produce liquid fuels, provide H_2 for fuel cells, or improve the combustion of biogas. A $Rh/\gamma Al_2O_3$ catalyst is successful in dry reforming biogas to syngas without deactivation from carbon formation at CH_4/CO_2 ratios of one or lower. In CH_4 rich mixtures, auto-thermal reforming (ATR) is effective because it provides additional oxidant that eliminates carbon formation and combusts a portion of the CH_4 in-situ to provide the heat needed for the endothermic reforming reactions.

In addition to CH_4 and CO_2, biogas also contains chlorocarbons that are potential catalyst poisons. Chlorocarbons are unique to biogas and bio-derived fuels due to the natural presence of chlorinated compounds in organic material that are released during decomposition or thermal treatment. Despite their presence in biogas in 10-50ppm concentrations, the effect of chlorocarbons on the dry reforming reaction has not been extensively studied. This work investigated the effect of CH_3Cl in particular on the activity and selectivity of CH_4 dry and auto-thermal reforming using a $Rh/\gamma Al_2O_3$ catalyst.

It was determined that CH_3Cl introduction into the reforming reaction deposits chloride on the alumina catalyst support, which increases the surface acidity, poisons the water-gas shift reactions by replacing basic hydroxyl groups, and poisons the dry reforming reaction by reducing hydrogen mobility and the affinity of CO_2 for the alumina support. CH_3Cl also likely competes and reacts preferentially over CH_4 for dry reforming sites. In CO_2 rich environments, the reverse water gas shift reaction is poisoned, resulting in an increase of the H_2/CO ratio, while in H_2O rich environments, the forward water gas shift reaction is poisoned, resulting in a decrease of the H_2/CO ratio. With 50 ppm addition of CH_3Cl into a dry reforming reaction, the H_2/CO ratio increases by 53% at a relatively low temperature of 350°C and increases by only 3% at 700°C.

The poisoning of the water gas shift and dry reforming reactions, and the resulting changes in product selectivity and dry reforming activity, are completely reversible upon removal of CH_3Cl from the feed. Therefore, the amount of chlorocarbon expected in a biogas mixture, between 10-50ppm, is not particularly harmful for the 4% $Rh/\gamma Al_2O_3$ catalyst. The degree of chloride poisoning is directly proportional to CH_3Cl concentration and inversely proportional to H_2O concentration and temperature. Therefore, O_2 or air co-feeding minimizes chloride poisoning because it produces H_2O and additional heat from the CH_4 combustion reaction, both of which decrease chloride poisoning. Auto-thermal reforming is therefore more effective than dry reforming biogas because it keeps the $Rh/\gamma Al_2O_3$ catalyst clean of carbon and chloride deposition, thereby maintaining the activity and selectivity of the catalyst for conversion of biogas into syngas.

Table of Contents

List of Figures

List of Tables

Chapter 1 : Introduction

1.1 Motivation

Biogas is a mixture of methane and carbon dioxide produced from the anaerobic microbial digestion of biomass. Methane and carbon dioxide are the most abundant carbon-containing gases in the Earth's atmosphere. They play an important role in the greenhouse effect in which atmospheric gases adsorb infrared radiation from the earth and trap it in the earth's atmosphere. Biogas from landfills alone is the second largest source of anthropogenic methane emissions in the United States[1].

Biogas is produced in landfills, in agricultural operations, and during the treatment of wastewater. Landfill gas is a particularly large source of biogas, producing 13.5 billion m^3 of methane per year. It is estimated that in the U.S. approximately 18% of this is used for energy[2, 3]. Wastewater digester gas, produced by anaerobic digestion of organic material in the purification of wastewater, is a source of biogas[4]. Only 2% of wastewater treatment plants that employ anaerobic digestion use digester gas for electricity[5]. CH_4 and CO_2 are also produced by the anaerobic digestion of biomass or animal manure. The CH_4 production potential from dairy and swine farms alone is 4.3 billion m^3 of methane per year and only 2% of farms in which anaerobic digestion would be technically feasible are capturing and using the CH_4[6-8]. In all these cases the CH_4 content of the biogas ranges from 40-70% [1, 5, 7] with the remainder being CO_2. The methane contained in these three sources of biogas is worth approximately $2.5 billion per year[9]. However, most of this fuel is wasted and not used for energy.

One of the reasons why biogas mixtures are not more widely used for energy is because the high CO_2 content decreases the heating value and flame stability of the gas mixture. This leads to increased CO, NO_X, and unburned hydrocarbon emissions when the biogas is combusted in an engine, turbine, or boiler compared to pure CH_4 or natural gas[10]. For these reasons biogas is often burned, or flared, and emitted to the atmosphere as CO_2 and H_2O, without extracting any of the latent chemical energy.

The CO_2 may be separated from the CH_4 to produce a pure CH_4 stream to use as a natural gas replacement or to produce compressed natural gas (CNG) or liquefied natural gas (LNG) that can be used as a transportation fuel. The separation of CO_2 from CH_4 is accomplished by membrane separation, pressure swing adsorption (PSA), or amine scrubbing. The methane is then compressed to above 3,000 psi to produce CNG or further cooled until the CH_4 liquefies to produce LNG. Due to the high pressures and cryogenic temperatures needed to produce CNG and LNG, the processes are expensive and usually most suitable for large CH_4/CO_2 flows where economies of scale can be obtained[11, 12].

These options for biogas use are summarized in Figure 1.1. Flaring is the most common method to dispose of CH_4/CO_2 mixtures, but wastes the heating value of the CH_4. Combustion of biogas in engines or turbines for electricity production, or in boilers for direct heating, are popular applications, but suffer from increased emissions due to the abundance of CO_2 in the biogas. CO_2 separation to pure CH_4 is used sporadically due to its high cost. Catalytic reforming is another option that has the potential to fully utilize the energy contained in the biogas.

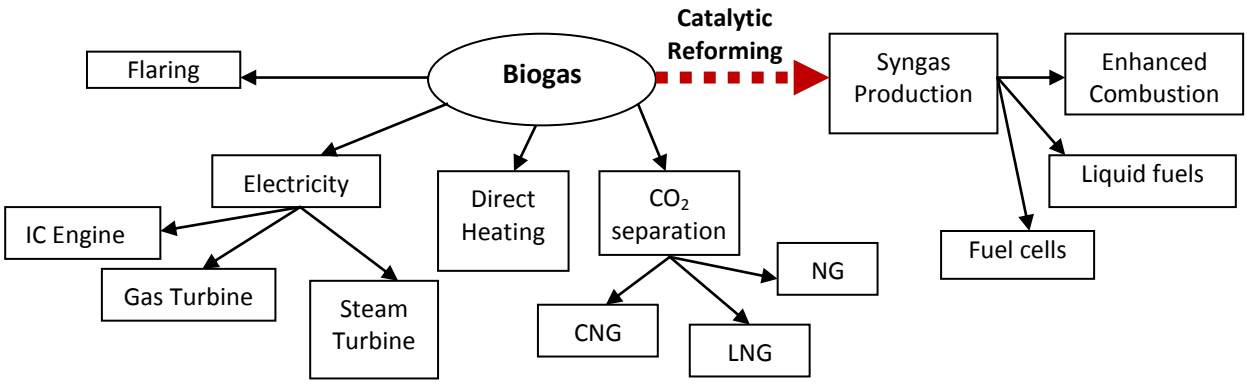

Figure 1.1: Summary of current technologies for CH_4/CO_2 utilization

Two methods of catalytic biogas reforming are explored in this work, dry reforming and auto-thermal reforming. Dry reforming of biogas is an endothermic reaction that directly converts the CH_4 and CO_2 into H_2 and CO. H_2 and CO, or syngas, is a valuable gas mixture because it can be used as a combustion enhancer or a feedstock for liquid fuels or fuel cells. Syngas acts as a combustion enhancer due to its high reactivity that improves the combustion efficiency of the biogas and reduces engine emissions when combusted[10]. The syngas can also be further upgraded to a H_2 rich feed for use in fuel cells, or it can be converted to liquid fuels using the Fischer-Tropsch process[13].

The dry reforming reaction was first studied by Franz Fischer and Hans Tropsch in 1928. Their interest in production of syngas from coal and gaseous fuels and the subsequent production of liquid fuels from syngas originated from the reality of resource availability in Western Europe at this time period, a reality heightened by two world wars. Coal, and to a lesser extent, gas, was readily available, allowing for stationary steam or electricity production, but liquid fuels, ideal for motor, air, or marine transportation, were relatively scarce. In 1925 Franz Fischer stated, "so long as electrical energy in large bulk cannot be carried more efficiently than present-day accumulators permit, so long are we restricted to the use of liquid fuels of relatively high

potential energy for motor propulsion[14]." This paradigm remains apropos almost a century later.

Auto-thermal reforming (ATR) is another catalytic method of converting CH_4 and CO_2 into syngas, using air as a co-reactant. The additional air combusts with a portion of the CH_4 within the catalytic reactor, producing CO_2, H_2O and heat that drive the endothermic dry reforming reactions. ATR also maintains the catalyst activity by providing additional oxidant that reduces the potential for carbon formation in the reactor, especially for biogas mixtures with high CH_4 content.

Both dry and auto-thermal reforming allow for the complete conversion of biogas into syngas. The catalytic reforming can be combined with existing processes, such as combustion of biogas in an engine or turbine, or it can be used in new applications to produce liquid fuels or power fuel cells from local and cheap sources of biogas. No matter the final application, converting biogas into syngas provides more opportunities to completely utilize the energy contained therein.

Biogas from landfills, wastewater, and agricultural waste will contain trace amounts of other compounds, such as nitrogen, sulfur and chlorinated compounds, shown in Table 1.1, in addition to CH_4 and CO_2. These trace compounds will contribute to undesired emissions and have the potential to poison a catalyst, reducing its effectiveness for the production of H_2 and CO.

Table 1.1: Poisons present in Landfill Gas [11, 15]		
Class	Examples	Amount (PPMV)
Chlorinated	Vinyl Chloride, Chlorocarbons	11-46
Sulfur	Hydrogen Sulfide, Methyl Sulfide	30
Aromatic	Toluene, Benzene, Xylene	98
C2s	Ethane, Ethanol	72
C3s	Propane, Acetone	27

The effect of chlorinated compounds, particularly chlorinated hydrocarbons, or chlorocarbons, on a catalyst is not extensively studied, although they are on the same order of magnitude as sulfur compounds in biogas. Sulfur is widely studied because it is commonly present in oil and its derivatives, gasoline for example[13]. Therefore extensive economic clout has been placed on the understanding of the effect of sulfur on catalysts used in oil refining and fuel reforming. Chlorocarbons are not as widely studied because they are not as prevalent in oil or natural gas although they are present in biogas[11, 15], as well as in the high and low temperature gasification products of biomass, coal, and municipal solid waste [16-19]. These chlorocarbons originate from the natural presence of chlorinated compounds in organic material that are released during low temperature decomposition, gasification or combustion of organic material. In fact, it is believed to be plant pectin or lignin that is responsible for the methylation of plant chlorides to produce CH_3Cl, the most abundant atmospheric halocarbon[16]. For this reason, CH_3Cl is used as the chlorocarbon surrogate in this work. Another benefit of using CH_3Cl is that it is chemically similar to CH_4 except for the replacement of one hydrogen atom with one chlorine atom. Therefore any differences observed in the catalyst activity and selectivity during exposure to CH_3Cl compared to CH_4 can be attributed to the presence of the additional chloride.

As the production of bio-derived fuels increases, the effect of chlorocarbons on reforming catalysts will become more important. This thesis discusses the process of dry and auto-thermal

reforming of CH_4 and CO_2 into syngas using a $Rh/\gamma Al_2O_3$ catalyst. The focus of this thesis is on the effect of CH_3Cl on the activity and selectivity of the reforming reactions using a $Rh/\gamma Al_2O_3$ catalyst to convert biogas to syngas. This thesis will contribute to the understanding of the field of chlorocarbon poisoning of the dry reforming reaction, and will be especially useful for biogas applications in which chlorocarbons are present and potentially problematic for a catalytic reactor.

1.2 Thesis Structure

This thesis begins with a background and review of literature relevant to dry reforming, auto-thermal reforming, water-gas shift, and the effect of chlorinated compounds on precious metal catalysts supported on γ-alumina in Chapter 2. Chapter 3 includes results from experimental work on the dry and auto-thermal reforming of CH_4/CO_2 mixtures on a $Rh/\gamma Al_2O_3$ catalyst. Chapter 4 focuses specifically on the effect of CH_3Cl, the chlorocarbon surrogate, on the dry reforming reaction over a Rh/γAl2O3 catalyst. The effect of HCl on the dry reforming reaction and the effect of CH_3Cl on the auto-thermal reforming reaction are discussed briefly. Chapter 4 also includes catalyst characterization results that helped to develop models and a proposed mechanism for the chlorination of the Rh/γAl2O3 catalyst.

Chapter 5 discusses the modification of a pre-existing alumina chlorination model to better represent the Rh/γAl2O3 catalyst, and the use of the chlorination model and trends found in experimental work to simulate the effect of O_2, H_2O, and CO_2 co-feeding as a means to reduce chloride poisoning of the catalyst. Chapter 5 also includes a proposed mechanism for the effect of CH_3Cl on the poisoning of the CH_4 dry reforming reaction. Chapter 6 summarizes the

conclusions of this work. The appendix includes the experimental methods used, including flow-through reactor and catalyst characterization techniques.

Chapter 2 : Background and Literature Review

2.1 Dry Reforming

2.1.1 Thermodynamics

The dry reforming reaction converts CH_4 and CO_2 into H_2 and CO shown in Equation 2.1 and Figure 2.1. It is a highly endothermic reaction, converting two stable molecules, CH_4 and CO_2, into syngas (H_2 and CO), a reactive, high value product and feed stock for other chemical processes. High temperatures, up to 900°C, as shown in Figure 2.1 are needed to fully convert the CH_4 and CO_2 into syngas.

Dry Reforming $CH_4 + CO_2 \rightarrow 2H_2 + 2CO$ $\Delta H=247\ kJ\ mol^{-1}$ 2.1

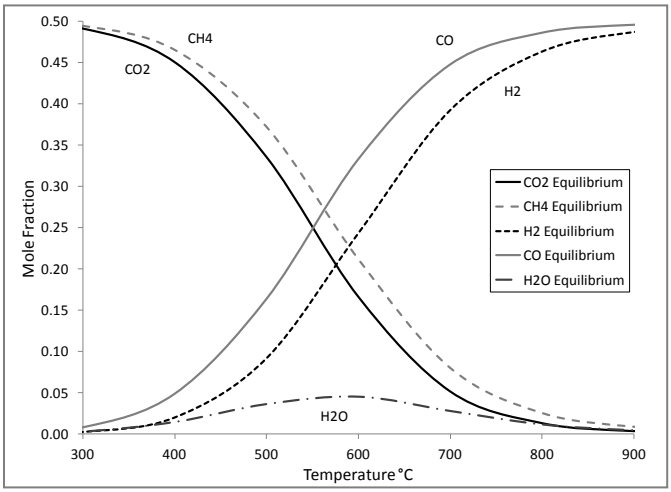

Figure 2.1: Equilibrium conversion of 50% CH_4 and 50% CO_2 between 300°C and 900°C; calculated using GASEQ at atmospheric pressure

Dry reforming is usually accompanied by other side reactions, such as the reverse water-gas shift reaction, Equation 2.2, and carbon forming reactions, Equations 2.3-2.5. The reverse water-gas shift reaction is slightly endothermic and is driven by the high concentration of CO_2 in the dry reforming feed, producing H_2O and decreasing the H_2/CO ratio to a value slightly less than one in the temperature range of 400°C-800°C. Above 900°C complete conversion of CH_4 and CO_2

can be achieved producing a H_2/CO ratio of one. A H_2/CO ratio of approximately one is ideal for certain Fischer-Tropsch processes to produce liquid fuels, particularly higher alcohols[20]. The Boudouard, CO reduction, and CH_4 decomposition reactions have the potential to produce carbon, reducing the selectivity to syngas.

Reverse Water-Gas Shift	$CO_2 + H_2 \leftrightarrow H_2O + CO$	ΔH=42 kJ mol^{-1}	2.2
Boudouard Reaction:	$2CO \leftrightharpoons CO_2 + C$	ΔH= -172 kJ mol^{-1}	2.3
CO reduction:	$CO + H_2 \leftrightharpoons H_2O + C$	ΔH= -131 kJ mol^{-1}	2.4
CH_4 decomposition:	$CH_4 \leftrightharpoons 2H_2 + C$	ΔH= 75 kJ mol^{-1}	2.5

Reactions 2.3-2.5 can be represented graphically in Figure 2.2. The free energy of the reactions in kJ/mole is shown as a function of temperature. The Boudouard and CO reduction reactions have a negative free energy at low temperatures, meaning they are spontaneous at low temperature. The methane decomposition reaction is more likely to occur at high temperatures. Therefore, there is no temperature range of operation in which the dry reforming reaction would occur thermodynamically free of carbon formation. The effect of these carbon forming reactions are more easily realized in an equilibrium plot of mole fraction with temperature, including solid amorphous carbon (C(A)) as a potential product, shown in Figure 2.3. The figure was produced using HSC, a chemical equilibrium calculation software.

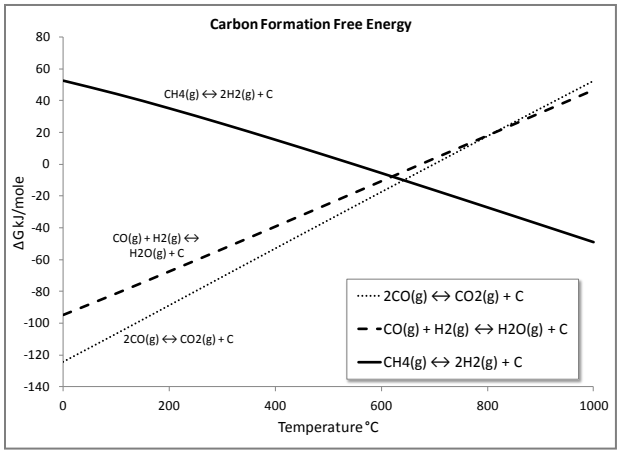

Figure 2.2: ΔG in kJ/mole as a function of temperature for the Boudouard, CO reduction, and CH_4 decomposition reactions at temperatures between 0°C and 1000°C, calculated using GASEQ

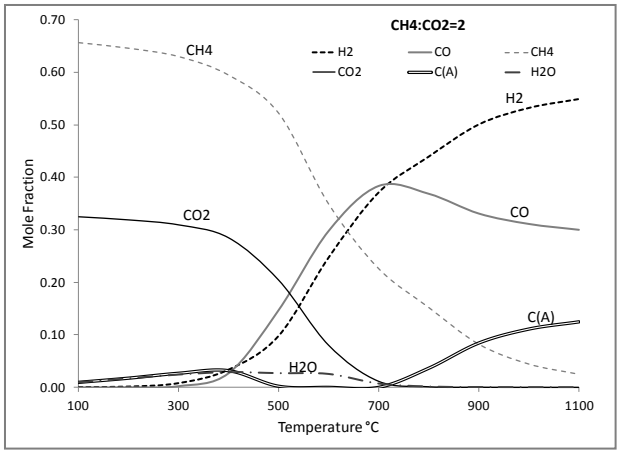

Figure 2.3: Equilibrium mole fractions of CH_4, CO_2, H_2, CO, H_2O, and solid carbon for a dry reforming feed with a CH_4/CO_2=2 at temperatures between 100°C and 1100°C; calculated using HSC

At CH_4/CO_2 ratios of one or less, carbon formation is not thermodynamically expected because there is sufficient oxygen from the CO_2 to oxidize the carbon from CH_4 and CO_2. However at CH_4/CO_2 ratios higher than one, carbon formation can occur. For example, Figure 2.3 shows that with a CH_4/CO_2 ratio of two, there are two temperature regimes in which carbon formation is likely, a low temperature range between 100°C and 500°C, and a high temperature range beginning at 700°C. The low temperature range corresponds to the temperatures at which the Boudouard and CO reduction reactions are spontaneous, while the high temperature range corresponds to the temperature at which methane decomposition is energetically favored. The CH_4 decomposition reaction (2.5) is apparent in Figure 2.3 beginning at 700°C, after CO_2 and H_2O are depleted, CH_4 continues to be consumed, and carbon and hydrogen are produced.

2.1.2 Catalytic Dry Reforming

Because the dry reforming reaction is endothermic and because carbon forming side reactions exist, catalysts are useful for lowering the activation energy of the dry reforming reaction and increasing selectivity to H_2 and CO while decreasing selectivity to carbon formation. Dry

reforming has historically been performed using both base and precious metal catalysts. Base metal catalysts such as nickel (Ni) are attractive due to their low cost compared to precious metal catalysts, but they are less effective because they catalyze the carbon forming Boudouard and methane decomposition reactions. The morphology of the carbon formation on Ni is unique, with carbon forming whiskers beginning at the Ni-support interface and growing outward, with Ni at the tip of the whisker. Interestingly, exposing the Ni catalyst to small amounts of sulfur reduces the carbon formation because the sulfur interrupts ensemble sites necessary for the growth of carbon whiskers. Other factors affecting particle size such as preparation method and surface area also have a major effect on carbon whisker growth[21, 22]. Despite the extensive research on dry reforming using nickel catalysts and the various methods for reducing carbon formation, nickel catalysts are inferior to precious metal catalysts for the dry reforming reaction due to extensive carbon formation[23]. The most ubiquitous method of producing syngas using Ni is by reacting CH_4 with steam instead of CO_2 which keeps carbon formation to a minimum[13].

Precious metal catalysts are extremely active for dry reforming and have lower selectivity for the carbon forming reactions compared to nickel. When this result was first reported in the 1990's, interest in the dry reforming reaction surged [24]. At this time, Rostrup-Nielsen compared the activity of various metals such as Rh, Ru, Pt, Pd, Ir, and Ni supported on MgO and found that Rh and Ru were the most active metals for dry reforming, followed by Ni, Ir, Pt, and Pd[23]. CH_4 decomposition experiments have shown that Ni has a much higher carbon formation rate than the precious metals. It was also noted that those catalysts that had the highest CO heat of adsorption were the least active for dry reforming, suggesting that CO adsorption poisons the dry reforming

reaction. Following this work that showed potential for rhodium as a dry reforming catalyst, rhodium was investigated on various supports [25]. Al_2O_3 was the most effective support compared to TiO_2, SiO_2, and MgO which may be attributed to higher rhodium dispersion, differences in rhodium crystal size, or the ability for carbon to migrate from the metal to the support. The role of the support on the dry reforming reaction will be discussed more thoroughly in section 2.1.3 after a description of the dry reforming mechanism.

2.1.3 Dry Reforming Mechanism

Perhaps because of these early studies that highlighted the superiority of Rh/Al_2O_3 as a dry reforming catalyst, Rh/Al_2O_3 became a popular catalyst for further investigations into the kinetic mechanism, the nature of carbon formation, and the effect of promoters on the dry reforming reaction. In a series of rigorous kinetic studies that excluded transport and thermodynamic effects and accounted for reverse reactions, Wei and Iglesia determined that in dry reforming the activation of the first C-H bond in methane is the only kinetically relevant step on a clean catalyst surface[26-29]. They found this to be true on Rh/Al_2O_3, Rh/ZrO_2, and Ni. In their proposed mechanism, CH_4 first completely decomposes via a step-wise dehydrogenation, producing a high coverage of C* and H* on the metal, and relatively few CH_X species. The C* then reacts with surface O* originating from the co-reactant, either CO_2 or H_2O. H* self reacts to form H_2 or reacts with O* to form OH*, which then reacts with another H* to form H_2O. Therefore the co-reactant is only important for the removal of surface carbon and hydrogen to keep the Rh surface clean. When the surface is clean, meaning vacant surface species, or *, is abundant, the activation of the first C-H bond is the rate determining step and the only rate constant in the rate expression. In this case, the rate is proportional to CH_4 and the co-reactant is irrelevant.

Other kinetic studies on Ni have agreed that the C-H bond activation is a kinetically relevant step, but that the activation of CO_2 to provide oxygen to the surface is also kinetically relevant, at least in some temperature regimes [30-34]. The necessity of the oxidizing co-reactant is apparent in practice because it is required to clean the surface of carbon and maintain activity of the catalyst, although it may not be a kinetically relevant step of a clean surface. However the difficulty involved in studying the dry reforming reaction without carbon formation, especially over base metal catalysts, may be the reason why many studies have reported that the activation of the co-reactant responsible for carbon removal, i.e. CO_2 in the dry reforming case, is kinetically relevant.

According to the micro kinetic mechanism developed by Maestri, Vlachos, Beretta, Groppi, and Tronconi[35], the CH_4 activation is the kinetically relevant process but they concluded that the step between CH_3 and CH_2 is the rate determining step, and all other reactions are quasi-equilibrated. A schematic of this mechanism, showing only the most important steps, is shown in Figure 2.4. The dry reforming reaction proceeds by a stepwise dehydrogenation of CH_4 to surface C*, which is then oxidized by OH* groups, not O*, to form CO. The OH* groups originate from CO_2 activation on the surface by adsorbed H*, or by H_2O activation to form OH* and H*. The surface reaction of CO_2* and H*

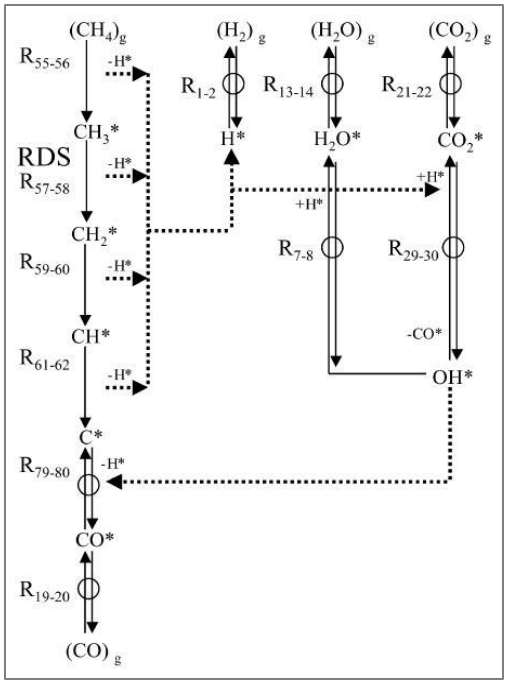

Figure 2.4: Schematic of important steps in the micro-kinetic mechanism for CH_4 dry reforming

produces the necessary OH* group to oxidize the carbon from CH_4 and produces CO from CO_2. Some of the adsorbed H* also reacts with the OH* to form small amounts of H_2O, via the reverse of water activation, and most self reacts to produce H_2. In this mechanism, the mobility of hydrogen on the surface for the dehydrogenation of CH_4 and activation of CO_2 is important.

The activation of CO_2 by H* is also supported indirectly by work on Rh/Al_2O_3 with TiO_2 and V_2O_5 promoters[36]. In this work, the promoters had a minimal effect on CH_4 decomposition but did have an effect on the dissociation of CO_2, and therefore increased the rate of the dry reforming reaction. It was also found that during pretreatment in H_2, TiO_2 was slightly reduced and V_2O_5 was significantly reduced. The ease of reduction may have introduced more H* to the support that helped to activate the CO_2. Oxidation followed by reduction of a Rh/Al_2O_3 catalyst without promoters has also been shown to increase dry reforming activity compared to oxidation alone [37]. This experimental work seems to support the micro-kinetic mechanism in which H* activates CO_2*.

Because the mobility of H and O atoms on the support is relevant to the reforming reaction, there have been efforts to explore different supports and promoters that enhance CO_2 activation or carbon removal reactions. Al_2O_3 is a common support because it has a high surface area and contains acidic and basic sites that can be catalytic in their own right. Indeed it is thought that the alumina support may be instrumental in dry reforming by activating the CO_2 and providing oxidizing species to the carbon originating from the CH_4, whose activation occurs over the metal[25, 38]. The support is also important for allowing hydrogen to migrate from the CH_4 on the metal to the support. ZrO_2 addition to Al_2O_3 improved the rate of the dry reforming reaction

on Ni by promoting the dissociation of CO_2 on the support into oxygen intermediates such as OH* and O* to react with coke on the metal [39]. The addition of CeO_2 also improves the oxygen storage capacity of the support which helps to reduce carbon formation, but it is also easily reduced and deactivated in H_2, a main product of the dry reforming reaction [40].

CeO_2, La_2O_3, and K_2O promoters on Ni/ZrO_2 have also been shown to increase the basicity of the support which favors CO_2 activation, an acidic molecule, and therefore provides more oxidant to reduce the rate of carbon formation[41]. These promoters, as well as MgO and SiO_2, also improve the dry reforming activity on noble metals because they increase surface basicity which is correlated with higher oxygen and hydrogen mobility[42, 43]. This increases the rate of hydrogen and oxygen exchange between the metal and the support, which therefore increases the rate of hydrogen assisted CO_2 activation and decreases carbon formation on the metal. The role of H_2 is significant because while various supports will improve CO_2 activation, in the presence of H_2, CO_2 dissociation is greatly enhanced, suggesting that hydrogen is more effective than the support alone in activating CO_2[25].

Isotopic experiments combined with FTIR, TPO, and TPR were performed to characterize the carbon formation on precious metal catalysts during dry reforming [44]. It was determined that the origin of the carbon formation is from CO_2, with a small contribution from CH_4, and that the carbon becomes less active with time on stream. Furthermore, less carbon is produced at higher temperatures due to increased rates of carbon gasification by H_2O and CO_2. Other work by Chen et al. on Ni catalysts also concluded that CO_2 is the likely carbon source [30]. The CH_4 decomposition reaction has also been reported as a source of carbon formation, although it is not

the dominant carbon formation mechanism on precious metal catalysts[45]. Support acidity may also play a role in carbon formation because more basic supports will increase the ability of the catalyst to chemisorb CO_2 which will oxidize surface carbon[45]. Therefore characteristics of both the support and the metal have an effect on the carbon formation during dry reforming.

In conclusion, dry reforming is an endothermic reaction with a high thermodynamic potential for carbon formation that requires a precious metal catalyst for the highest CH_4 conversion and selectivity to syngas. There is agreement that on precious metal catalysts the dry reforming mechanism generally proceeds by a dehydrogenation of CH_4, which is the slow step, followed by an oxidation of the surface carbon by the co-reactant. The mechanism of CO_2 activation and the resultant oxidizing species is debated. According to the two micro-kinetic mechanisms previously presented [28, 35], CO_2 either decomposes to CO* and O*, proving O* to the surface C* as the oxidizing species, or it reacts with H* to produce CO* and OH*, providing OH* as the oxidizing species. Studies on various supports have shown that there is a correlation between basicity of the support and the degree of CO_2 activation and dry reforming activity. On amphoteric supports such as Al_2O_3, the basicity primarily originates from surface hydroxyl (OH) groups[46] and the acidity can originate from Lewis acid sites or more likely Brönsted acid sites in the presence of H_2O[47]. Both the protons from the Brönsted acid sites and the hydroxyl groups can be mobile[42]. Therefore a support like Al_2O_3 is amenable to an activation of CO_2 on basic sites, assisted by hydrogen that is mobile between the metal and support, to produce CO and OH, a process that is better represented by the micro-kinetic mechanism of Maestri et al[35].

2.2 Auto-thermal Reforming

2.2.1 Thermodynamics

Auto-thermal reforming is defined here as the addition of air or oxygen to the dry reforming reaction to combust with a portion of the CH_4, providing heat and co-reactants to drive the endothermic reforming reactions. The oxygen may fully oxidize the CH_4 to H_2O and CO_2 (Equation 2.6) or partially oxidize it to H_2 and CO (Equation 2.7). The CO_2 produced in the combustion may react with methane via dry reforming (Equation 2.8) and the H_2O produced from the combustion may react with methane in the steam reforming reaction (Equation 2.9). The forward or reverse water-gas shift reaction (Equation 2.10) may also occur.

Methane Combustion	$CH_4 + 2O_2 \rightarrow 2H_2O + CO_2$	ΔH=-802 kJ mol^{-1}	2.6
Methane Partial Oxidation	$CH_4 + \frac{1}{2}O_2 \rightarrow 2H_2 + CO$	ΔH=-36 kJ mol^{-1}	2.7
Dry Reforming	$CH_4 + CO_2 \rightarrow 2H_2 + 2CO$	ΔH=247 kJ mol^{-1}	2.8
Steam Reforming	$CH_4 + H_2O \rightarrow 3H_2 + CO$	ΔH=206 kJ mol^{-1}	2.9
Water-Gas Shift	$H_2O + CO \leftrightarrow CO_2 + H_2$	ΔH=-42 kJ mol^{-1}	2.10

Equilibrium conversion of a $CH_4/CO_2/O_2$ gas mixture at a ratio of 1/1/0.5, or 40% CH_4, 40% CO_2, 20% O_2, is shown in Figure 2.5. O_2 is completely consumed rapidly in the reaction and therefore does not appear in the products. The oxidation reactions, combustion and partial oxidation, produce large amounts of CO_2 and H_2O and some H_2 and CO at low temperatures, less than 500°C. As the temperature increases, CH_4, CO_2, and H_2O are consumed, producing more H_2 and CO, via dry and steam reforming. As the temperature increases the H_2/CO ratio of the syngas decreases because the reverse water-gas shift reaction becomes more active, especially above 700°C.

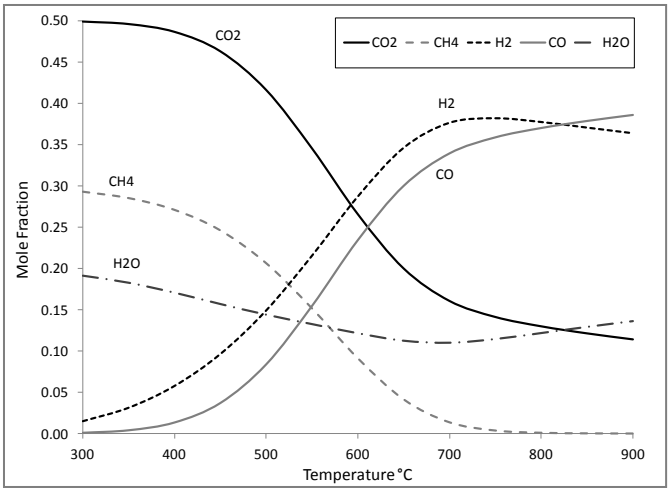

Figure 2.5: Equilibrium conversion of 40% CH_4, 40% CO_2, and 20% O_2 between 300°C and 900°C; calculated using GASEQ at atmospheric pressure

Auto-thermal reforming has the additional benefit of reducing carbon formation potential due to the additional oxidant in the system[24]. The oxygen can combust with surface carbon to produce CO_2, or the steam produced from the combustion may gasify carbon [48], cleaning the rhodium surface. The presence of H_2O also increases the H_2/CO ratio of the product gas via the water-gas shift reaction (Equation 2.10), and therefore the H_2/CO ratio of the syngas can be tuned by altering the amount of O_2 added[45].

2.2.2 Catalytic Auto-thermal Reforming and Mechanism

The reaction of CH_4 and O_2 on Rh/Al_2O_3 is very well understood due to numerous auto-thermal reforming and catalytic partial oxidation studies. Rh is a superior catalyst for methane oxidation compared to other precious and base metals. Ni is likely to form NiO during oxidation which is inactive in the reforming reaction and can volatize[49]. Rh is thermally stable, does not form coke, and has the highest selectivity to H_2 and CO over H_2O and CO_2 compared to Pt due to a high activation energy for OH formation which promotes the release of H_2 before it can be fully oxidized to H_2O[50].

There has been much debate in the literature over whether the production of syngas on a Rh catalyst occurs via a direct route in which H_2 and CO are produced on the catalyst and then desorbed, or via an indirect route in which H_2O and CO_2 are produced from the complete combustion of O_2, followed by steam and CO_2 reforming to syngas. Schmidt et al. have specialized in short contact time reactors at very high temperatures and conversions and have claimed that syngas is produced via the direct route. Because the oxidation reaction is mass transport limited, high space velocities increase conversion and selectivity to H_2 and CO rather than H_2O and CO_2 [51-53]. They propose a mechanism in which CH_4 is dehydrogenated to surface C* that then reacts with surface O* to produce CO, and H_2 is produced from the recombination of surface H*[51-53].

Spatially resolved data in a catalyst bed has revealed that when CH_4 and O_2 are introduced, oxidation occurs in the first part of the bed, rapidly consuming the O_2 and producing a temperature rise, called a “hot spot” in the inlet portion of the reactor. In the literature there is a debate as to the proportions of H_2, CO, H_2O, and CO_2 produced in this oxidation regime, due to the debate over which mechanism, direct or indirect, produces the syngas. Once the O_2 is consumed, the H_2O and CO_2 react with the remaining CH_4 to produce H_2 and CO via steam and dry reforming [54-61]. In some cases, CO_2 reforming is not observed in the downstream portion of the bed, meaning that H_2O is the preferential reactant of CH_4 [55].

One explanation for the debate between the direct vs. indirect mechanism of syngas formation during methane partial oxidation is that both routes occur, but on different sites. A strong

correlation has been observed between oxidation state and CO selectivity. A study by Rabe et al. [62] has shown that at low temperatures, less than 600°C, in the presence of CH_4 and O_2 the Rh is in an oxidized state, and the selectivity to CO/CO_2 is low. At higher temperatures, as the reaction proceeds, the Rh is reduced, and the CO selectivity compared to CO_2 is higher. Therefore, oxidized Rh particles may participate in complete oxidation that would lead to complete combustion followed by the reforming reactions. Reduced Rh particles would not favor complete oxidation and would be more likely to produce syngas directly without complete oxidation to H_2O and CO_2 [62]. X-ray adsorption spectroscopy has shown that after ignition of the CPOX reaction, the entrance zone of the bed is oxidized while the downstream, reforming zone is reduced. Because the oxidation state of Rh is a balance between the rate of oxidation and the rate of CH_4 reaction [63], different oxidation states can exist contiguously, leading to different methane partial oxidation mechanisms within the same zone.

The micro-kinetic mechanism developed by Maestri et al. for dry reforming[35] can also be extended to steam reforming and oxidation reactions[64-67], because the mechanism of dry reforming, methane partial oxidation, and steam reforming are all analogous. The CO_2, O_2, and H_2O are all co-reactants that supply oxygen to the support to oxidize carbon or CH_X species originating from the CH_4 decomposition. In the partial oxidation case, the Maestri model reveals that in the first reaction zone, CH_4 and O_2 are present in the bulk gas and O* is the most abundant reaction intermediate (MARI), leading to complete oxidation of CO* and H* to CO_2 and H_2O. In the second zone, O* is depleted from the surface but is still present in the bulk gas in small amounts, and so H* and CO* become the MARIs, producing H_2O, CO_2, H_2 and CO. In this regime, H_2 and CO desorption compete with their complete oxidation. In the third zone, all

O_2 is consumed and H* and CO* dominate the surface, producing H_2 and CO via the indirect reforming route [35, 66].

It can be summarized that on a catalyst operating at very low residence times, approximately 10^{-3} seconds, and high temperatures, above 1000°C, with low species surface coverage, the direct production of syngas is a good description. On working catalysts with higher residence times and possibly more mass transport restrictions, the complete combustion followed by reforming is the more probable mechanism[68].

While this discussion has focused on the reaction of CH_4 and O_2 alone, the effect of CO_2 on the CH_4 combustion and partial oxidation reactions have also been explored. The kinetics of the catalytic methane partial oxidation reaction with H_2O and CO_2 co-feeding was investigated and it was determined that the CH_4 conversion is independent of O_2, H_2O, and CO_2 [59, 60, 69], analogous to the dry reforming reaction kinetics proposed by Wei and Iglesia, in which CH_4 activation is the only kinetically relevant step[28]. In the reforming zone H_2O and CO_2 addition affect the syngas production according to the water-gas shift reaction: H_2O addition results in more H_2 and CO_2 addition results in more CO. Furthermore, it is suggested that true dry reforming does not occur at all, but rather a combination of steam reforming and water-gas shift, which is stoichiometrically equivalent. This has been an ongoing discussion in literature [23, 45] but it has been difficult to prove because in most studies the reverse water-gas shift reaction is at equilibrium and therefore it is difficult to determine if the CH_4 is reacting with the CO_2 directly or if the CO_2 is converting to H_2O via reverse water-gas shift and then reacting with the CH_4. In the work of Donazzi et al, however, the space velocities are high and the reverse water-gas shift

is non-equilibrated, so it could be shown to control the rate of methane conversion, meaning the reverse water-gas shift reaction is necessary for the dry reforming reaction to occur. Therefore experimentally and mechanistically, dry reforming has been shown to be simply a combination of steam reforming and water-gas shift. For convenience, however, we will continue to refer to dry reforming (Equation 2.13) and express it as the stoichiometric sum of steam reforming (Equation 2.11) and reverse water-gas shift (Equation 2.12).

Steam reforming	$CH_4 + H_2O \rightarrow 3H_2 + CO$	$\Delta H=206\ kJ\ mol^{-1}$	*2.11*
Reverse Water-Gas Shift	$CO_2 + H_2 \leftrightarrow H_2O + CO$	$\Delta H=42\ kJ\ mol^{-1}$	*2.12*
Dry Reforming	$CH_4 + CO_2 \rightarrow 2H_2 + 2CO$	$\Delta H=247\ kJ\ mol^{-1}$	*2.13*

2.2.3 Carbon Formation Potential

Auto-thermal reforming has the additional benefit of reducing carbon formation potential due to the additional oxidant in the system[24]. This is illustrated in the following figures that show an equilibrium calculation of carbon formation at 700°C, in Figure 2.6, and 900°C, in Figure 2.7, performed using HSC. The ordinate is the H/C ratio of the gas mixture, and the abscissa is the O/C ratio. The angled y axis is the CO_2/CH_4 ratio, and the upper horizontal axis is the O_2/CH_4 ratio. Therefore a gas mixture with mostly CH_4 and little CO_2 or O_2 would be on the upper left region of this chart, where the H/C ratio is equal to 4.00 and the O_2/CH_4 ratio is equal to 0.0. The shaded grey region is the region in which carbon formation is thermodynamically likely.

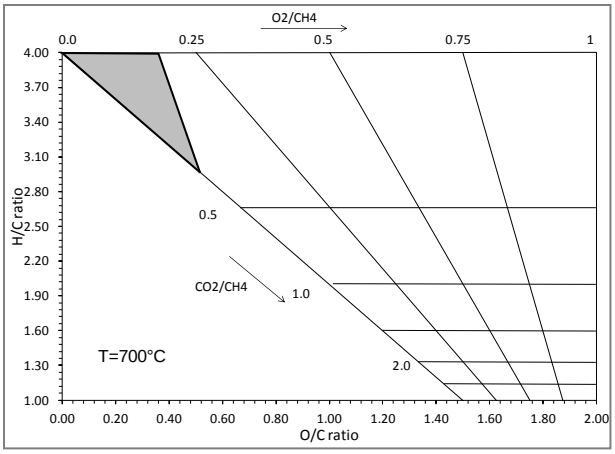

Figure 2.6: Equilibrium calculation of solid carbon formation for various $CH_4/CO_2/O_2$ mixtures at 700°C calculated using HSC. The shaded grey region indicates where carbon formation is favorable.

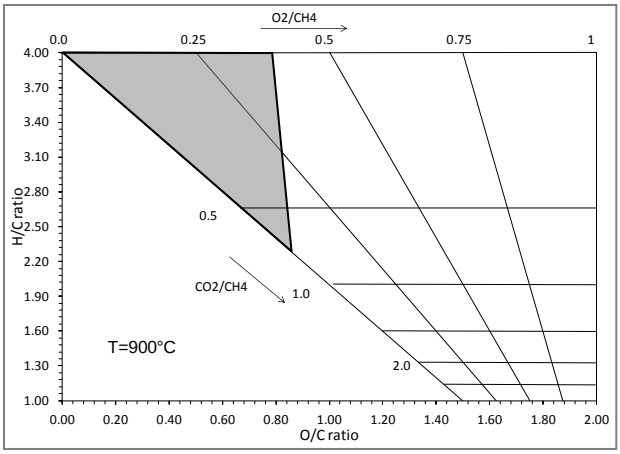

Figure 2.7: Equilibrium calculation of solid carbon formation for various $CH_4/CO_2/O_2$ mixtures at 900°C calculated using HSC. The shaded grey region indicates where carbon formation is favorable.

Both plots show that carbon formation is thermodynamically favorable for $CH_4/CO_2/O_2$ mixtures with low O_2 and CO_2 content. They also show that O_2 is a more effective oxidizer than CO_2. For example, at 900°C, at least 0.4 moles of O_2/mole CH_4 is necessary to be outside of the carbon formation regime, while 0.8 moles of CO_2/mole CH_4 is needed for the same result. As temperature increases, the region in which carbon formation is thermodynamically favorable grows in size, as observable by comparing the size of the shaded grey regions in Figure 2.6 to Figure 2.7. Furthermore, these plots show that even at 900°C, carbon formation is not thermodynamically favorable at a CH_4/CO_2 ratio of one, but as the CH_4 content of the mixture increases, carbon formation becomes more probable. Therefore air addition to the dry reforming reaction has the beneficial effect of reducing the likelihood of carbon formation, especially for CH_4 rich mixtures.

The aforementioned literature has shown that when sufficient O_2 is supplied to react with all of the CH_4 in a CH_4/CO_2 gas mixture, the CH_4 will combust or partially oxide to produce H_2, CO, H_2O, and CO_2, and the CO_2 will not participate in the reaction to a large extent, except in the reverse water-gas shift reaction, thereby altering the H_2/CO ratio. Therefore, large amounts of

O_2 addition to a CH_4/CO_2 mixture would not provide the benefit of converting CO_2 into valuable products. However, a small amount of O_2 or air addition is still beneficial for combusting surface carbon to keep the rhodium surface clean, oxidizing a portion of the CH_4 to produce heat to drive the endothermic reforming reactions, and providing H_2O from the CH_4 combustion that can increase the H_2/CO ratio and provide another reactant for carbon gasification. When CH_4 and CO_2 are already present in a gas mixture, as is the case for landfill gas, biogas, wastewater treatment gas, and some natural gas, reforming the mixture using a Rh/Al_2O_3 catalyst, with or without the addition of air, is a method of converting a low quality fuel mixture into higher value products.

2.3 Water-gas shift reaction

2.3.1 Thermodynamics

The water-gas shift reaction has been mentioned in the previous sections because it usually occurs parallel to dry reforming and auto-thermal reforming reactions. The water gas shift reaction is shown in Equation 2.14.

Water-Gas Shift $H_2O + CO \leftrightarrow CO_2 + H_2$ ΔH=-42 kJ mol^{-1} 2.14

The reaction is reversible, mildly exothermic and the equilibrium constant decreases with temperature. In the range of 315°C to 480°C the equilibrium constant is given by Equation 2.15.

$$K_{eq,WGS} = exp\left[\left(\frac{4577.8}{T}\right) - 4.33\right] \quad 2.15$$

Figure 2.8 shows the equilibrium concentrations of H_2O, CO, H_2 and CO_2 as a function of temperature. Because the forward water-gas shift reaction is exothermic, it is favored at low temperatures, producing H_2 and CO_2. At high temperatures, the reverse-water gas shift reaction is favored, producing H_2O and CO.

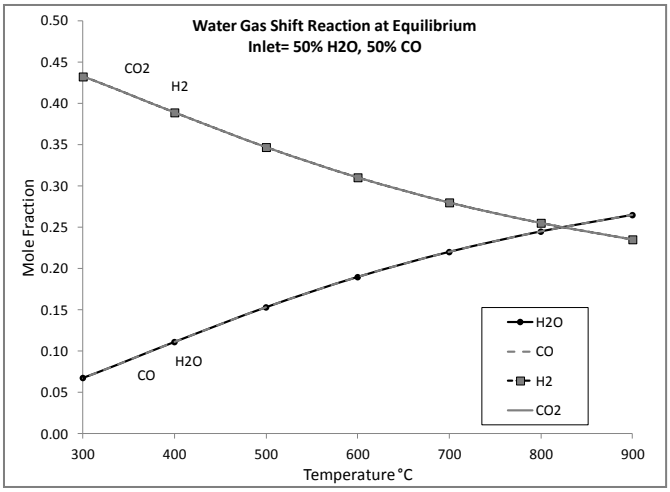

Figure 2.8: Equilibrium conversion of 50% CO_2 and 50% H_2 between 300°C and 900°C; calculated using GASEQ at atmospheric pressure

In the dry reforming reaction, because the CO_2 inlet concentration is high and the reaction is typically performed at high temperatures to achieve maximum conversion of CH_4 to syngas, the reverse-water gas shift reaction is favored, producing additional H_2O and CO. This is the source of H_2O in the dry reforming reaction, and the reason why the H_2/CO ratio of the resulting syngas is often less than one.

2.3.2 Water-gas Shift Mechanism

Many mechanisms have been proposed for the water-gas shift reaction, but in general they fall into two types. One type is an Eley-Rideal mechanism in which the rate limiting step is the reaction of a gas phase species with a surface species such as gas phase CO reacting with surface oxygen to produce CO_2. Another type is a Langmuir-Hinshelwood mechanism in which the rate limiting step is a reaction between two absorbed species, such as surface CO* and O* reacting to form CO_2[70]. On precious metal catalysts supported on non-reducible supports, such as Rh/Al_2O_3, the prevailing mechanism is a Langmuir-Hinshelwood type in which the CO adsorbs on the noble metal and the H_2O is activated on the support to form OH* and H*. Reaction of

CO* and OH* or H_2O* then produces the intermediate formate, or carboxyl group, *COOH, on the metal which rapidly decomposes into CO_2 and H_2 [70-73].

It is widely accepted that the rate limiting step in the forward water-gas shift reaction is the production of the formate intermediate [70-73] either due to diffusion of the CO from the metal to the support, or diffusion of H_2O* or OH* from the support to the metal. A recent study of water-gas shift on Rh/Al_2O_3 used a steady state isotopic transient kinetic analysis (SSITKA) technique coupled with mass spectrometry to follow the labeled H from H_2O and labeled C from CO on the catalyst surface. It was determined that a large pool of OH* and H* existed on the surface of the alumina support and that this pool of OH* was much larger than what could theoretically exist around the periphery of the rhodium particles and much larger than the concentration of carbon species on the surface. The authors therefore concluded that the diffusion of OH* from the support to the active metal, where CO is present, is the slow step in the water-gas shift reaction. Whether the rate limiting step is the diffusion of the CO from the metal to the support or the diffusion of OH* from the support to the metal, in either case OH* is a necessary co-reactant to form the primary reaction intermediate, formate. The rate of the water-gas shift reaction is therefore directly related to the concentration and possibly the mobility of surface hydroxyl groups.

Because the water-gas shift reaction is very reversible, the mechanism and primary surface intermediate will depend on the reaction conditions. In the forward water-gas shift reaction, previously discussed, the primary intermediate is formate, while in the dry reverse water-gas shift reaction, research suggests both a formate and a carbonate intermediate depending on the reaction conditions [74, 75]. When H_2O is added to the feed it accelerates the decomposition of

both formate and carbonate species so conditions can exist in which either species is the primary surface intermediate in the reverse water gas shift reaction [75]. However in the presence of H_2, carbonate species are not likely to be stable because the carbonate species are easily reduced to formate species [76, 77]. Therefore, in reforming conditions in which CO_2, H_2O, H_2 and CO will all exist simultaneously, the surface intermediate is likely to be formate in both the forward and reverse water-gas shift reaction.

In the reverse water-gas shift reaction, the CO_2 is adsorbed on basic sites on the support to produce carbonate species that are quickly reduced by hydrogen to form formate. The H_2 is activated on the rhodium metal and spilled over onto the support. The CO_2 adsorption on the alumina requires basic oxygen anions to form the short lived carbonate[75], and the production of formate requires hydrogen mobility, which is higher on more basic supports[42, 43]. The CO_2 may also adsorb on basic hydroxyl sites forming the formate group directly[46]. Therefore the activity of the reverse water-gas shift reaction, as well as the forward water-gas shift reaction, is related to the basicity of the support, which originates primarily from alumina hydroxyl (OH) groups[46, 78, 79].

2.4 Effect of Chlorinated Compounds on Catalytic Reforming

The effect of chlorocarbons on a catalyst during the dry reforming reaction has not been widely studied. However, other systems involving precious metal supported catalysts and chlorine compounds have been studied that can be used to gain insight on the effect of chlorocarbons on the dry reforming reaction. For example, catalysts are often prepared with chlorinated precursors, and therefore much is known about the interaction between the catalyst support, metal, and chlorine content during catalyst preparation. This provides some understanding of the effect of chlorinated compounds during catalyst use. Other well developed relevant fields of

research include the steam reforming of chlorocarbons, hydro-dechlorination of chlorocarbons, and naphtha reforming in which chlorinated compounds are added to the naphtha feed periodically to rejuvenate the catalyst and enhance the acidity of the alumina support. These four categories: the effect of chlorinated compounds in catalyst preparation, chlorocarbon steam reforming, hydrodechlorination, and naphtha reforming, will be discussed in turn. Because an understanding of the alumina support surface is helpful in the following sections, it will be discussed first.

2.4.1 Alumina Support Structure and Effect of Chloride

Alumina, also known as aluminum oxide or Al_2O_3, is an amphoteric oxide[79] often used as an adsorbent or catalyst support. Alumina is produced from bauxite ore originating from the weathering of aluminum rich rocks. The ore also contains silicas, iron oxides, and titanium dioxide which can remain as trace impurities in alumina supports. The bauxite is purified to aluminum oxide using the Bayer process, developed in 1887 by Carl Josef Bayer who was developing a method to supply alumina, then used as a mordant, to the textile industry. After purification, calcining the alumina in air removes water and results in pure alumina[80].

The temperature and conditions in which the alumina is calcined determines the crystal structure and the surface area of the alumina. For example, gamma alumina calcined at 800°C will have a surface area of approximately 100 m^2/g. Alpha alumina is produced by calcining up to 1200°C and has a surface area of approximately 5 m^2/g. Gamma alumina exhibits a cubic spinel structure, with aluminum interacting in tetrahedral and octahedral configurations with the oxygen atoms. Gamma alumina is the most widely used commercial catalyst support due to its balance of thermal and mechanical stability and high surface area[13].

Figure 2.9 shows the 100 plane, one of the potentially exposed planes on a catalyst, of an ideal structure of dry and hydrated alumina[81]. After calcination in dry air, if the calcination temperature is high enough to remove all of the hydroxyl groups (occurs at approximately 1100°C[46]) an ideal alumina surface will look like the model on the left side of the figure, in which only aluminum and oxide ions are present. On the top layer there is one oxide ion for every two oxide ions beneath it, and the stoichiometry of these two layers is Al_2O_3. As the hydroxyl ions are removed, some "defect" sites can be formed and the alumina model will diverge from the ideal. For example, two or more oxygen ions may remain adjacent to each other as a result of uneven dehydroxylation. These defect sites are important because they can have strong acidic or basic properties.

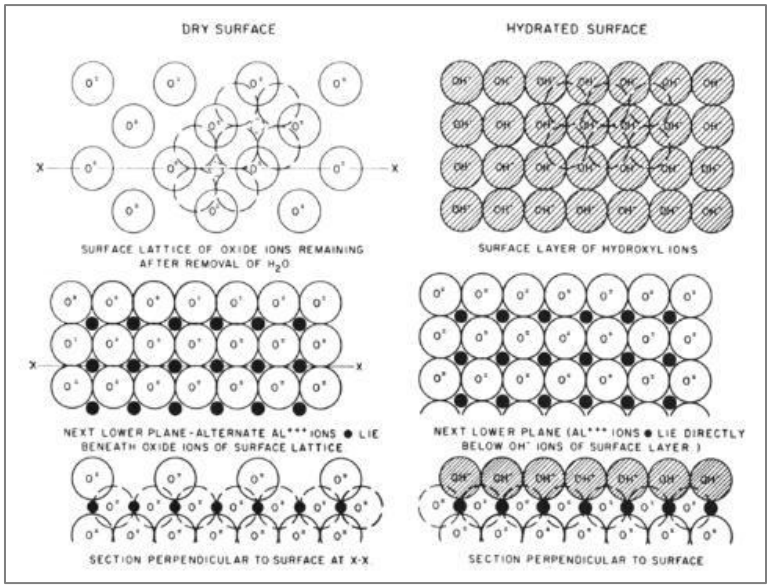

Figure 2.9: 100 plane of an ideal structure of dry and hydrated alumina

After the alumina is calcined, when it is exposed to moisture in room air, the alumina will chemisorb at least a monolayer of water, forming a layer of hydroxyl ions[82]. The model of a

hydrated alumina surface is shown on the right side of the figure. If the alumina is fully hydrated, there is one hydroxyl OH group for each aluminum ion.

In a working catalyst at elevated temperatures in the presence of H_2O, the concentration of OH groups on the surface will result from a balance between the water concentration which favors hydroxylation and the temperature which if high will promote dehydroxylation. Therefore depending on the H_2O concentration and the temperature, the catalyst surface will contain aluminum ions, oxygen ions, and hydroxyl groups. The aluminum ions act as Lewis acids, and the oxygen ions and hydroxyl groups act primarily as bases. The hydroxyl groups can also exhibit weak Brönsted acidity in some configurations. Five common configurations of hydroxyl groups on an ideal (100) plane of alumina are shown in Figure 2.10, labeled A-E. The "A" groups are the most basic because they have the largest number of neighboring oxide ions which stabilize the OH group through the inductive effect. Conversely, the "C" groups, without neighboring oxide groups, are the most acidic[81].

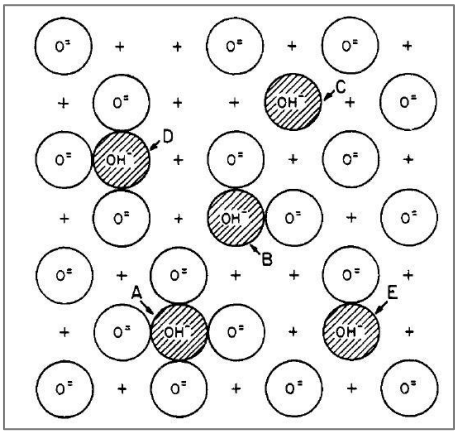

Figure 2.10: Peri model of five possible configurations of OH groups on an Al_2O_3 surface leading to varying amounts of acidity

Another model of the properties of surface hydroxyl groups, proposed by Knozinger and Ratnasamy, considered the three crystal planes of alumina; (111), (110), and (100)[79]. According to this model, the net charge of the alumina hydroxyl groups, determined by their coordination to either tetrahedral or octahedral alumina, influences the IR frequency of the OH

group. Figure 2.11 shows the various hydroxyl group configurations with their calculated net charges. According to the model, the species with the most negative net charge should be the most basic, and those with the most positive net charge should be acidic.

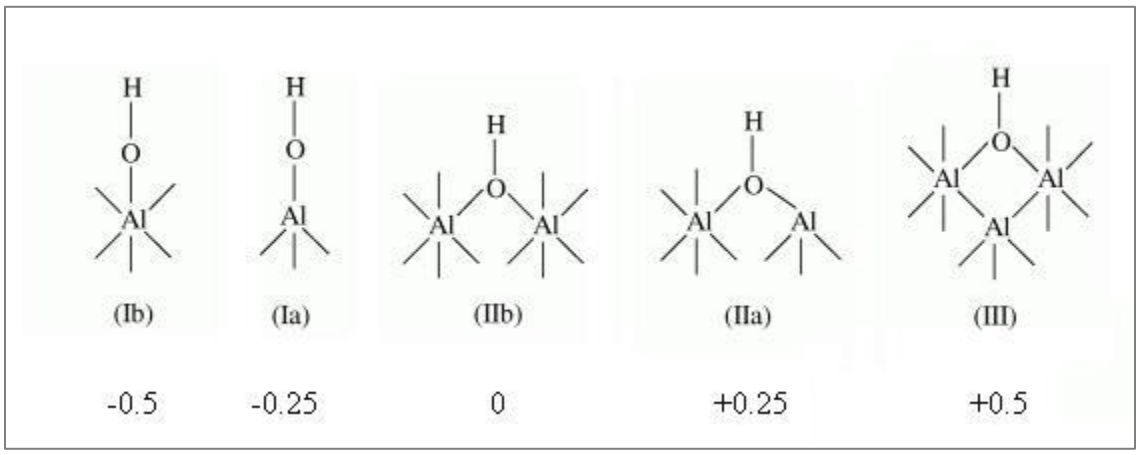

Figure 2.11: Knozinger and Ratnasamy model of various types of alumina hydroxyl groups

In practice the correlation of net charge with acidity is not always accurate because species Ia can be more basic than species Ib, and strong acidity has not been observed for species III[78]. However in general this is still a useful model that is used often to correlate observed IR frequency bands with particular hydroxyl groups[78]. It also illustrates the fact that hydroxyl groups can exhibit acidity or basicity, but usually basicity, depending on their configuration.

Another source of Brönsted acidity on the alumina surface can result due to the interaction of H_2O with Lewis acid sites to produce Brönsted acid-base pairs, as shown in Figure 2.12.

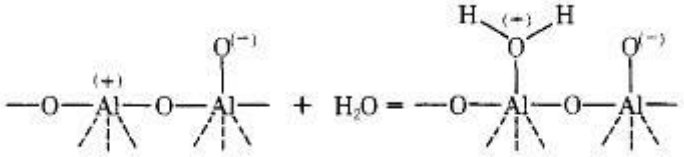

Figure 2.12: Interaction of H_2O with Lewis acid-base pairs to form weaker Brönsted acid-base pairs

Therefore the alumina support is a complex surface that can possess both Lewis acid sites, Brönsted acid sites, and basic sites, leading to the amphoteric nature of alumina[46, 79]. The number of Lewis and Brönsted acid sites on γAl_2O_3 determined with NH_3 adsorption ranges from 0.65 to 0.69 mmol/g [46, 83] and on 5% Rh/Al_2O_3 the number of acid sites has been reported to be 0.47 mmol/g[84]. The amount of basic sites have been measured using CO_2 adsorption and found to be in the range of 0.09-0.21 mmol/g[46]. Therefore the Al_2O_3 is more acidic than basic, but it does contain both types of sites.

The acidic and basic sites on alumina impart catalytic activity. In general alumina catalyzes bond dissociation of H-H and C-H bonds as well as dehydrohalogenation, hydration, deamination and aldol condensation reactions. It is thought that acid-base pairs on the alumina are responsible for its catalytic activity[46]. Because these acidic and basic sites can play a role in catalytic activity, the effect of a strong acid, such as HCl, will certainly affect the acidity and perhaps the activity of the support. It has been proposed that on a working alumina catalyst, in which a mixture of Lewis acid, Brönsted acid, and basic sites exist, HCl dissociates on the catalytic acid base pairs to form Al-Cl, Al-OH, and H_2O, as shown below in Figure 2.13[47].

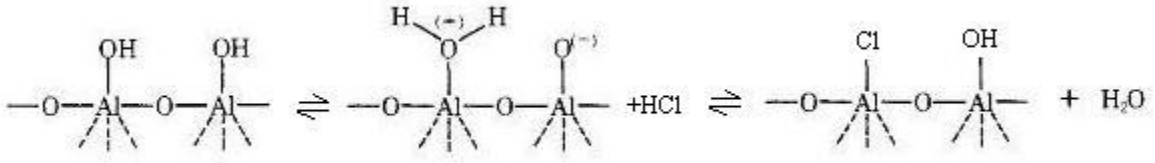

Figure 2.13: Interaction of HCl with a Brönsted acid-base pair to produce Al-Cl, Al-OH, and H_2O

As illustrated in Figure 2.13, H^+ protons from HCl react with basic aluminum anions, while the Cl^- anions react with Brönsted acid sites, resulting in a deposition of chloride and a release of one water molecule. The net reaction is a replacement of a hydroxyl group with a chloride. Another proposed mechanism for the interaction of HCl with alumina is shown in Figure 2.14.

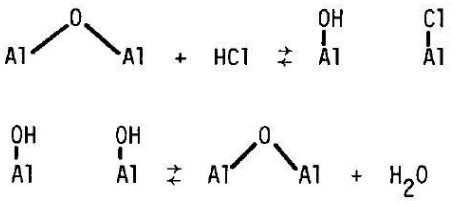

Figure 2.14: Interaction of HCl with bridged oxygen on alumina to product Al-Cl, Al-OH, and H_2O

In this model HCl attacks a bridged oxygen species to form an alumina hydroxyl group and a chloride[85]. In this case the chloride attacks the bridged oxygen-alumina species as if it were a Lewis acid-base pair, as illustrated in Figure 2.12. Therefore the chloride reacts with the alumina cation, the Lewis acid, and the proton from HCl reacts with the basic oxygen anion. If another hydroxyl group is present, the two groups will react to release a molecule of H_2O and replace the bridged oxygen species. In this case, the net reaction is also a replacement of an alumina hydroxyl group with a chloride species and a release of H_2O, shown in Figure 2.15.

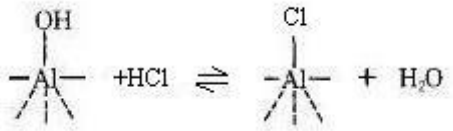

Figure 2.15: Net reaction of alumina chlorination

Therefore in either model, HCl dissociates to react with acid base pairs on the alumina. The chloride reacts with either a Brönsted or Lewis acid, and the proton reacts with an oxygen anion. The net result is a replacement of a hydroxyl groups, which in most configurations is basic, which therefore increases the acidity of the alumina[86]. The net reaction also illustrates the importance of the H_2O content on the chlorination of alumina. Because the chlorination is reversible by reaction with H_2O, the H_2O/HCl ratio and the equilibrium constant of the reaction play a role in the resulting chlorine content on the alumina[85-87].

Chloride may also increase the Brönsted acidity of neighboring OH groups by polarizing the lattice of hydroxyl groups and weakening the remaining O-H bonds [86, 88]. This effect leads to increased proton mobility and hydrogen spillover on the catalyst surface. Hydrogen spillover is the migration of hydrogen atoms from the active metal to the support, which can increase dry reforming activity, as mentioned previously in section 2.1. On Rh, above 75°C, the spillover of hydrogen from the Rh to the alumina is fast, while the surface diffusion of hydrogen is rate limiting. Therefore, increased proton mobility will increase this surface diffusion and therefore improve the dry reforming reaction rate. However it is worth noting that Brönsted acidity is not always directly correlated to hydrogen mobility because protons can also migrate on basic oxides if the oxygen mobility is high, and the hydroxyl groups can move over the surface without the O-H bond dissociation[42].

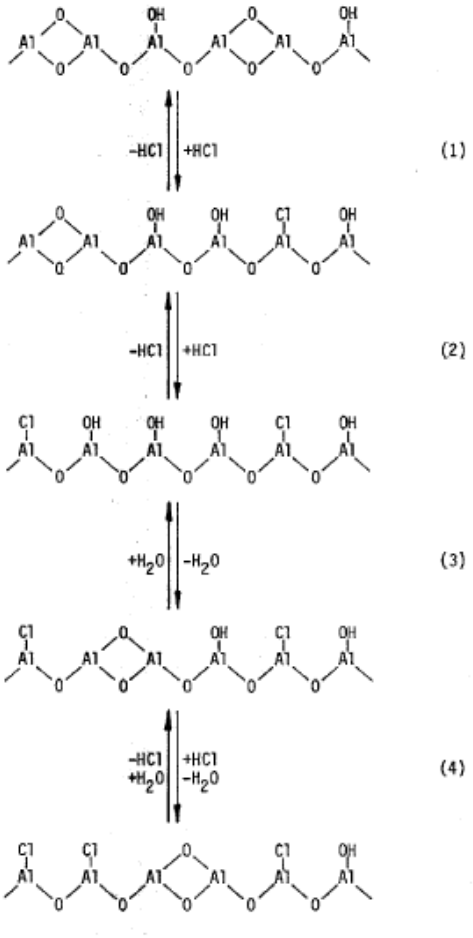

Figure 2.16: Model for successive chlorination of alumina surface, leading to a decrease in hydrogen mobility

An instructive model of the effect of alumina chlorination on hydrogen mobility is presented in Figure 2.16. In step 1, HCl reacts with the bridged Al_2O group to deposit Cl and an OH on the surface. This is the same mechanism as the reaction in Figure 2.14. The chlorination continues until the surface is covered with chloride and hydroxyl groups (step 2 of Figure 2.16). The surface equilibrium of OH

groups is maintained by the subsequent removal of H_2O. This produces more sites for reaction with HCl. This continues until the alumina is saturated with chloride.

The highest hydrogen mobility occurs when half of the surface is covered with Cl, likely because in this configuration the H atoms on the OH groups are acidic due to the aforementioned polarizing of the hydroxyl groups and weakening the O-H bond. The H atoms are therefore more mobile and enhance the rate of H diffusion over the surface. Once the surface is more fully saturated by Cl, however, the number of OH groups decrease, thus decreasing hydrogen mobility[88].

In summary, the alumina support contains a mixture of Lewis acid sites, Brönsted acid sites, and hydroxyl groups that can exhibit basicity or acidity depending on their configuration. In general the alumina has more acidic sites than basic sites. Acid species such as HCl attack acid base pairs, a reaction that has the net effect of replacing OH groups with chloride, therefore increasing the acidity of the alumina. This increased acidity increases H_2 mobility up to the point at which more than half of the basic hydroxyl groups are replaced with chloride. The increased H_2 mobility may increase the rate of the dry reforming reaction by enhancing hydrogen spillover and diffusion from the metal through the support.

2.4.2 Role of Chlorinated Compounds in Catalyst Preparation

Precious metal catalysts are usually produced by incipient wetness impregnation, in which a high surface area support, such as γ-Al_2O_3, is saturated with soluble salts of catalytic metals. After impregnation the catalysts are dried and calcined, or heated in air, which decomposes the metal salts to oxides. The metals are sometimes reduced following the calcination treatment[89]. One

of the most important goals in catalyst preparation is to produce a high dispersion of the precious metal which increases metal surface area and catalyst activity.

In acidic solution, the OH, or hydroxyl groups, of the alumina behave as bases. In reaction A of Figure 2.17 below, the hydroxyl group is protonated and interacts electrostatically with the anion X^-. In reaction B, the hydroxyl group exchanges with the anion to form Al-X and H_2O. In reaction C, scission of an Al-O bond can occur, producing $AlOH_2$ and AlOH [90].

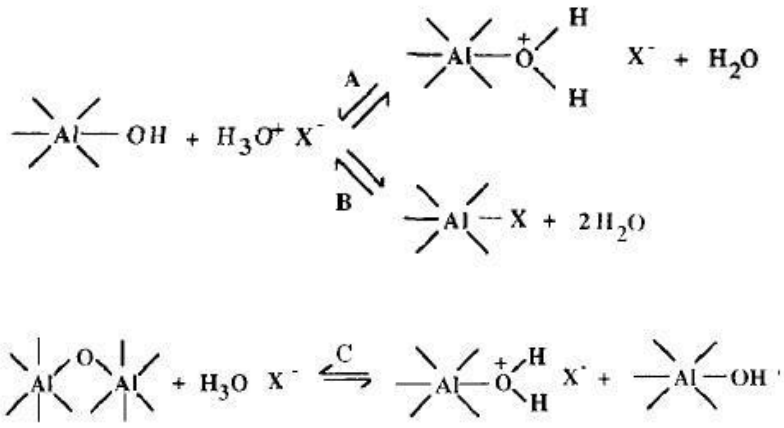

Figure 2.17: Behavior of alumina in acidic solution leading to the interaction of the anion, X^- with the alumina surface

In all three of these reactions, alumina acts as an anion exchanger, with the maximum quantity of anions that can be exchanged being related to the number of alumina hydroxyl groups or the equilibrium constants of the reactions. Therefore, as pH decreases, the equilibrium constants will increase. The exchange of the anion is kinetically very fast and is only limited by diffusion of the anions into the alumina pores[90]. This fact is important in catalyst preparation because usually the metal precursors are acids that can exchange with the alumina very rapidly.

For example, in the impregnation of platinum onto alumina, H_2PtCl_6 acid is used. In solution the hexachloroplatinic acid dissociates into H^+ ions and $PtCl_6^{2-}$ anions. These ions are exchanged with the hydroxyl groups on the alumina, as in reactions A-C, to form the Pt/Al_2O_3 catalyst. However the interaction between $PtCl_6^{2-}$ anions and the Al_2O_3 is very strong, and therefore the anions are fixed very rapidly without ample time for diffusion through the Al_2O_3. This results in a heterogeneous distribution of Pt. To distribute the Pt more homogeneously, HCl is added to produce Cl^- anions that act as competitors to the $PtCl_6^{2-}$ anions. The amount of HCl added is adjusted so that the $PtCl_6^{2-}$ ions remain in solution long enough to diffuse throughout the alumina support and result in an even distribution of Pt. Therefore chloride ions may be introduced into a catalyst via the metal salt or as a competitor ion in catalyst preparation.

While the use of chlorinated precursors and HCl increases the metal dispersion[91], which should theoretically improve catalyst activity, catalysts prepared in this way actually have lower catalytic activity for methane oxidation and reforming reactions because the chloride blocks the active metal sites from reaction. Thus after catalyst preparation using chlorinated precursors or HCl, a reduction step in H_2 is necessary to remove the chloride from the metal surface which improves catalytic activity[92], although some chloride still remains on the alumina support[93], which does not negatively affect the catalytic activity. However the chloride that remains on the alumina support is an important parameter for the acidity and hydrogen spillover activity of the alumina, as discussed in section 2.4.1

2.4.3 Chlorocarbon Steam Reforming

Steam reforming of various chlorocarbons over base and precious metal catalysts supported on γAl_2O_3 has been studied by the Richardson group. The chlorocarbons studied include CH_3Cl

[94-96], chloro-ethanes [97], chloro-aromatics [98], trichloroethylene (TCE) [99, 100] and polychlorinated biphenyls (PCBs) [101]. The steam reforming reaction, shown for CH_3Cl, is shown below in Equation 2.16.

CH_3Cl Steam Reforming: $CH_3Cl + H_2O \rightarrow 2H_2 + CO + HCl$ $\Delta H=123\ kJ\ mol^{-1}$ 2.16

The research group found that in every case deposited chloride poisons the forward water-gas shift reaction, Equation 2.17, but not the chlorocarbon steam reforming activity, Equation 2.16.

Water-Gas Shift $H_2O + CO \leftrightharpoons CO_2 + H_2$ $\Delta H=-42\ kJ\ mol^{-1}$ 2.17

The most active catalyst for the steam reforming was Rh, followed by Cu, Re, Ir, Ru, Ni, and then Co, in decreasing activity. On the Ni catalysts carbon formation was a major deactivation mechanism. On the precious metal catalysts carbon formation occurred to some extent but was not a major cause for activity loss. On all catalysts, a loss in water-gas shift activity was observed via an increase in CO and a decrease in CO_2 at temperatures lower than 700°C[94]. When 1% CH_3Cl was added into a CH_4 steam reforming feed, the activity of CH_4 steam reforming decreased but the CH_3Cl conversion remained at 100%. After CH_3Cl was removed the CH_4 steam reforming activity returned. This suggests that CH_4 and CH_3Cl may be competing for reforming sites and that CH_3Cl reacts preferentially.

Regeneration of the water gas shift activity with H_2O was possible in each case, likely because it converted surface chloride to HCl, removing it from the surface. To explain these results, it was suggested that chloride effectively replaces Al-OH sites that are in equilibrium with steam, as suggested previously for chloride in the catalyst preparation [88] and illustrated in Figure 2.15. By replacing these Al-OH sites, chloride poisons the WGS reaction which is also dependent on

these OH sites. It was also suggested that chloride deposition could contribute to carbon formation by decreasing the hydrogen spillover, as discussed previously, which would increase carbon formation by reducing the $C + 2H_2 \rightarrow CH_4$ reaction. The increase in surface acidity due to the deposited chloride may also promote carbon cracking reactions [99].

To probe the effect of surface acidity on carbon formation, a test was performed by adding HCl instead of CH_3Cl to a methane steam reforming reaction[99]. In this experiment, HCl did not contribute to carbon formation, but did poison the water-gas shift activity. Any carbon formation due to the introduction of chlorocarbons therefore originates from the excess carbon introduced by the chlorocarbons and not the increase in surface acidity due to the chloride deposition. In summary, carbon formation enhancement by chlorocarbons or HCl is not a likely deactivation mechanism. However, chloride deposition on the alumina seems clearly to be a reversible water-gas shift site poison.

To evaluate the effect of the alumina support on the chlorocarbon reforming activity, experiments were also performed on a ZrO_2 support [100]. On a Pt/ZrO_2 catalyst, water-gas shift poisoning was not seen, and the chlorocarbon reforming remained high and close to equilibrium. It was proposed that ZrO_2 is not poisoned by chloride or HCl and that it maintains a constant number of hydroxyl groups. It is important to note that ZrO_2 has weaker acid and basic sites than Al_2O_3, which may be the reason why it is more resistant to chloride poisoning. The lower acidity provides fewer acid sites for the chloride anion to attack, thereby reducing the potential for chloride deposition.

2.4.4 Hydrodechlorination of chlorocarbons

The hydrodechlorination of a chlorocarbon is the reaction of a chlorocarbon with H_2 to replace the chlorine(s) atoms with H, and convert the chloride to HCl. The mechanism of this reaction has been studied on precious metals supported on alumina and carbon, and may be relevant to understanding the mechanism of chlorocarbon reforming in the dry reforming reaction, in which H_2 is a product. It is thought that during hydrodechlorination the chlorocarbon deposits on the surface and reacts with H_2 or surface H* to remove the chloride as HCl [102-105]. The HCl may then compete with the chlorocarbon for active sites, reducing the chlorocarbon conversion [102].

It has been proposed that the rate limiting step is the scission of the first C-Cl bond [105, 106], analogous to the Wei and Iglesia mechanism of CH_4 reforming, in which the rate limiting step was the scission of the first C-H bond[26-29]. The C-Cl rate limiting step is supported by the fact that the overall chlorocarbon reaction rate is correlated to the C-Cl bond strength of the chlorocarbon[105]. The bond dissociation energy of a CH_3-H bond is 439 kJ/mole while that of a CH_3-Cl bond is 350 kJ/mole[107], so it is likely that in a reforming reaction with CH_4 and CH_3Cl present, the C-Cl bond will break before the C-H bond of the CH_4. This is supported by the result from Richardson et al. that CH_3Cl reacts preferentially over CH_4 on a precious metal catalyst.

2.4.5 Use of Chlorocarbons in Catalyst Rejuvenation in Naphtha Reforming

Naphtha is the low-molecular weight mixture of hydrocarbons in the C_5 to C_{12} range produced from the distillation of crude oil. Naphtha reforming is the process of upgrading low octane naphtha into higher octane branched alkanes and aromatic compounds through a sequence of dehydrogenation, dehydrocyclisation, and isomerization reaction[89]. In general an acid

function is needed to catalyze the isomerization reactions and a metal site is needed to catalyze the dehydrogenation reactions[13]. For this reason Pt/Al_2O_3 or $Pt\text{-}Re/Al_2O_3$ are common catalysts for naphtha reforming. The catalyst is more effective when prepared with chlorinated precursors as opposed to Pt nitrates due to the increased acidity of the alumina imparted by the chloride. The discovery of the ability of chloride or fluoride promoters to increase catalyst acidity and isomerization activity in the 1950's was a breakthrough in naphtha reforming technology[89].

In addition to preparation with chlorinated metal precursors and HCl, acidity of the catalyst is maintained during naphtha reforming by introduction of a gas phase chloride such as CCl_4[13]. The amount of chloride deposited on the catalyst surface is important because too little chloride content will decrease catalyst activity and too much chloride will promote the formation of low carbon number alkanes[85]. The optimum chloride content is 0.9-1.3 wt% to maintain a high activity for isomerization. To reach this optimum chloride content, Castro et al. developed a model to describe the weight percent of chloride as a function of the steam and HCl content in the regenerative feed stream. Because the net reaction of alumina chlorination, presented previously in Figure 2.15 and shown again in Figure 2.18 is a function of HCl and H_2O content, the relative ratio of these compounds determines the alumina chlorination content.

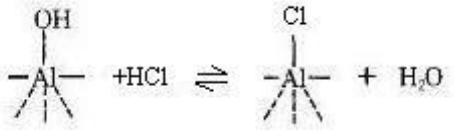

Figure 2.18: Alumina chlorination reaction

Using the net reaction shown in Figure 2.18 and calling K the equilibrium constant of the reaction (Equation 2.19), L the sum of chloride and OH surface species (Equation 2.20), and R

the ratio of H_2O/HCl (Equation 2.21) [85, 87], an expression for the chloride equilibrium concentration on the alumina surface can be developed as shown in Equations 2.22 to 2.24.

$$K = \frac{[Cl][H_2O]}{[OH][HCl]} \quad 2.19$$

$$L = [Cl] + [OH] \quad 2.20$$

$$R = \frac{[H_2O]}{[HCl]} \quad 2.21$$

$$[Cl] = \frac{K[OH][HCl]}{[H_2O]} \quad 2.22$$

$$[Cl] = \frac{K[OH]}{R} \quad 2.23$$

$$[Cl] = \frac{K(L-[Cl])}{R} \quad 2.24$$

Therefore, the chloride equilibrium concentration on the alumina surface is presented in Equation 2.25.

$$[Cl^*] = \frac{KL(1/R)}{1+K(1/R)} \quad 2.25$$

Both K and L only depend on temperature. This model is a good description of the dependence of chloride deposition on H_2O, HCl, and hydroxyl group concentration, which will be illustrated in Chapter 5.

Another function of chlorination in naphtha reforming is to re-disperse agglomerated or sintered metal, usually Pt and Re, using oxy-chlorination[89]. This process produces volatile platinum oxychloride complexes that react with alumina hydroxyl groups to form smaller crystallites. The catalyst is then reduced in H_2 to remove the chloride associated with the platinum, while

unaffecting the chloride associated with the alumina[89]. This process increases metal dispersion and therefore increases naphtha reforming activity[108].

In the dry reforming reaction there is no air present and therefore the volatilization of Rh as $RhCl_3$, or a rhodium oxychloride complex, is unlikely. Furthermore, during the dry reforming reaction a significant amount of H_2 is produced which means the catalyst is in a reduced state, and therefore chloride is unlikely to deposit or remain on the rhodium metal. However, the chlorination of the alumina support is very likely, and therefore the chlorination model proposed by Castro et al. is likely representative of the alumina chlorination process during dry reforming.

2.5 Summary of Literature

There has been a great deal of work and progress on understanding the reactions and mechanisms of the dry reforming, auto-thermal reforming, and water-gas shift reactions. There is also a thorough understanding of the γAl_2O_3 support and the effect of chlorinated compounds on the support in the areas of catalyst preparation, chlorocarbon steam reforming, and acidity doping for naphtha reforming. Despite this relevant research, there is no work to the author's knowledge on the effect of CH_3Cl on a Rh/γAl2O3 catalyst for the dry reforming reaction. The most relevant work is on the steam reforming of chlorocarbons in order to convert them into more benign compounds such as HCl[94-101, 109]. Dry reforming will likely be quite different because there is little steam in the feed except that produced by the reverse water-gas shift reaction, and the focus is not on the destruction of CH_3Cl but the effect of ppm amounts of CH_3Cl as a poison for the dry reforming reaction. The work presented in this thesis will contribute to the understanding of the field of chlorocarbon poisoning of reforming reactions for syngas production.

Chapter 3 : Dry and Auto-thermal Reforming Results

3.1 Dry Reforming

3.1.1 Comparison to Equilibrium

The ability of the 4% Rh/γAl2O3 catalyst to catalyze the dry reforming reaction and minimize selectivity to carbon formation reactions was investigated experimentally using a flow-through reactor and thermo-gravimetric analysis. HSC and GASEQ, two chemical equilibrium programs, were used to calculate equilibrium concentrations of carbon as well as other relevant reactant and product species. For convenience the dry reforming reaction is shown again below in Equation 3.1.

Dry Reforming $CH_4 + CO_2 \rightarrow 2H_2 + 2CO$ $\Delta H=247$ *kJ/mole* *3.1*

Figures 3.1 to 3.4 show a comparison of experimental data to equilibrium conversion of CH_4 and CO_2 to H_2, CO, and H_2O calculated using GASEQ. The experimental data was collected over a wide range of space velocities and inlet CH_4/CO_2 ratios, noted in each figure. Space velocity is a measure of the contact time of the reactants on the catalyst. One measure of space velocity is the gas hourly space velocity (GHSV), measured as the volumetric flow rate of the product feed in ml/hour divided by the volume occupied by the catalyzed monolith, shown in Equation 3.2. The unit of GHSV is therefore $hour^{-1}$ and is the inverse of contact time.

$$GHSV\ \left(\frac{1}{hour}\right) = \frac{volumetric\ flow\ rate\ \left(\frac{ml}{hour}\right)}{volume\ of\ monolith\ (cm^3)} \qquad 3.2$$

The solid lines are the results of the equilibrium calculations and the data points are experimental results.

Comparison of equilibrium values, calculated using GASEQ, to experimental values

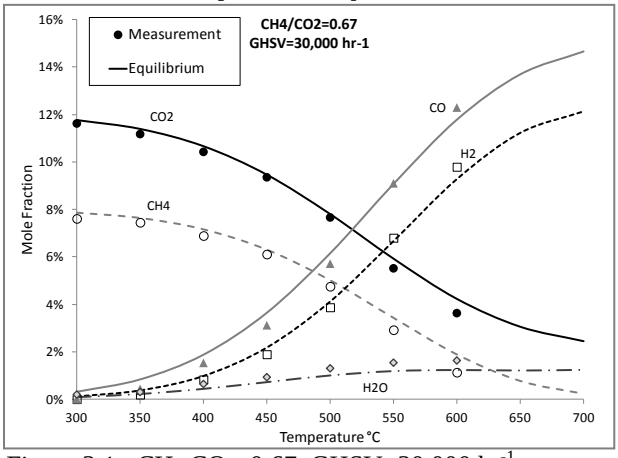

Figure 3.1: CH_4:CO_2=0.67, GHSV=30,000 hr^{-1}

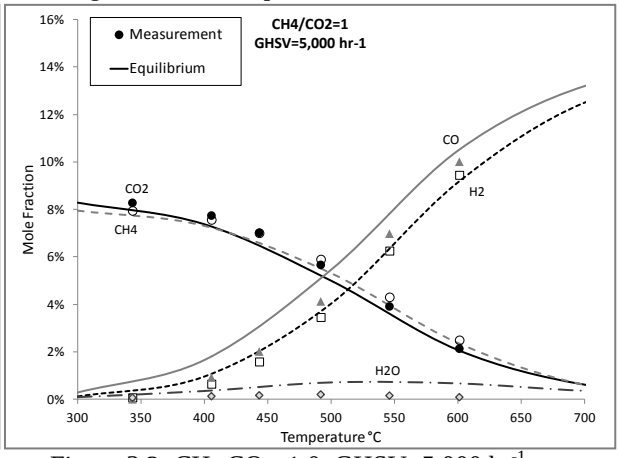

Figure 3.2: CH_4:CO_2=1.0, GHSV=5,000 hr^{-1}

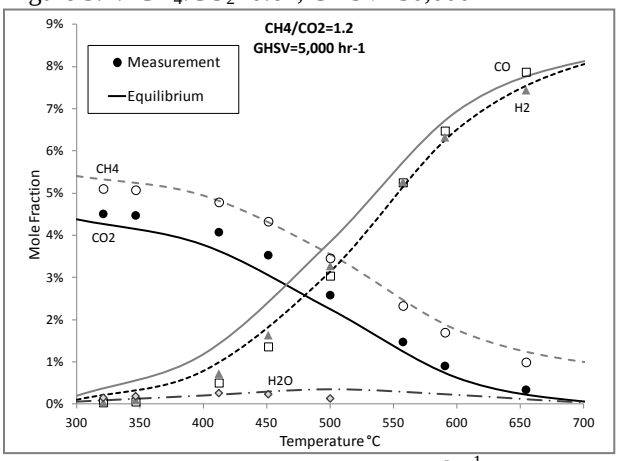

Figure 3.3: CH_4:CO_2=1.2, GHSV=5,000 hr^{-1}

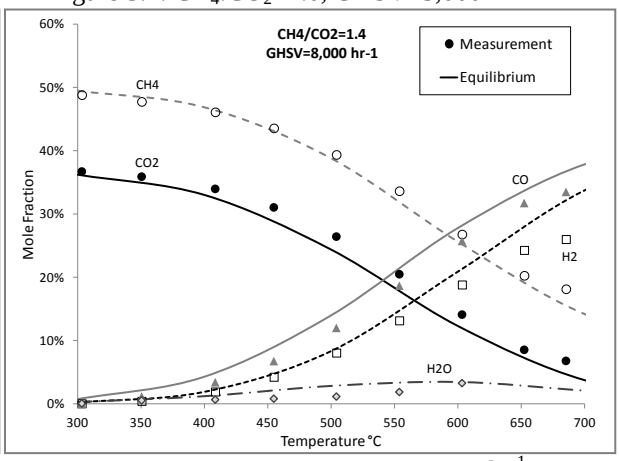

Figure 3.4: CH_4:CO_2=1.4, GHSV=8,000 hr^{-1}

As the CH_4 content of a CH_4/CO_2 mixture increases, carbon formation is more thermodynamically favorable especially at high temperatures. For this reason, Figures 3.1-3.3 show that the Rh/γAl2O3 catalyst reaches equilibrium conversions of CH_4 and CO_2 to H_2, CO, and H_2O at all temperatures, but in Figure 3.4, at a CH_4:CO_2 ratio of 1.4, at high temperatures the experimental data begins to diverge from equilibrium. This is due to carbon formation on the catalyst that blocks rhodium active sites for reforming. The figures also show the effect of CH_4/CO_2 ratio on product selectivity. A high CO_2 fraction, shown in Figure 3.1, produces a

lower H_2/CO ratio due to the occurrence of the reverse water-gas shift reaction (Equation 3.3). As the CO_2 fraction decreases, the H_2:CO ratio increases and approaches 1.0 as long as carbon formation is not significant, as shown in Figures 3.1-3.3.

Reverse Water-Gas Shift $CO_2 + H_2 \leftrightarrow H_2O + CO$ $\Delta H=42\ kJ\ mol^{-1}$ 3.3

3.1.2 Durability

To further evaluate the performance of the Rh/γAl2O3 catalyst experimentally, a 4% Rh/γAl2O3 wash-coated monolith calcined at 725°C in air was exposed to a dry reforming feed (20% CH_4, 20% CO_2, and 60% N_2) for 60 hours to observe any decreases in dry reforming activity that may occur over time. Figure 3.5 shows the results from this test at 925°C and a GHSV of 8,000hr^{-1}. Mole percent is shown as a function of time for CH_4, CO_2, H_2, CO, and H_2O.

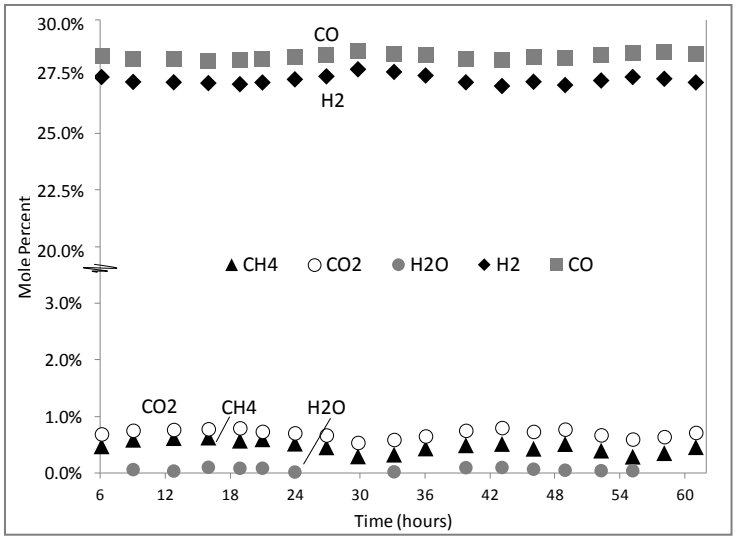

Figure 3.5: Dry reforming of a 20% CH_4, 20% CO_2, 60% N_2 mixture for 60 hours on a 4% Rh/γAl_2O_3 catalyzed monolith at 925°C and a GHSV of 8,000hr^{-1}

Throughout the 60 hours of testing, the CH_4 conversion remained stable at approximately 98%. The rate of change was slightly negative, -0.06%/hour, indicating that the CH_4 conversion was actually slightly increasing over time. H_2 and CO production were also stable at 27% and 28%,

respectively, resulting in a H_2/CO ratio of 0.97. H_2O was not measured using the GC and was therefore calculated from the H_2 balance; it varied between 0.6% and 1.0% throughout the experiment. All species were within 2% of equilibrium values. This data shows that 4% Rh/γAl2O3 catalyst is active for dry reforming 1:1 CH_4:CO_2 mixtures at full conversion for at least 60 hours and likely much longer, without deactivation.

3.1.3 Kinetics

Insight into the kinetics of the dry reforming reaction can be gleaned by observing the conversion of CH_4 and CO_2 to H_2 and CO as a function of position in the monolith. Figure 3.6 shows the mole percent of the products and reactants as a function of axial position in the monolith, obtained using the capillary sampling technique described in section A.1.3. The secondary y axis shows the monolith temperature obtained using multiple thermocouples placed at various axial positions in the monolith. The feed consisted of 20% CH_4, 20% CO_2, and 60% N_2 at a GHSV of 8,000hr^{-1} and a reactant inlet temperature of 925°C. Just before the entrance to the monolith, the gas composition is primarily CH_4 and CO_2. As the axial position in the monolith increases, CH_4 and CO_2 concentrations decrease while H_2 and CO concentrations increase, showing that dry reforming (Equation 3.1) is the primary reaction occuring. Some H_2O is also produced, indicating that the reverse water-gas shift reaction (Equation 3.3) is also active.

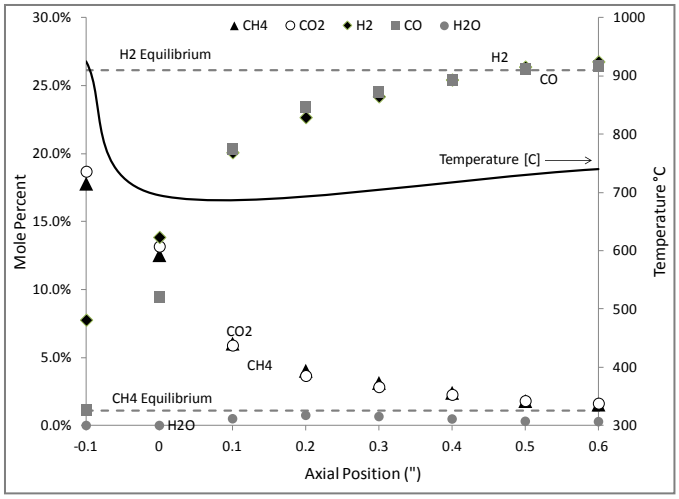

Figure 3.6: Mole percent of CH_4, CO_2, H_2, CO, and H_2O for an inlet concentration of 20% CH_4, 20% CO_2, and 60% N_2 at a GHSV of 8,000 hr^{-1} and a furnace temperature of 925°C as a function of axial position

By the exit of the monolith, equilibrium concentrations have been reached, as shown by the CH_4 and H_2 equilibrium lines on the figure, calculated using the monolith outlet temperature. The monolith temperature is a function of the endothermic dry reforming reaction. Before the inlet of the monolith, the gas temperature is 925°C, the same temperature as the furnace. As the axial position increases along the monolith and the reaction proceeds, the monolith temperature drops rapidly to 700°C. As the reaction proceeds along the monolith, the reaction rate decreases as shown by the decrease in the rate of H_2 and CO production and the stabilization and then slight increase of the monolith temperature.

The data shown in Figure 3.6 can be used to obtain kinetic parameters such as the activation energy and reactant orders in the dry reforming reaction. The dry reforming rate can be written as below in Equation 3.4, as a function of a pre-exponential factor k_o, the activation energy of the reaction, E_a, and the concentration of the reactants CH_4 and CO_2 raised to orders α and β, respectively, neglecting reverse reactions.

$$Rate = k_o \exp\left(\frac{-E_a}{RT}\right)(CH_4)^{\alpha}(CO_2)^{\beta} \qquad 3.4$$

Monoliths are typically not used for kinetic studies because the gas flow is laminar within the channels of the monolith which reduces mass transfer to the catalytic sites. Temperature and concentration gradients are also harder to control in long monoliths, as evidenced by the previous Figure 3.6. However if a capillary is used to take data close to the entrance of the monolith, the flow path is turbulent, resulting in higher mass transfer to the catalytic sites, resulting in kinetic data that is more intrinsic to the catalytic active sites. Furthermore, at the entrance of the monolith when CH_4 conversion is low and heat and mass transfer is high, the temperature can be approximated to be the inlet temperature of the gas, and kinetics can be obtained at known temperatures without temperature gradients within the monolith.

A preliminary implementaion of this technique confirmed that the reaction is more kinetically limited in the first portion of the monolith due to high mass tranport rates, and is therefore the best location to measure kinetic data. The experimental and calculation method is described in more detail in appendix section A.2. The results for CH_4 and CO_2 orders at 550°C in both the turbulent entrance region of the monolith and the laminar, downstream region of the monolith, and the calculated activation energy is shown in Table 3.1. The activation energy is calculated using data between 400°C and 700°C from both the turbulent and laminar regions of the monolith.

Table 3.1: Summary of reaction orders at 550°C and E_A obtained from the capillary sampling technique

Summary of Reaction Orders at 550°C and E_A		
	CH_4 order	CO_2 order
Turbulent Region	0.58	0.50
Laminar Region	0.26	0.65
Activation energy, E_A=95.44 kJ/mole.		

Table 3.1 shows that in the turbulent region of the monolith, where it is expected that the system is more kinetically limited, the reaction rate is more sensitive to CH_4 than CO_2. In the laminar region of the monolith, where a boundary layer develops between the gas phase and the surface and it is therefore expected that mass transfer will have an effect on the reaction rate, the reaction rate is more sensitive to CO_2 than CH_4. The difference in reaction orders may also be due to different gas mixtures that result from CH_4 and CO_2 conversion to H_2 and CO occurring throughout the monolith.

Literature values for the activation energy of the dry reforming reaction are shown in Table 3.2 and range from 53.3 to 111 on a Rh/Al_2O_3 catalyst. The activation energy obtained in this study is 95.55 kJ/mole. Literature values for the reaction orders of CH_4 and CO_2 in the dry reforming reaction span a wide range from 0.04 to 1 for CH_4 and 0 to 0.51 for CO_2. In the rigorous isotopic kinetic studies performed by Wei and Iglesia, discussed in section 2.1.2, it was determined that in dry reforming the activation of the first C-H bond in methane is the only kinetically relevant step on Rh/Al_2O_3, Rh/ZrO_2, and Ni catalysts [26-29]. This means that in the absence of transport effects and carbon formation, the reaction should be first order in methane and zero order in CO_2. It is important to note that in the turbulent region of the monolith the reaction orders are closer to this approximation. This is consistent with the hypothesis that the system is more kinetically controlled in this region.

Table 3.2: Summary of literature values for reaction orders and activation energy in kJ/mole for various catalysts

Summary of Literature values for Reaction Orders and E_A				
Ea kJ/mole	CH_4 Order	CO_2 Order	Catalyst	Reference
95.5	0.58	0.50	4% Rh/Al_2O_3	This Work
111	1.0	0.0	0.4% Rh/Al_2O_3	[28]
74.1	0.04-0.16	0.03-0.09	4% Rh/Al_2O_3	[110]
76.15	0.14-0.22	-0.06-0.43	1% Rh/Al_2O_3	[25]
53.3	0.61	0.37	0.6% Rh/La_2O_3	[111]
31.1	0.52-0.82	0.10-0.51	8% wt Ni/Al_2O_3	[33]

This preliminary kinetic study using capillary sampling shows promise for the determination of kinetic parameters using capillary sampling, with modifications that involve further reduction of heat and mass transfer limitations. For example, the coupling of pellet or powder catalyst beds or catalyst foams with the capillary sampling technique may provide a better system for the measurement of kinetic data.

3.1.4 Carbon formation

The Rh/Al_2O_3 catalyst is at the greatest risk for carbon formation while dry reforming CH_4/CO_2 mixtures with a CH_4/CO_2 ratio higher than one. To understand this potential for carbon formation, thermo gravimetric studies were performed with a gas mixture of 43% CH_4, 35% CO_2, and 22% N_2, giving a CH_4:CO_2 ratio of 1.2. A 4% $Rh/\gamma Al_2O_3$ powder was used to catalyze the dry reforming reaction in the TGA. The temperature program consisted of 20 minute isotherms at 100°C intervals from 300°C to 800°C. The product gases and catalyst weight was measured throughout the experiment, shown in Figure 3.7.

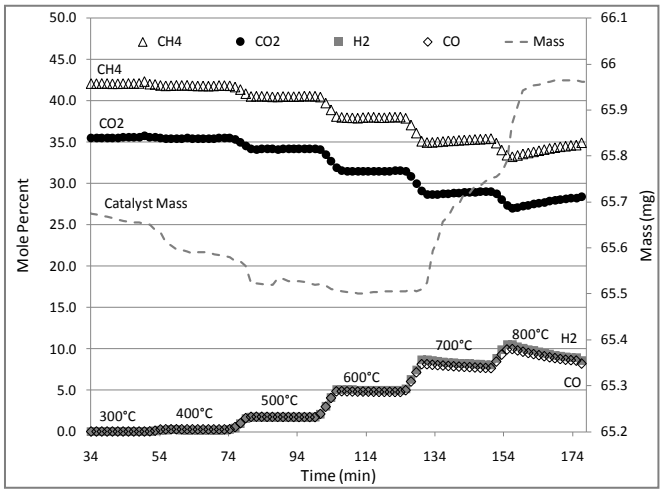

Figure 3.7: Mole percent of CH_4, CO_2, H_2, and CO and catalyst mass (mg) while reforming a mixture of 43% CH_4, 35% CO_2, and 22% N_2 at temperatures between 300°C and 800°C, performed in TGA

Between isotherms of 300°C and 600°C while exposed to CH_4 and CO_2, the catalyst weight decreased, possibly due to a loss of moisture from the catalyst surface. The catalyst was calcined at 725°C in air prior to this test, but was then exposed to room air which results in a hydration of alumina. At each isotherm between 300°C and 600°C, the gas concentrations were stable. Beginning at 700°C, however, the concentration of product gases H_2 and CO decreased during an isotherm, while CH_4 and CO_2 increased. This was coupled with a gain in the catalyst mass, indicative of carbon deposition on the catalyst surface leading to deactivation.

The deactivation rate was calculated in each isotherm as the change in CH_4 molar flowrate during each isotherm, divided by the original CH_4 molar flowrate, shown in Equation 3.5. It is assumed that the change in CH_4 molar flowrate is one measure of the dry reforming activity.

$$Deactivation\ Rate\ (\%/hour) = \frac{CH_{4,f}\left(\frac{moles}{\min}\right) - CH_{4,i}\left(\frac{moles}{\min}\right)}{time_f - time_i\ (\min) * CH_{4,i}\left(\frac{moles}{\min}\right)} * 60\left(\frac{min}{hour}\right) * 100 \qquad 3.5$$

The deactivation rate at each temperature is plotted in the following figure.

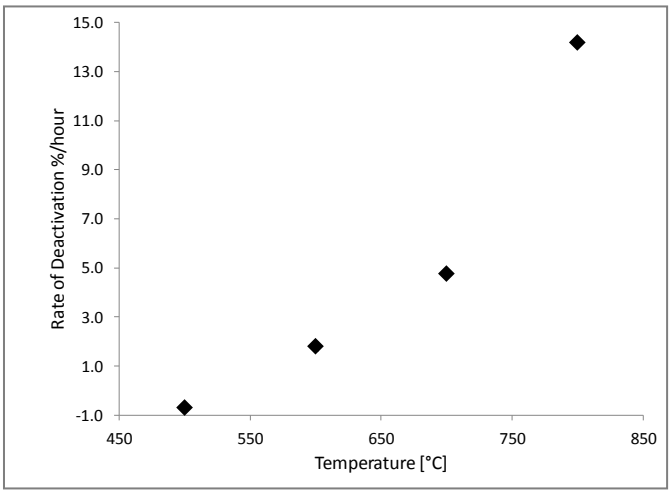

Figure 3.8: Deactivation rate in %/hour as a function of temperature calculated from the experimental data shown in Figure 3.7

Figure 3.8 shows clearly that the deactivation rate increases with temperature. This is consistent with the thermodynamic carbon formation calculations previously discussed in Chapter 2.2.3. After these experiments, the catalyst was exposed to 10% O_2 in N_2 in a temperature ramp from 100°C to 550°C. CO_2 evolved from the sample beginning at 200°C until 400°C. After the regeneration, the activity returned to within 10% of the original activity, further indication that carbon formation was the cause of the catalyst deactivation. In these experiments the $Rh/\gamma Al_2O_3$ catalyst did not begin to form carbon extensively until the catalyst reached a temperature of 700°C. This indicates that for CH_4/CO_2 mixtures with high CH_4 content, there may be conditions in which dry reforming can operate without significant carbon formation and deactivation. Furthermore, if carbon formation does occur, the catalyst has the ability to be regenerated in air.

These experiments and carbon formation calculations define a theoretical working envelope for methane reforming. Theoretically and in practice, carbon will deposit on the Rh/Al_2O_3 catalyst as long as methane is in excess, or the co-reactants CO_2 and O_2 are low or non-existent. However, increasing the CO_2 or O_2 content in the feed can help to reduce carbon formation. According to the carbon formation plots, O_2 in particular is more effective than CO_2 in removing carbon from the surface. This is the basis for why the introduction of O_2 or air into a reforming feed of CH_4 and CO_2 reduces carbon formation and therefore maintains the activity of the Rh/Al_2O_3 catalyst.

3.2 Auto-Thermal Reforming

3.2.1 Comparison to Equilibrium

The ability of the 4% Rh/γAl2O3 catalyst to catalyze the auto-thermal reforming reactions was investigated experimentally using a flow-through reactor and a 4% Rh/γAl2O3 catalyzed

monolith. GASEQ was used to calculate equilibrium concentrations of the product species. The reactions involved in auto-thermal reforming are shown again below in Equations 3.6 to 3.10.

Methane Combustion	$CH_4 + 2O_2 \rightarrow 2H_2O + CO_2$	ΔH=-802 kJ mol^{-1}	3.6
Methane Partial Oxidation	$CH_4 + \frac{1}{2}O_2 \rightarrow 2H_2 + CO$	ΔH=-36 kJ mol^{-1}	3.7
Dry Reforming	$CH_4 + CO_2 \rightarrow 2H_2 + 2CO$	ΔH=247 kJ mol^{-1}	3.8
Steam Reforming	$CH_4 + H_2O \rightarrow 3H_2 + CO$	ΔH=206 kJ mol^{-1}	3.9
Water-Gas Shift	$H_2O + CO \leftrightarrow CO_2 + H_2$	ΔH=-42 kJ mol^{-1}	3.10

Figures 3.9 to 3.12 show a comparison of experimental data to equilibrium conversion of CH_4, CO_2, and varying amounts of O_2 to H_2, CO, and H_2O. In each case, the inlet CH_4/CO_2 ratio was 1, and the CH_4/O_2 ratio varied from 1.6 to 8.0. The experiments were performed at GHSVs between 5,000 and 8,000 hr^{-1}. The solid lines are the results of the equilibrium calculations and the data points are experiment results.

Comparison of equilibrium values, calculated using GASEQ, to experimental values

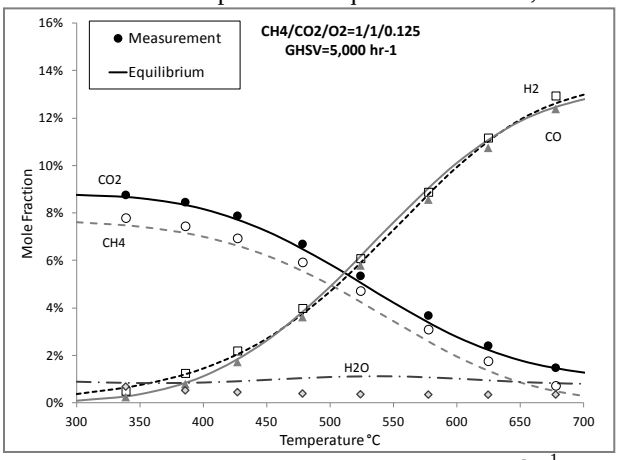

Figure 3.9:$CH_4/CO_2/O_2$=1/1/0.125 GHSV=5,000 hr^{-1}

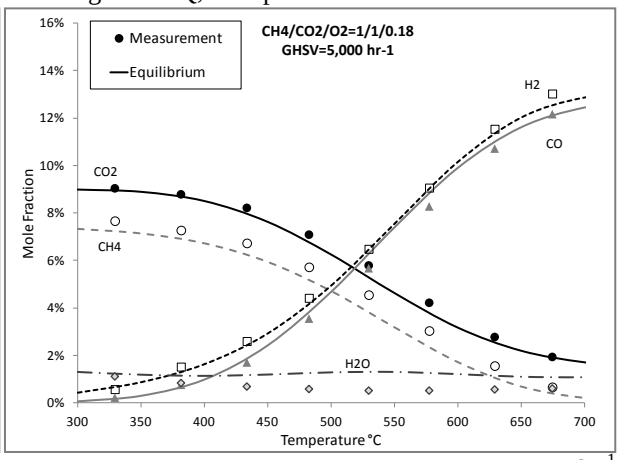

Figure 3.10:$CH_4/CO_2/O_2$=1/1/0.18 GHSV=5,000 hr^{-1}

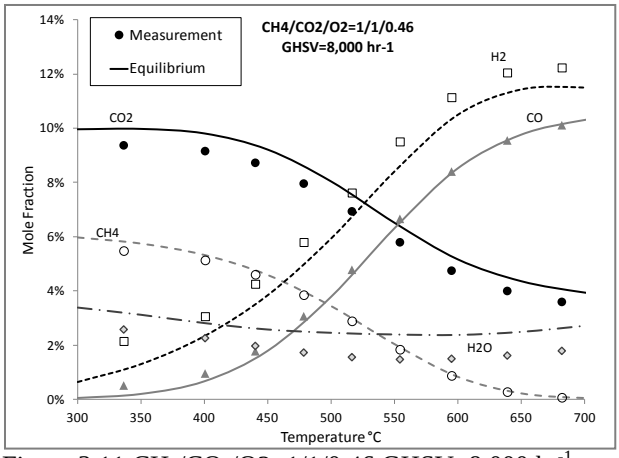

Figure 3.11:$CH_4/CO_2/O2=1/1/0.46$ GHSV=8,000 hr^{-1}

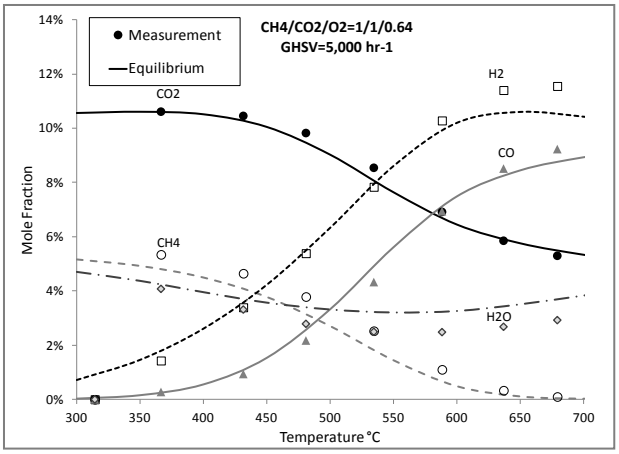

Figure 3.12:$CH_4/CO_2/O2=1/1/0.64$ GHSV=5,000 hr^{-1}

In each Figure 3.9-3.12, the experimental values follow equilibrium values without any deactivation. In each case, at low temperatures, CH_4 conversion produces CO_2, H_2O, H_2, and CO due to the combustion and partial oxidation reactions. As temperature increases, CH_4, CO_2, and H_2O are consumed in reforming and water-gas shift reactions, producing more H_2 and CO. As the O_2 content of the feed increases, CO_2, H_2O, H_2 and CO production increases due to the oxidation reactions. Also as O_2 content increases, the H_2/CO ratio of the syngas increases, due to the additional H_2O in the system from the combustion of CH_4. The H_2O participates in the forward water-gas shift reaction, especially at low temperatures at which it is more thermodynamically favored. Larger amounts of O_2 also increase the CH_4 conversion rate, but even at the lowest O_2 content the CH_4 is completely converted to products at 700°C.

It is important to note that although O_2 introduction increases the H_2/CO ratio, the amount of H_2 and CO produced is smaller at high O_2 concentrations because the syngas is diluted in the combustion products, CO_2 and H_2O. Therefore there is a tradeoff between H_2/CO ratio and syngas production. This is illustrated in Figures 3.13 and 3.14 that show only experimental data from Figures 3.9 to 3.12. Figure 3.13 shows the H_2/CO ratio as a function of syngas production

(H_2+CO mole fraction) for each O_2 concentration. Figure 3.14 shows the H_2/CO ratio as a function of temperature for each O_2 concentration.

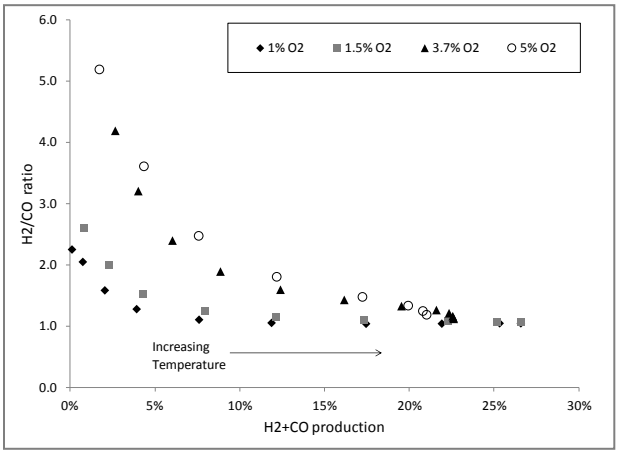

Figure 3.13: Experimental data from Figures 3.9-3.12 that shows the H_2/CO ratio of the syngas as a function of syngas production

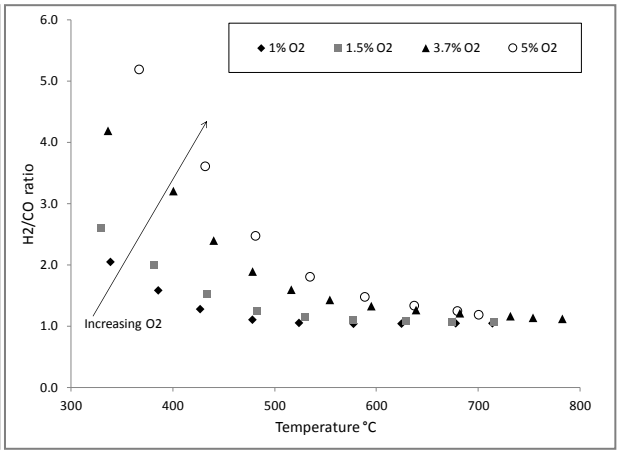

Figure 3.14: Experimental data from Figures 3.9-3.12 that shows the H_2/CO ratio of the syngas as a function of temperature

Generally, higher syngas production is correlated with higher reactor temperatures, as shown in Figures 3.13. Therefore, as temperature and syngas production increase, the H_2/CO ratio of the product decreases due to the reverse water-gas shift reaction (Equation 3.2), shown in both Figures 3.13 and 3.14. At high temperatures therefore, the H_2/CO ratio converges to 1.0, the CH_4 conversion reaches 100%, and the syngas production is maximized at a given O_2 concentration. At a low O_2 feed concentration of 1%, the maximum syngas concentration is 26.6%, while at a high O_2 feed concentration of 5%, the maximum syngas concentration is 21.0% because the syngas is diluted in CO_2 and H_2O. At low temperatures the effect of O_2 addition is more obvious because in this regime the forward water-gas shift reaction is favored. Therefore, increasing O_2 will increase the H_2O production from the CH_4 combustion, which will increase the H_2/CO ratio of the syngas at low temperatures but will decrease the concentration of syngas in the products.

One of the main benefits of introducing air or O_2 into CH_4/CO_2 mixtures is that it reduces the carbon formation potential of the gas mixture. According to the thermodynamic carbon formation regime plots shown in Chapter 2.2.3, at 900°C a mixture of 8% CH_4 and 6% CO_2 is likely to form carbon, but addition of only 0.35% O_2 removes the mixture from the theoretical carbon formation regime. Therefore, only small amounts of O_2 are needed to keep the Rh/γAl2O3 catalyst clean of carbon formation. In light of the previous results summarized in Figures 3.13 and 3.14, the largest syngas production also occurs with small amounts of O_2 introduction and at high reactor temperatures. Therefore, a small amount of O_2, in the range of CH_4/O_2 ratios of 10-20, provides the benefit of carbon removal from the catalyst without producing excessive CO_2 and H_2O from the combustion of CH_4 that dilutes the syngas.

3.2.2 Auto-thermal Reforming Reaction Sequence

The series of reactions involved in auto-thermal reforming; methane combustion, methane partial oxidation, dry reforming, steam reforming, and water-gas shift (Equations 3.6-3.10) that combine to convert CH_4, CO_2, and O_2 to H_2, CO, H_2O, and CO_2 are better resolved using mole fraction data as a function of axial position in the monolith. A capillary sampling method was developed to obtain this type of data. This technique is especially useful for reaction systems with very disparate reaction rates that will take place in different regions of the reactor bed. For example, in the catalytic oxidation of methane, the oxidation reactions are much faster than the reforming reactions. In a monolith reactor, the oxygen involved in the oxidation reactions is consumed quickly in the monolith, while the downstream portion of the bed is depleted of O_2 but has a high concentration of partial oxidation and combustion products. In this situation, with only the outlet gas concentrations, it is very difficult to understand how concentration varies with reaction time. A capillary sampling technique provides data at multiple points along the axis of the monolith

and therefore gives more insight into the reaction rates. More detail on the technique is provided in the appendix section A.1.3.

Figures 3.15 and 3.16 below show plots of mole fraction and monolith temperature as a function of axial position. The catalyst used was a 4% Rh/γAl2O3 wash-coated monolith. Figure 3.15 shows the reaction of 20% CH_4, 10% CO_2, and 10% O_2 at GHSV 52,000 hr^{-1} and a furnace temperature of 500°C. CH_4, CO_2, and O_2 are introduced in the monolith and immediately the oxidation reactions initiate, raising the temperature of the monolith to 800°C and consuming all of the O_2 in the first 0.1" of the monolith. Concurrently, H_2, CO, CO_2, and H_2O are produced. After the oxygen is consumed, the endothermic dry reforming reactions continue, reducing the temperature in the monolith and producing more H_2 and CO with the consumption of CH_4, H_2O, and CO_2. The final H_2/CO ratio of the product gas is 1.5 and the temperature at the end of the bed is 723°C.

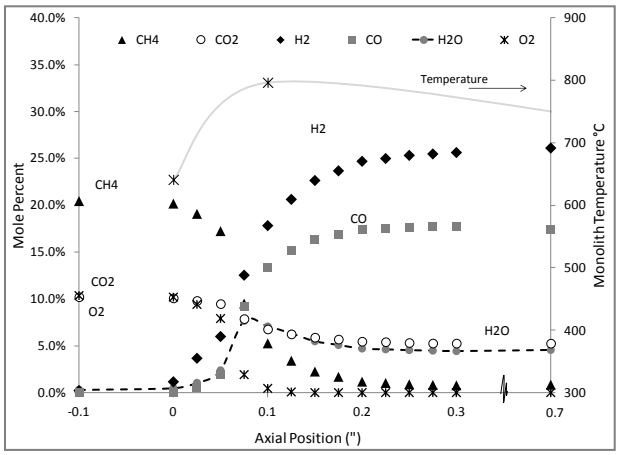

Figure 3.15: Mole fraction of CH_4, CO_2, O_2, H_2, CO, and H_2O and monolith inlet temperature as a function of axial position in the 4% Rh/γAl2O3 monolith for the reaction of 20% CH_4, 10% CO_2, 10% O_2, and 60% N_2 at GHSV 52,000 hr^{-1} and a furnace temperature of 500°C

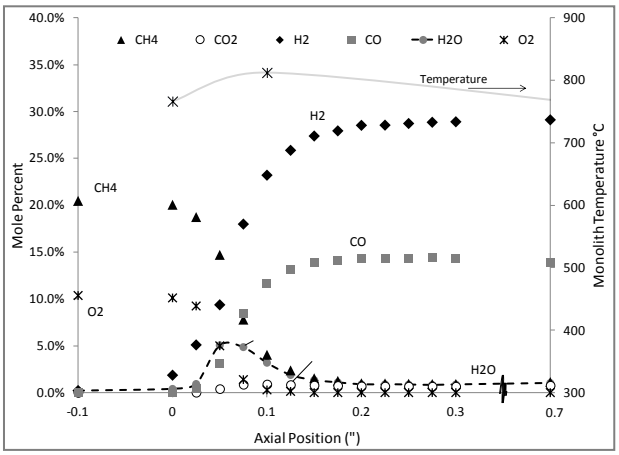

Figure 3.16: Mole fraction of CH_4, CO_2, O_2, H_2, CO, and H_2O and monolith inlet temperature as a function of axial position in the 4% Rh/γAl2O3 monolith for the reaction of 20% CH_4, 10% O_2, and 70% N_2 at GHSV 52,000 hr^{-1} and a furnace temperature of 500°C

According to the data shown in Figures 3.15 and 3.16, the monolith can theoretically be divided into two zones; an oxidation zone and a reforming zone. The oxidation zone occurs in the first 0.1" inch of the monolith, in which O_2 is present and CH_4 and O_2 are consumed to produce H_2, CO, H_2O, and CO_2. This zone produces a temperature rise in the monolith. After the O_2 is consumed, the remainder of the monolith is a reforming zone, in which CH_4, H_2O, and CO_2 are consumed to produce more H_2 and CO.

CO_2 is both a product of the complete combustion reaction and a reactant in the dry reforming reaction, and therefore the CO_2 content of the CH_4/CO_2 mixture plays a role in the selectivity of the reaction. Figure 3.16 shows the same reaction of 20% CH_4 and 10% O_2 at a GHSV of 52,000 hr^{-1} and reactant inlet temperature of 500°C, but without any CO_2 in the feed. In this case, the final H_2/CO ratio of the product gas is 2.1 and the temperature at the end of the bed is 812°C. The monolith temperature and H_2/CO ratio with and without CO_2 are summarized in Figure 3.17.

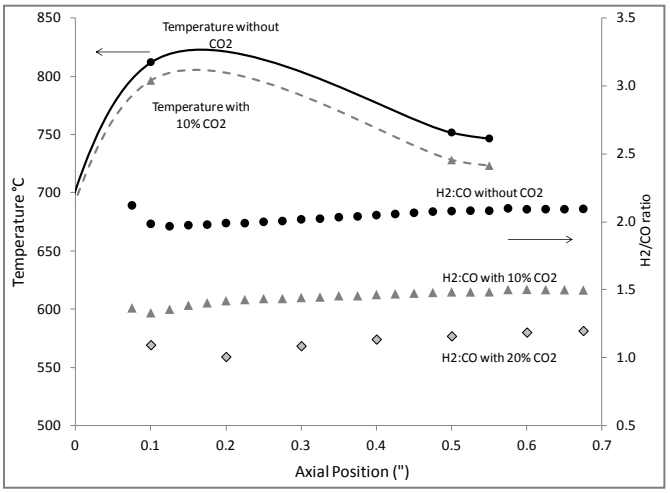

Figure 3.17: Experimental data from Figures 3.15 and 3.16 for monolith inlet temperature and syngas H_2/CO ratio as a function of axial position

The lower monolith temperature caused by CO_2 in the feed could be a result of increased endothermic dry reforming or reverse water-gas shift reaction, or a result of CO_2 acting as a

diluent. However, during the oxidation and reforming zones the CH_4 conversion with and without CO_2 is almost identical, so it does not seem that CO_2 is playing a large role as a diluent in the oxidation zone or increasing the rate of the dry reforming reaction in the forming zone. The reverse water-gas shift reaction must be active to produce the lower H_2/CO ratio due to production of CO and H_2O in favor of H_2 and CO_2. This reaction is slightly endothermic and would account for the difference in temperature with and without CO_2. Therefore it seems that the primary effect of CO_2 in auto-thermal reforming is to participate in the reverse water-gas shift reaction. This is consistent with previous work examining the effect of H_2O and CO_2 on the catalytic partial oxidation of CH_4 [69]. In this work it was determined that the rate of CH_4 reforming is independent of H_2O and CO_2, and that these species affect the product selectivity by participating in the forward and reverse water-gas shift reactions, respectively. Furthermore, while co-feeding both H_2O and CO_2, it was determined that H_2O is the preferential co-reactant of CH_4 via the steam reforming reaction.

3.2.3 Auto-thermal Operation without External Heating

One of the major benefits of air introduction into the CH_4 reforming reaction is that the heat produced from the oxidation reactions can sustain the endothermic reforming reactions and eliminate the need for external heating. This was demonstrated at both a low and a high space velocity. The low GHSV scenario was operated at 8,000 hr^{-1} with a feed of 41% CH_4, 29% CO_2, 19% O_2, and 11% N_2. The CH_4:CO_2 ratio was 1.4 and the O_2:CH_4 ratio was 0.5. Mole percent and temperature are shown as a function of time in Figure 3.18.

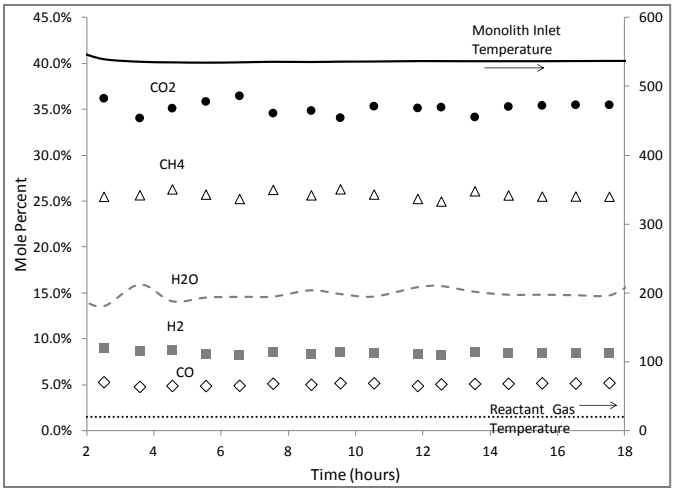

Figure 3.18: Mole percent and monolith inlet temperature as a function of time on stream for the reaction of 41% CH_4, 29% CO_2, 19% O_2, and 11% N_2 at a GHSV of 8,000 hr^{-1}

In this experiment the $CH_4/CO_2/O_2$ mixture was ignited by heating the reactant gases to 600°C. The ignition occurred at approximately 300°C. The reactor furnace was then turned off but remained closed to provide insulation to the reactor. After ignition, the monolith inlet temperature stabilized at 520°C while the outlet temperature stabilized at 400°C, resulting in a CH_4 conversion of 48% and H_2 and CO production of 8.4% and 5.2%, for a H_2/CO ratio of 1.6.

In the high GHSV experiment, the reaction was operated at 41,000 hr^{-1} with a 1.4:1 CH_4:CO_2 mixture composed of 20% CH_4, 14% CO_2 and 10% O_2 in a balance of N_2. The monolith inlet temperature stabilized at 563°C while the outlet stabilized at 482°C. The higher space velocity enabled higher heat and mass transfer throughout the monolith, resulting in CH_4 conversion of 61% and H_2 and CO production of 13.4% and 8.7%, for a H_2/CO ratio of 1.5. This experiment operated for 20 hours without loss of dry reforming activity. These experiments illustrate the importance of high space velocity during auto-thermal operation to achieve high heat and mass transfer to maximize syngas production and eliminate the need for external heating.

These dry and auto-thermal reforming experiments show that a $Rh/\gamma Al_2O_3$ monolith is successful at reaching equilibrium conversion of CH_4 and CO_2 to H_2, CO, and H_2O, with CH_4/CO_2 ratios close to 1.0. However, at higher CH_4:CO_2 ratios the additional CH_4 decomposes on the surface leaving solid carbon, leading to catalyst deactivation. Auto-thermal reforming, however, eliminates carbon formation due to the higher O/C ratio and can operate without external heating at high space velocities.

Chapter 4 : Effect of CH_3Cl on CH_4 Reforming

The effect of CH_3Cl at amounts between 10 and 50ppm in the dry reforming reaction was investigated using flow-through reactor and characterization techniques. Flow-through reactor experiments were used to determine the effect of CH_3Cl on CH_4 conversion, syngas production and product selectivity. Flow-through reactor experiments also tested the effect of HCl on the dry reforming reaction, and the effect of CH_3Cl on the auto-thermal reforming reaction. XPS, acidity, basicity, chemisorption, thermo-gravimetric analysis, and BET characterization were used to develop the mechanism by which CH_3Cl reacts on the catalyst surface.

4.1 Flow-through Reactor Testing

4.1.1 The Effect of CH_3Cl on Dry Reforming

Flow-through reactor tests were performed by exposing the 4% Rh/γAl2O3 powder catalyst to a mixture of 6% CH_4, 7% CO_2 in a balance of N_2 until the reactor temperature and conversion stabilized. CH_3Cl at a concentration of 10, 25, or 50ppm CH_3Cl was introduced for 1 hour. In every experiment, the weight hourly space velocity, defined as the mass flow rate divided by the catalyst mass, was 1,050 hr^{-1}, roughly corresponding to a volumetric space velocity of 700,000 hr^{-1}. CH_3Cl was then removed and the test continued to run for 1 hour with the initial gas mixture. When CH_3Cl was introduced, the N_2 was reduced to maintain a constant flow rate. Product species were monitored throughout the experiment.

The effect of 50ppm CH_3Cl exposure for 1 hour at 400°C on CH_4, CO_2, H_2, CO, H_2O, and CH_3Cl mole concentrations is shown in Figure 4.1. Before CH_3Cl introduction, the CH_4, CO_2, H_2, CO, and H_2O concentrations are stable and the CH_4 conversion is 5.94%. Immediately after CH_3Cl introduction, from 4.4 to 4.5 hours on stream, CO_2 increases by 73 μmoles/min, H_2 increases by 16

μmoles/min, CO decreases by 19 μmoles/min and H_2O decreases by 7 μmoles/min. The immediate CH_4 change is negligible. The CH_3Cl outlet flow rate is 0.8 μmoles/min, giving a conversion of 66%. Due to the stoichiometry of the change in product selectivity, at least a portion of the initial effect of CH_3Cl is a poisoning of the reverse water-gas shift reaction (Equation 4.1), or an enhancement of the water-gas shift reaction, producing more H_2 and CO_2 at the expense of H_2O and CO.

Reverse Water-Gas Shift $CO_2 + H_2 \leftrightarrow H_2O + CO$ $\Delta H=42\ kJ\ mol^{-1}$ 4.1

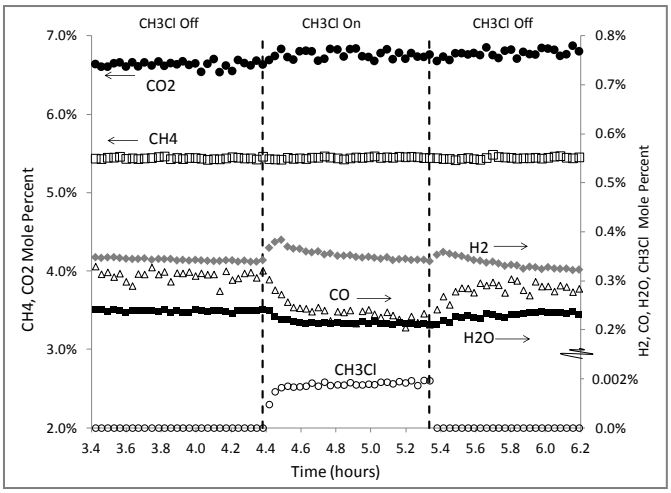

Figure 4.1: The effect of 50ppm CH_3Cl exposure for 1 hour at 400°C in a feed of 6% CH_4 and 7% CO_2 in a balance of N_2 on CH_4, CO_2, H_2, CO, H_2O, and CH_3Cl mole percent

After the immediate change in selectivity, throughout the hour-long CH_3Cl pulse from 4.5 to 5.4 hours, CO_2 is stable within the margin of error produced due to variation in the gas chromatograph readings, CH_4 slightly increases by 7 μmoles/min, H_2 decreases by 15 μmoles/min and CO decreases by 22 μmoles/min. H_2O and CH_3Cl are relatively stable. The stoichiometry of this change appears to be a loss in the activity of the dry reforming reaction, shown in Equation 4.2.

Dry Reforming $CH_4 + CO_2 \rightarrow 2H_2 + 2CO$ $\Delta H=247\ kJ/mole$ 4.2

The net change in product species one hour after the CH_3Cl is removed, at 6.2 hours compared to values before CH_3Cl is introduced, at 4.2 hours, seems to indicate a loss of dry reforming activity overall. CH_4 increases by 11 μmoles/min, CO_2 increases by 58 μmoles/min, H_2 decreases by 10 μmoles/min and CO decreases by 8 μmoles/min. H_2O is relatively unchanged. A summary of the changes in H_2/CO ratio and CH_4 conversion as a result of CH_3Cl exposure is presented in Table 4.1. The error windows arise from the variation of the GC readings.

Table 4.1: Effect of CH_3Cl on H_2/CO, CH_4 Conversion, and Syngas Production at 400°C

Condition	H_2/CO ratio	CH_4 Conversion	H_2+CO production
Before CH_3Cl (4.2h)	1.11 ± 0.05	$5.94\% \pm 0.22\%$	$0.65\% \pm 0.01\%$
Immediately After CH_3Cl (4.5h)	1.42 ± 0.02	$5.97\% \pm 0.22\%$	$0.64\% \pm 0.02\%$
1 hour with CH_3Cl (5.4h)	1.59 ± 0.09	$5.60\% \pm 0.22\%$	$0.56\% \pm 0.01\%$
1 hour after CH_3Cl removed (6.2h)	1.10 ± 0.01	$5.75\% \pm 0.22\%$	$0.61\% \pm 0.01\%$

The effect of CH_3Cl is indicative of an immediate poisoning of the reverse water-gas shift activity, followed by a more gradual decrease of the dry reforming activity. The change in reverse water-gas shift activity is fast and reversible, producing an increase of the H_2/CO ratio of the products while CH_3Cl is on, but reverts back to the original H_2/CO ratio after CH_3Cl is removed. The effect of CH_3Cl is likely a poisoning of the reverse water-gas shift reaction rather than an enhancement of the forward water-gas shift reaction because the high concentration of CO_2 in the product mixture favors the reverse water-gas shift direction. This is calculated and illustrated in more detail in section 4.1.4. The loss of the dry reforming activity is gradual and only partly reversible at this time scale, as illustrated by the change in CH_4 conversion in each segment. CH_4 conversion does not change immediately upon introduction of CH_3Cl, but does gradually decrease, resulting in less total syngas production (H_2 + CO). After the CH_3Cl is removed, some CH_4 conversion and syngas production does return, but not completely within the one hour time segment.

The effect of CH_3Cl on the dry reforming activity may be due to a competition for reforming sites between CH_4 and CH_3Cl. The bond dissociation energy of a CH_3-H bond is 439 kJ/mole while that of a CH_3-Cl bond is 350 kJ/mole[107], meaning CH_3Cl is likely to react preferentially over CH_4. However, the loss in CH_4 reforming is more than what would be expected assuming a 1:1 competition for sites between CH_4 and CH_3Cl, so the cause is likely more than the direct site competition. Another effect of the CH_3Cl could be a chlorination of the alumina surface, as suggested previously in literature, that would increase the acidity of the alumina and therefore decrease the affinity of the support for the acidic CO_2 molecule. This could decrease the rate of the dry reforming reaction, but would be reversible after CH_3Cl is removed. Musso et al. showed that small amounts of alumina chlorination can increase the hydrogen spillover effect which may increase the rate of CH_4 conversion and overall dry reforming activity. However larger amounts of chlorination will cover the alumina with chloride ions and decrease the hydrogen spillover effect and likely the CH_4 conversion[88]. Therefore another explanation for the loss of dry reforming activity in this case could be excessive chlorination of the alumina surface which decreases hydrogen spillover from the CH_4 on the metal to the alumina support, thereby decreasing CH_4 conversion and dry reforming activity.

In order to better understand the effect of CH_3Cl on the dry reforming activity loss, it is useful to compare the rate of deactivation in the CH_3Cl segment to the rate of deactivation before CH_3Cl introduction. The deactivation rate is calculated as the change in CH_4 molar flowrate during a time segment of operation, divided by the original CH_4 molar flowrate, shown in Equation 4.3. It is analogous to a percent change in CH_4 over time. It is assumed that the change in CH_4 molar flowrate is one measure of the dry reforming activity. The equation is shown below.

$$Deactivation\ Rate\ (\%/hour) = \frac{CH_{4,f}\left(\frac{moles}{min}\right) - CH_{4,i}\left(\frac{moles}{min}\right)}{time_f - time_i\ (min) * CH_{4,i}\left(\frac{moles}{min}\right)} * 60\left(\frac{min}{hour}\right) * 100 \qquad 4.3$$

The deactivation rate in each segment is shown in Figure 4.2. In the experiment shown in Figure 4.1, the deactivation rate before CH_3Cl introduction was -0.01%/hr; effectively no deactivation. After CH_3Cl introduction, the deactivation rate was 0.25%/hr. Clearly CH_3Cl introduction increases the rate of dry reforming deactivation. One hour after CH_3Cl was turned off, the deactivation rate decreased to 0.11%/hr. As the dry reforming reaction continues without CH_3Cl, the deactivation rate continues to decrease over time, reaching a level of zero deactivation. This was shown in an experiment performed in exactly the same way as in Figure 4.1, except that it examined the effect of 50ppm CH_3Cl on dry reforming using time segments longer than one hour. The deactivation rate of the catalyst 6 hours after exposure to CH_3Cl is also shown in Figure 4.2.

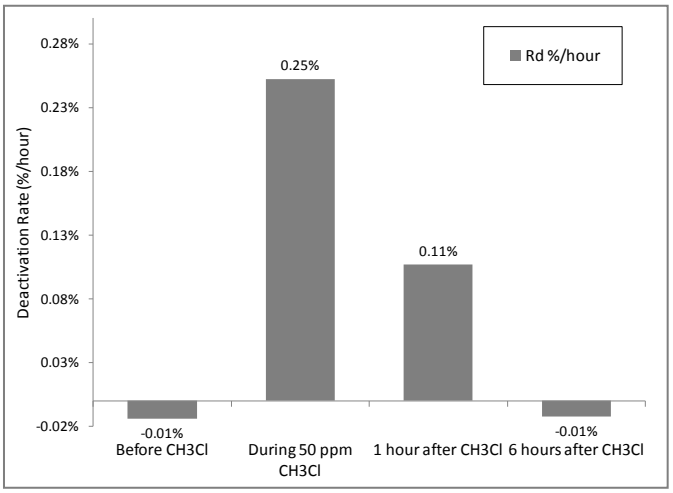

Figure 4.2: Dry reforming deactivation rate measured before, during, and after 50ppm CH_3Cl introduction into a feed of 6% CH_4, 7% CO_2 in a balance of N_2 at 400°C on a 4% Rh/γAl2O3 powder catalyst

Six hours after the CH_3Cl is removed, the dry reforming deactivation rate of the catalyst returns to -0.01%. Therefore Figure 4.2 shows that after the CH_3Cl is removed, given enough time, the

deactivation rate will return to its initial value of effectively no deactivation at 400°C, indicating that the effect of CH_3Cl on the dry reforming activity is fully reversible at 400°C.

Overall it can be concluded that at 400°C, CH_3Cl decreases the rate of the methane reforming reaction while it is on-stream, but when CH_3Cl is removed, the reforming rate eventually returns to its previous value. The cause of the dry reforming poisoning may be due to competition between CH_3Cl and CH_4 for reforming sites, or a chlorinating effect of CH_3Cl on the support that reduces CO_2 activation and/or hydrogen spillover. Chloride is not expected to deposit on the rhodium metal in the presence of H_2, as previously discussed in the literature review, so metal site blocking is not a likely explanation for the dry reforming activity loss. Therefore the effect of chloride deposition on the support may explain both the change in water gas shift and dry reforming activity.

The effect of 50ppm CH_3Cl at other temperatures between 350°C and 700°C was also explored, shown in the following figures. Figure 4.3 shows how CH_4 conversion changes before, during, and after a 1 hour pulse of 50ppm CH_3Cl. In general, as temperature increases, the difference between the CH_4 conversion before CH_3Cl introduction to CH_4 conversion during 50ppm CH_3Cl exposure decreases. This means that the loss in CH_4 reforming activity due to CH_3Cl introduction decreases with temperature. This also suggests that catalysts operating at higher temperatures are not as affected by CH_3Cl. The conversion of CH_3Cl increases with temperature, so the reduced effect of CH_3Cl at higher temperatures is not due to reduced adsorption or surface reaction of CH_3Cl. After removal of CH_3Cl, the CH_4 conversion generally

returned to its original value, indicating that the effect of CH_3Cl on CH_4 conversion is reversible at each temperature.

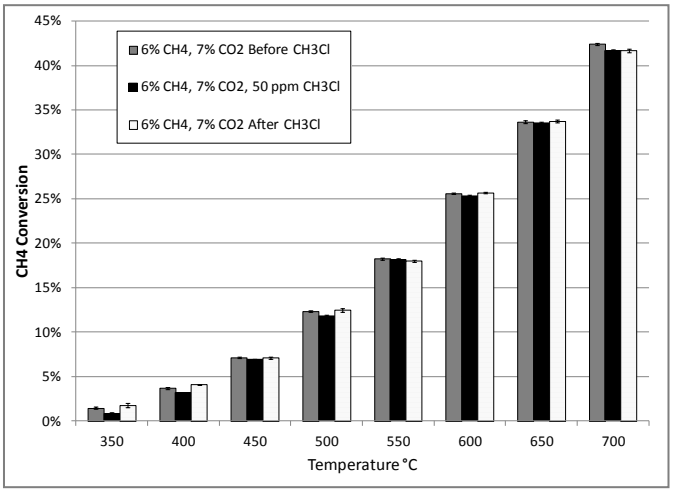

Figure 4.3: CH_4 conversion as a function of temperature before, during, and after 50ppm CH_3Cl introduction into a feed of 6% CH_4 and 7% CO_2 in a balance of N_2 over a 4% Rh/γAl2O3 powder catalyst

Figure 4.4 shows how the H_2/CO ratio changes before, during, and after a 1 hour pulse of 50ppm CH_3Cl. The H_2/CO ratio is a measure of the water-gas shift activity as illustrated in Equation 4.1. High H_2/CO ratios indicate a high water-gas shift activity, while low H_2/CO ratios indicate a low water-gas shift activity, or a high reverse water-gas shift activity. According to Figure 4.4, as temperature increases from 350°C to 700°C, the effect of CH_3Cl on the H_2/CO ratio decreases. At low temperatures, CH_3Cl appears to strongly poison the reverse water-gas shift reaction, causing an increase in the H_2/CO ratio. At high temperatures the change is very small, suggesting only a slight poisoning of the reverse water-gas shift reaction. This is further evidence that the poisoning effect of CH_3Cl is temperature sensitive. The plot also shows that the change in the H_2/CO ratio, or the poisoning of the reverse water-gas shift is completely reversible at every temperature except for 350°C. At 350°C the deposition of CH_3Cl or chloride may be partially irreversible, or take longer than one hour to be completely removed.

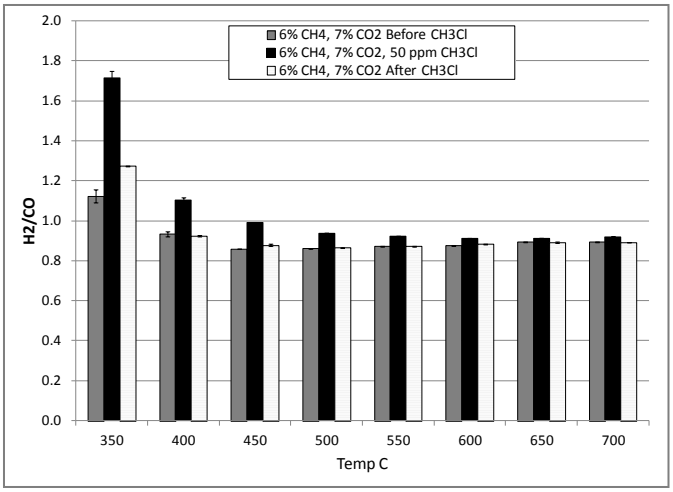

Figure 4.4: H_2/CO ratio as a function of temperature before, during, and after 50ppm CH_3Cl introduction into a feed of 6% CH_4 and 7% CO_2 in a balance of N_2 over a 4% Rh/γAl2O3 powder catalyst

In addition to 50ppm CH_3Cl, 25ppm and 10ppm concentrations of CH_3Cl were tested for their effect on the dry reforming reaction. As expected, the lower the CH_3Cl concentration, the lesser the effect on methane conversion and change in product selectivity, shown in the following two figures. Figure 4.5 shows the effect of a one hour pulse of 10ppm CH_3Cl on the product species. During the hour-long CH_3Cl pulse, CH_4 decreased by 12 μmoles/min, indicating an increase in CH_4 conversion, but the effect was barely statistically significant. CO_2 increased by 20 μmoles/min, H_2 increased by 12 μmoles/min, CO decreased by 9 μmoles/min and H_2O decreased by 6 μmoles/min. The CH_3Cl conversion was 59%.

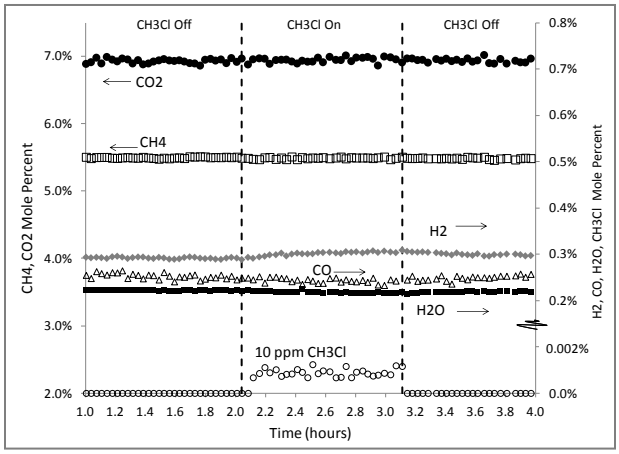

Figure 4.5: The effect of 10ppm CH_3Cl exposure for 1 hour at 400°C in a feed of 6% CH_4 and 7% CO_2 in a balance of N_2 on CH_4, CO_2, H_2, CO, H_2O, and CH_3Cl mole percent

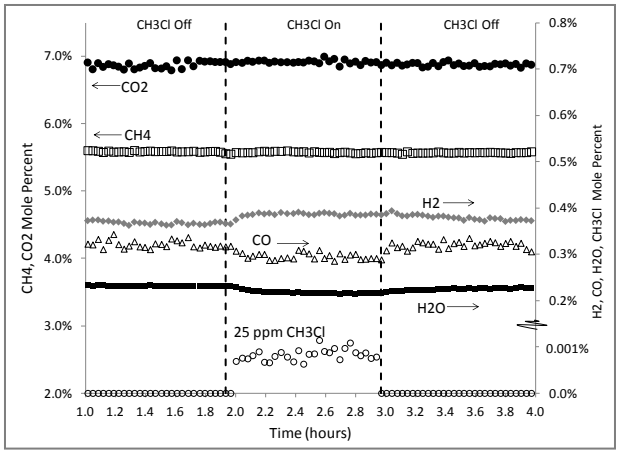

Figure 4.6: The effect of 25ppm CH_3Cl exposure for 1 hour at 400°C in a feed of 6% CH_4 and 7% CO_2 in a balance of N_2 on CH_4, CO_2, H_2, CO, H_2O, and CH_3Cl mole percent

Figure 4.6 shows the effect of a one hour pulse of 25ppm CH_3Cl on the product species. During the hour-long CH_3Cl pulse, CH_4 decreased by 20 µmoles/min (indicating an increase in CH_4 conversion), CO_2 decreased by 5 µmoles/min, H_2 increased by 17 µmoles/min, CO decreased by 25 µmoles/min and H_2O decreased by 15 µmoles/min. The CH_3Cl conversion was 64%. The results of the experiments shown in Figures 4.5 and 4.6 are summarized and compared to 50 ppm introduction of CH_3Cl in Figures 4.7 and 4.8. Figure 4.7 shows the CH_4 conversion before, during, and after the pulse of CH_3Cl for 1 hour. Figure 4.8 shows the H_2/CO ratio before, during, and after CH_3Cl introduction for 10, 25, and 50 ppm concentrations of CH_3Cl.

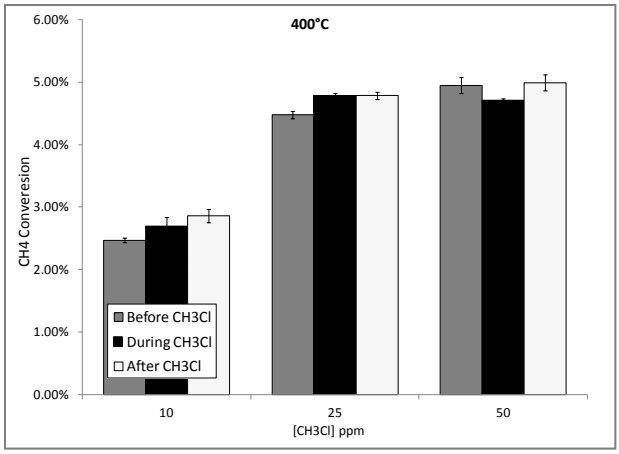

Figure 4.7: CH_4 conversion as a function of CH_3Cl concentration before, during, and after CH_3Cl introduction into a feed of 6% CH_4 and 7% CO_2 in a balance of N_2 over a 4% Rh/γAl2O3 powder catalyst at 400°C

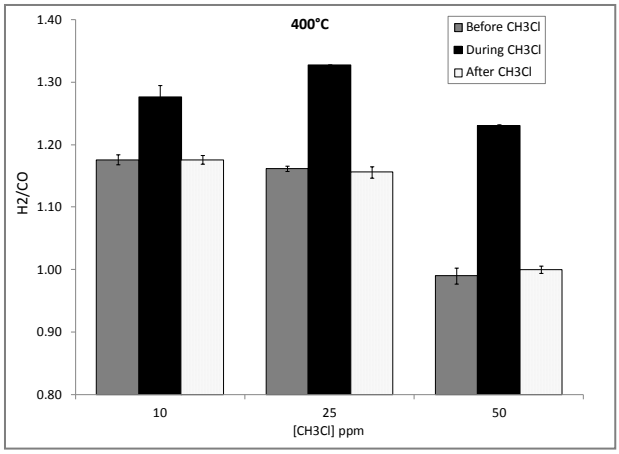

Figure 4.8: H_2/CO ratio as a function of CH_3Cl concentration before, during, and after CH_3Cl introduction into a feed of 6% CH_4 and 7% CO_2 in a balance of N_2 over a 4% Rh/γAl2O3 powder catalyst at 400°C

Figure 4.7 shows that at low concentrations of CH_3Cl, CH_3Cl introduction actually improves CH_4 conversion, while at 50 ppm, CH_3Cl introduction decreases CH_4 conversion. After CH_3Cl is removed, the CH_4 conversion returns to either the original value before CH_3Cl introduction or a value slightly higher, depending on the CH_3Cl concentration. These results suggest that low concentrations of CH_3Cl exposure may be beneficial for the activity of the dry reforming reaction. High concentrations of CH_3Cl however have a poisoning effect while it is on stream, but the effect is completely reversible. Figure 4.8 shows that as the CH_3Cl concentration increases, the change in H_2/CO ratio increases. The effect is reversible at each concentration of CH_3Cl exposure. These results indicate that the change in water-gas shift activity is directly related to the concentration of CH_3Cl exposure, and likely related to the degree of CH_3Cl or chloride deposition on the catalyst.

The effect of CH_3Cl concentration on CH_4 conversion was shown to be a repeatable effect. The effect was tested in two ways. In one method, a new catalyst bed was used for each one hour pulse of CH_3Cl. The result of these experiments were just discussed in the previous two figures.

In another method, the same powder bed was used for multiple CH_3Cl pulses. In both methods, the trend shown in Figures 4.5-4.8 was observed, with low concentrations of CH_3Cl slightly improving the activity of the dry reforming reaction, and high concentrations reversibly poisoning the activity of the dry reforming reaction. This may be related to the degree of hydrogen spillover, as proposed by Musso, that increases with small amounts of chlorination but decreases with larger amounts of chlorination. These results at 400°C are summarized in Figure 4.9, illustrating the change in CH_4 conversion as a result of CH_3Cl introduction on the primary y axis and the change in H_2/CO ratio as a result of CH_3Cl introduction on the secondary y axis, as a function of CH_3Cl concentration. As CH_3Cl concentration increases, the change in CH_4 conversion decreases, changing from an improvement of the dry reforming activity to a poisoning of the dry reforming activity at approximately 30ppm CH_3Cl. As CH_3Cl increases, the change in H_2/CO ratio increases linearly.

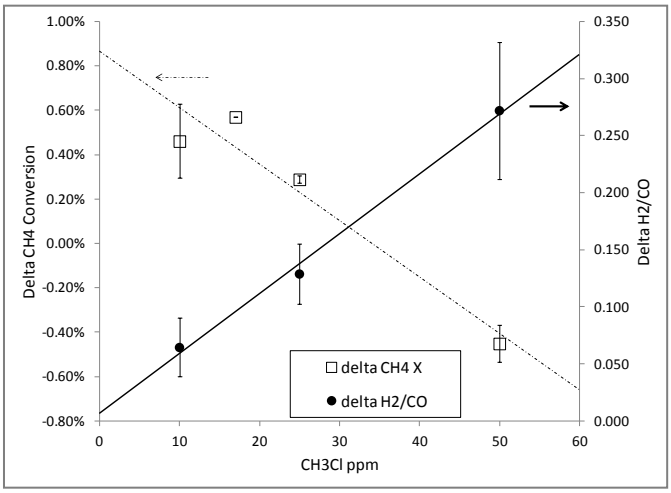

Figure 4.9: Change in CH_4 conversion and change in H_2/CO ratio as a function of CH_3Cl concentration before, during, and after CH_3Cl introduction into a feed of 6% CH_4 and 7% CO_2 in a balance of N_2 over a 4% Rh/γAl2O3 powder catalyst at 400°C

The linear change of H_2/CO ratio with CH_3Cl and the total reversibility of the change when CH_3Cl is removed strongly suggests that the change in H_2/CO ratio is a direct result of CH_3Cl or chloride deposition on the catalyst. The change in H_2/CO is most likely caused by a poisoning of

the reverse water-gas shift reaction, so the CH_3Cl or chloride deposition is likely inhibiting sites necessary for the reverse water-gas shift reaction.

The enhancement of the dry reforming activity at small amounts of CH_3Cl introduction may be explained by an enhancement of the hydrogen spillover effect which can increase CH_4 conversion. Enhancement of reforming activity as a result of chlorocarbon exposure has also been demonstrated for Pt/Al_2O_3 catalysts exposed to oxygen and chlorine in the oxy-chlorination process[89] for naphtha reforming. As discussed previously in the literature review, it is a common practice in naptha reforming to "rejuvenate" catalysts by exposing them to HCl or CCl_4 to redisperse the metal on the support, as well as to increase the acidity of the catalyst. This process produces volatile platinum oxychloride complexes that react with alumina hydroxyl groups to form smaller crystallites. The catalyst is then reduced in H_2 to remove the chloride associated with the platinum, while unaffecting the chloride associated with the alumina[89]. This process increases metal dispersion and therefore increases activity[108] of the naphtha reforming reaction. In the experiments discussed here the catalyst was not exposed to any oxygen, and in fact was exposed to a reducing atmosphere due to the H_2 produced from the dry reforming reaction. Therefore, it is unlikely that the same mechanism would result in a redispersion of rhodium, but perhaps there is another similar mechanism at work that results in the redispersion and increase of rhodium surface area. For example, perhaps the CO_2 and H_2O present have a local oxidizing effect, leading to a production of rhodium oxide species that are more mobile. In conclusion, the changes in dry reforming activity may be attributed to direct competition between CH_3Cl and CH_4 or a chlorination of the alumina support, as discussed previously, or an interaction of CH_3Cl with the rhodium metal, increasing dispersion or rhodium

availability. Both the change in H_2/CO ratio and the change in CH_4 conversion with CH_3Cl exposure will be discussed in more detail in subsequent sections in light of catalyst characterization results.

4.1.2 The Effect of HCl on Dry Reforming

Thus far two effects of CH_3Cl have been observed: a rapid, reversible change in the product selectivity attributed to a poisoning of the reverse water-gas shift reaction, and a slower reversible poisoning of the dry reforming reaction. The change in the reverse water-gas shift reaction is thought to be a result of CH_3Cl or chloride poisoning of the surface due to its rapidly reversible nature, while the change in the dry reforming reaction may be partly due to competition of CH_3Cl with CH_4 and partly due to support poisoning which decreases the activation of CO_2 on the support and affects the hydrogen mobility on the alumina. To attempt to separate these effects, HCl introduction at 50ppm was investigated at 400°C and 700°C, because HCl may deposit chloride but not compete with CH_4 for dry reforming sites in the same way as CH_3Cl. The effect of HCl at 50ppm on CH_4 conversion and H_2/CO ratio is shown in the following figures. Figure 4.10 shows the CH_4 conversion before, during, and after exposure to 50ppm HCl at 400°C and 700°C. Figure 4.11 shows the H_2/CO ratio of the products before, during, and after exposure to 50ppm HCl at 400°C and 700°C.

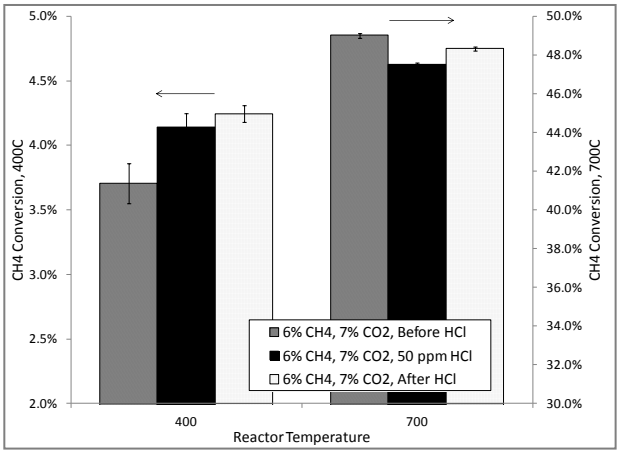

Figure 4.10: CH_4 conversion as a function of reactor temperature before, during, and after 50ppm HCl introduction into a feed of 6% CH_4 and 7% CO_2 in a balance of N_2 over a 4% Rh/γAl2O3 powder catalyst

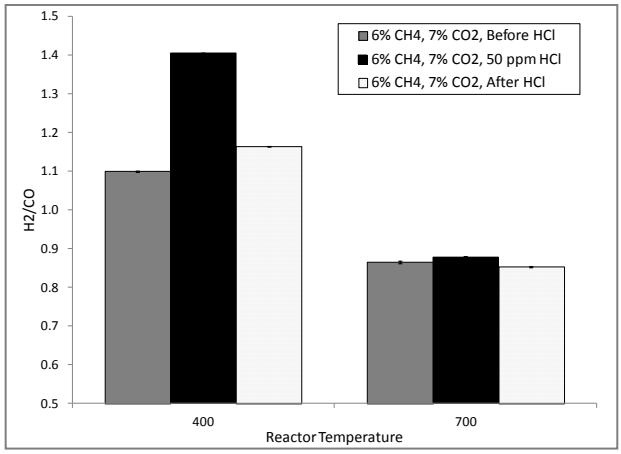

Figure 4.11: H_2/CO ratio as a function of reactor temperature before, during, and after 50ppm HCl introduction into a feed of 6% CH_4 and 7% CO_2 in a balance of N_2 over a 4% Rh/γAl2O3 powder catalyst

Figure 4.10 shows that the introduction of 50 ppm HCl increases CH_4 conversion at 400°C, and after the HCl is removed, the conversion remains high. This is similar to the effect of 10 or 25ppm CH_3Cl on CH_4 conversion. At 700°C, 50 ppm HCl decreases CH_4 conversion slightly while on stream, but the conversion returns after HCl is removed. In this case, the effect of HCl is similar to the effect of 50 ppm CH_3Cl at 700°C. The effect of 50 ppm HCl on H_2/CO ratio is the same as the effect of 50 ppm CH_3Cl at both 400°C and 700°C. HCl increases H_2/CO while it is on-stream, and the increase is greater at 400°C than at 700°C.

One working hypothesis was that HCl would affect the reverse water-gas shift reaction in a similar way as CH_3Cl, because both of these species would supply chloride species to the catalyst. This hypothesis is confirmed at both low and high temperatures, because the effect on H_2O, CO, H_2, and CO_2 concentrations is similar for both CH_3Cl and HCl at 50 ppm. For example, with 50 ppm CH_3Cl at 400°C, the increase in H_2/CO ratio ranged from 0.15 to 0.40. With 50 ppm HCl at 400°C, the increase in H_2/CO ratio is 0.30, in the same range as the CH_3Cl experiments. At 700°C with 50 ppm CH_3Cl, the increase in H_2/CO ratio ranged from no change

to 0.03 while with 50 ppm HCl the increase in H_2/CO ratio was 0.01, again in the same range as the CH_3Cl experiments. The HCl experiments also support the hypothesis that the species chlorinating the catalyst may not be CH_3Cl, but either a surface chloride or HCl, because the selectivity effect was the same for both CH_3Cl and HCl.

The other working hypothesis was that HCl would have less of an effect on the dry reforming activity loss because it would not compete directly with CH_4 for dry reforming metal sites. At 700°C the effect of 50 ppm HCl is very similar to the effect of 50 ppm CH_3Cl; with CH_3Cl, the net change in CH_4 conversion, from before CH_3Cl introduction to 1 hour after CH_3Cl removal, was a loss of 0.74%. With HCl, the net change in CH_4 conversion was a loss of 0.68%, slightly less than the CH_3Cl case, but the difference is not statistically significant. This does not support the hypothesis that HCl should have less of a poisoning effect because it does not compete with CH_4 for reforming sites. This, however, supports the idea that the primary cause of the changes seen in dry reforming activity are caused by chloride provided to the alumina support by either HCl or CH_3Cl, and not due to competition with CH_4 for metal reforming sites.

At 400°C with 50 ppm CH_3Cl, the change in CH_4 conversion from before CH_3Cl introduction to during the CH_3Cl 1 hour pulse, ranged between a loss of 0.24% to 0.69% CH_4 conversion. With HCl, the change was a gain of 0.20% CH_4 conversion. This is similar to the effect of small amounts of CH_3Cl, which at 10 ppm resulted in a gain of CH_4 conversion between 0.23% and 0.70%, and at 25 ppm resulted in a gain between 0.27% and 0.31% of CH_4 conversion. There are a number of explanations for this trend. One explanation could be that HCl does not interact with the surface as much as CH_3Cl and therefore deposits less chloride on the catalyst, causing a

change in CH_4 conversion similar to the smaller concentrations of CH_3Cl. However, the effect of HCl on the H_2/CO ratio is the same as the 50 ppm CH_3Cl experiments, which indicates that both CH_3Cl and HCl are depositing chloride in similar amounts to produce the same poisoning effect seen in the reverse water-gas shift activity.

Another explanation is that, as originally postulated, HCl does not compete with CH_4 for dry reforming sites so its introduction does not decrease the methane reforming activity. However, this alone does not explain why 50 ppm HCl and 10-25 ppm amounts of CH_3Cl increase the methane reforming activity. In the case of 10-25 ppm amounts of CH_3Cl the increase in CH_4 conversion was attributed to enhanced mobility of hydrogen on the alumina support due to small amounts of chloride deposition. However it is not definitive if this is the case for 50 ppm HCl because the effect of HCl on the H_2/CO ratio is the same as the 50 ppm CH_3Cl experiments. Another explanation could be a redispersion of the metal as a result of exposure to chlorinated species, as previously discussed in Chapter 4.1.1. This phenomenon could be occurring here, with HCl and CH_3Cl increasing metal dispersion which increases the dry reforming activity. Further characterization tests would be necessary to determine if exposure of the catalyst to HCl and CH_3Cl increase metal dispersion or availability. This will be discussed further in section 4.2.

In summary, the introduction of 50 ppm HCl suggested, at least at 700°C, that the changes in CH_4 conversion observed during the CH_3Cl experiments were primarily due to the deposition of chloride, not a competition between CH_3Cl and CH_4 for reforming sites. This is aligned with the fact that the conversion changes seen during dry reforming with CH_3Cl introduction were greater than what would have been expected assuming a 1:1 competition for sites between CH_4 and

CH_3Cl. The introduction of 50 ppm HCl at 400°C also showed, unexpectedly, that the CH_4 conversion improved, similar to the experiments with 10-25 ppm CH_3Cl introduction into the dry reforming feed. This may be due to an increase in hydrogen mobility, affinity of the support for CO_2, or higher rhodium dispersion caused by the interaction of HCl with the rhodium metal.

4.1.3 Catalyst Deactivation

The preceding discussion on the effect of temperature and reactant composition on the CH_4 reforming activity can be summarized in the following figure which shows the deactivation rate in %/hour as a function of temperature for either 50ppm CH_3Cl or HCl. The method for calculating the dry reforming deactivation rate was previously explained and illustrated in Equation 4.3. The results are shown in Figure 4.12. For ease of reading, the clusters of data points are slightly offset around the reaction temperature, although all of the experiments in a temperature cluster were performed at the same exact temperature indicated, either 400°C, 500°C, 600°C, or 700°C. A positive deactivation rate means that deactivation occurred, a negative deactivation rate means that the dry reforming activity improved.

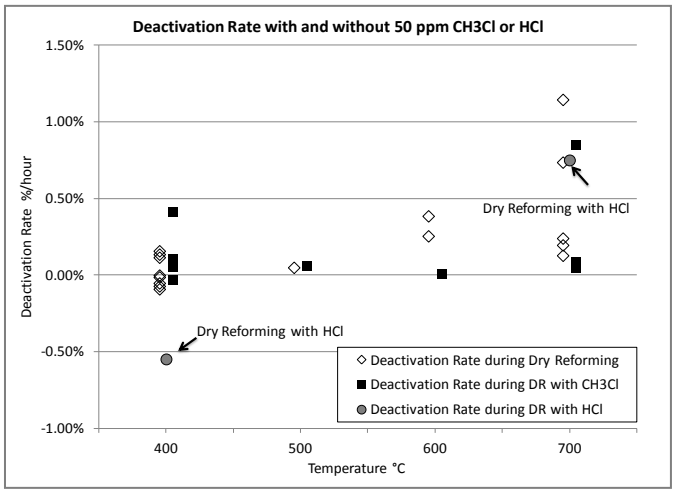

Figure 4.12:Dry reforming deactivation rate in %/hour as a function of temperature for a dry reforming feed of 6% CH_4, 7% CO_2 in a balance of N_2 alone or with 50ppm CH_3Cl or 50ppm HCl

The plot shows that as temperature increases, in general the deactivation rate of the catalyst during dry reforming increases. This is expected according to the discussion on dry reforming in Chapter 3, because deactivation due to carbon formation during dry reforming is more likely at high temperatures. The trend of deactivation rate during dry reforming with 50 ppm CH_3Cl is not as clear as with dry reforming alone because there are fewer data points at 500°C and 600°C, but it seems that in general deactivation rate also increases with temperature. At low temperatures, 400°C and 500°C, the dry reforming deactivation rate during CH_3Cl exposure seems to be in the same range or slightly higher than dry reforming without CH_3Cl. At high temperatures, 600°C and 700°C, the deactivation rate is on the low end of the range of deactivation rates for dry reforming alone. For the dry reforming case with 50 ppm HCl, at 400°C the deactivation rate is significantly lower than dry reforming with and without CH_3Cl, while at 700°C the deactivation rates are all in the same range. Therefore the rate of deactivation at high temperatures due to dry reforming alone overwhelms the impact of CH_3Cl or HCl. This is consistent with previous discussion in section 3.1 that dry reforming deactivation is likely to occur at high temperatures due to carbon formation, regardless of the presence of CH_3Cl or HCl.

In summary, at low temperatures (400°C), 50ppm CH_3Cl exposure increases the dry reforming deactivation rate, causing a decrease in CH_4 conversion, but the effect is completely reversible. This effect is likely due to chloride deposition on the catalyst as previously discussed. At high temperatures(700°C), 50ppm CH_3Cl exposure does not have a significant effect on the deactivation rate, either because CH_3Cl does not poison the surface to the same extent at high temperatures, or because the deactivation is caused by carbon formation which occurs irrespective of the CH_3Cl concentration. The fact that CH_3Cl does not poison the surface to the

same extent at high temperatures is confirmed by the changes in H_2/CO ratio which also decrease as the temperature increases. Therefore it is very likely that the effect of CH_3Cl is smaller at high temperatures.

4.1.4 The Effect of CH_3Cl on Auto-thermal Reforming

The effect of 50 ppm CH_3Cl on auto-thermal reforming at 400°C and 700°C was also investigated. The experimental method was the same, except that O_2 was also added to the feed. The Rh/γAl2O3 powder catalyst was first exposed to a mixture of 6% CH_4, 7% CO_2, and 2.5% O_2 in a balance of N_2 and the furnace was heated until reaction light-off occurred and the reactor temperature and conversion stabilized. The inlet temperature of the gases was maintained at either 400°C or 700°C depending on the experiment, but the combustion of the CH_4 in the reactor released heat that resulted in a slightly higher temperature in the catalyst bed that will be noted in each case. After temperature stabilization, the CH_3Cl was introduced for 1 hour. CH_3Cl was then removed and the test continued to run for at least 1 hour with the initial gas mixture. When CH_3Cl was introduced, the N_2 was reduced to maintain a constant flow rate. Product species were monitored throughout the experiment.

The effect of CH_3Cl on CH_4 conversion, syngas production and H_2/CO ratio are shown in Figures 4.13 and 4.14. At a gas preheat temperature of 400°C, the catalyst bed temperature rose to 460°C due to the exothermic combustion of CH_4. At a gas preheat temperature of 700°C, the catalyst bed temperature remained at 700°C because the increased rate of the endothermic reforming reactions negated the heat release from the exothermic oxidation reactions. Figure 4.13 shows that at a gas preheat temperature of 400°C the introduction of CH_3Cl decreased the CH_4 conversion by 0.32% and at 700°C the decrease due to CH_3Cl introduction was 0.09%.

This trend is similar to dry reforming; as temperature increases, the effect of CH_3Cl on CH_4 conversion decreases. After CH_3Cl is removed, the CH_4 conversion increases at both temperatures, at 400°C it increases by 1.38% and at 700°C by 0.60%. This is similar to the HCl introduction case at 400°C in which CH_4 conversion remained higher after HCl removal compared to before HCl introduction.

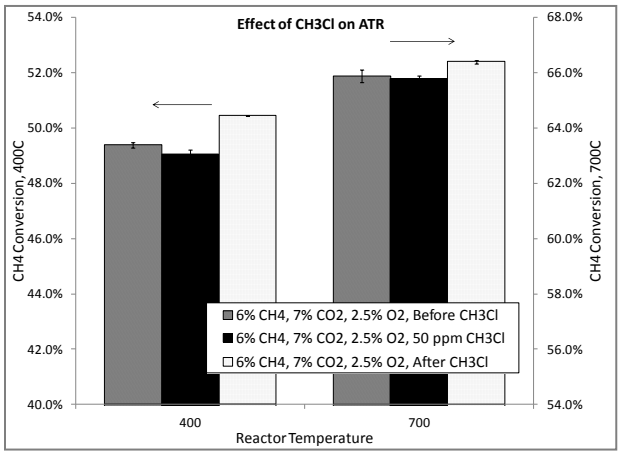

Figure 4.13: CH_4 conversion as a function of reactor temperature before, during, and after 50ppm CH_3Cl introduction into a feed of 6% CH_4, 7% CO_2, and 2.5% O_2 in a balance of N_2 over a 4% Rh/γAl2O3 powder catalyst

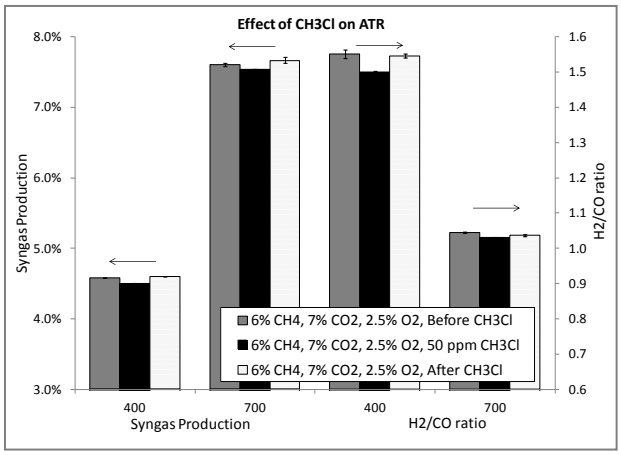

Figure 4.14: Syngas production and H_2/CO ratio as a function of reactor temperature before, during, and after 50ppm CH_3Cl introduction into a feed of 6% CH_4, 7% CO_2, and 2.5% O_2 in a balance of N_2 over a 4% Rh/γAl2O3 powder catalyst

The improvement in methane reforming activity could be due to an increase of hydrogen mobility and CH_4 conversion, or the oxy-chlorination effect previously discussed, which can increase catalyst dispersion. In this experiment, CH_3Cl and oxygen were present, which could have formed volatile rhodium particles in the same way that volatile platinum oxychloride complexes are formed during reaction with chlorocarbons an oxygen. This would lead to an increase of rhodium dispersion and an increase in dry reforming activity, even after CH_3Cl is removed. It is important to note that if the rhodium particles become volatile, this could result in a loss of rhodium metal and catalytic activity. No evidence of rhodium loss was observed, however, and so this theory requires further investigation.

The syngas production, shown in Figure 4.14, follows the trends shown in Figure 4.13. When CH_3Cl is introduced, at both temperatures the syngas production decreases, and when CH_3Cl is removed the syngas production returns to values slightly higher than before CH_3Cl introduction. The effect of CH_3Cl on H_2/CO ratio is very interesting in light of previous dry reforming results. In this case, CH_3Cl introduction decreases the H_2/CO ratio, by 0.05 at 400°C and by 0.01 at 700°C. This is the opposite effect observed with dry reforming. In addition, the absolute change is smaller compared to the dry reforming reactions, which caused an increase of the H_2/CO ratio by 0.17 at 400°C and by 0.03 at 700°C. One reason for this could be that in ATR the gas composition is different; there is much more H_2O, H_2, and CO in the products due to the combustion and partial oxidation of CH_4. To illustrate this, the following table shows species concentrations in mmoles/min (moles/min*10^3) for both ATR and dry reforming before, during, and after exposure to 50ppm CH_3Cl at 400°C. Table 4.2 shows that while dry reforming CH_4 and CO_2, the CH_4 conversion is lower resulting in less H_2, CO, and CO_2 while in ATR the CH_4 conversion is higher resulting in more H_2, CO, and H_2O. In the ATR case, CH_3Cl and O_2 conversion was 100%. The table also shows in more detail that when 50 ppm CH_3Cl is introduced in the ATR reaction, H_2 decreases, CO slightly increases, CO_2 decreases, and H_2O increases, which are changes consistent with a poisoning of the water-gas shift reaction, or a promotion of the reverse water-gas shift reaction. In dry reforming the changes are in the opposite direction, with what appears to be a poisoning of the reverse water-gas shift reaction.

Table 4.2: H_2, CH_4, CO, CO_2 and H_2O concentration in mmoles/min for both ATR and dry reforming before, during, and after exposure to 50ppm CH_3Cl on a 4% Rh/γAl2O3 powder catalyst at 400°C

Unit=mmoles/min	**Auto-thermal Reforming**					**Dry Reforming**				
Condition	H_2	CH_4	CO	CO_2	H_2O	H_2	CH_4	CO	CO_2	H_2O
Before CH_3Cl	2.68	2.39	1.73	5.45	1.91	0.41	5.21	0.42	6.39	0.22
Immediately After CH_3Cl	2.62	2.41	1.74	5.43	1.94	0.44	5.22	0.38	6.49	0.21
1 hour with CH_3Cl	2.60	2.39	1.74	5.39	1.94	0.41	5.23	0.33	6.52	0.20
1 hour after CH_3Cl removed	2.69	2.34	1.74	5.48	1.92	0.41	5.21	0.41	6.46	0.22

From the product species shown in Table 4.2, the reaction quotient, Q (Equation 4.5) and the equilibrium constant, K (Equation 4.6), can be calculated for the water-gas shift reaction (Equation 4.4) using the stoichiometry of the reaction and the following formulas.

Water-Gas Shift $H_2O + CO \leftrightarrow CO_2 + H_2$ ΔH=-42 kJ mol^{-1} *4.4*

$$Q, WGS = \frac{[H_2][CO_2]}{[H_2O][CO]} \quad 4.5 \qquad K, WGS = \frac{[H_2,eq][CO_2,eq]}{[H_2O,eq][CO,eq]} \quad 4.6$$

Q, the reaction quotient, is calculated using the product species in Table 4.2. K, the equilibrium constant, is calculated using equilibrium concentrations of H_2, CO_2, H_2O, and CO at the experiment temperature, i.e. 460°C for ATR and 400°C for dry reforming. The results of Q and K are presented in Table 4.3 along with the conclusion from Table 4.2 of which direction the water-gas shift reaction appears to be poisoned in each set of experiments.

Table 4.3: K and Q for both ATR and dry reforming before, during, and after exposure to 50ppm CH_3Cl on a 4% Rh/γAl2O3 powder catalyst

	ATR			**DR**		
Condition	K, WGS	Q, WGS	Reaction Poisoned	K, WGS	Q, WGS	Reaction Poisoned
Before 50ppm CH_3Cl	7.07	4.43	WGS	12.31	27.89	RWGS
After 1 hr 50ppm CH_3Cl	7.07	4.17		12.31	39.58	
After 50ppm CH_3Cl	7.07	4.42		12.31	29.05	

In general, Q is a measure of closeness to equilibrium. When Q is smaller than K, the reaction shifts to the right (assuming that as written the products of the reaction are on the numerator) and when Q is larger than K the reaction is shifting to the left. Because these experiments are operated in the kinetic regime, the flow rate is too fast for the gas concentrations to reach equilibrium, and so Q is not equal to K, even before CH_3Cl introduction. In the ATR case, Q is less than K meaning the water-gas shift reaction is shifting to the right, in the forward direction. In the dry reforming case, Q is greater than K meaning the reaction is shifting to the left, in the reverse water-gas shift direction. In the ATR case when CH_3Cl was introduced, Q decreased even further, moving farther away from K, meaning that the water-gas shift reaction moved farther away from equilibrium, suggesting that the forward water-gas shift reaction was poisoned. In the dry reforming case, Q increased when CH_3Cl was introduced, meaning that the reverse water-gas shift reaction moved farther from equilibrium and was therefore poisoned.

Therefore the direction in which the reaction is progressing is apparently poisoned by CH_3Cl. This was noted previously in CH_3Cl steam reforming experiments in which Q was much less than K, especially at lower temperatures, indicating that the forward water-gas shift reaction was poisoned[95]. This is evidence that CH_3Cl poisons a site necessary for the water-gas shift reaction in either direction. Characterization tests are used to further elucidate the mechanism of CH_3Cl poisoning.

4.2 Catalyst Characterization Results

To better understand the mechanism of CH_3Cl reforming on the Rh/γAl2O3 catalyst, XPS analysis, acidity and basicity characterization, CO chemisorption, TGA analysis, and BET surface area measurements were performed on a Rh/γAl2O3 powder catalyst that was exposed to either a dry

reforming mixture (6% CH_4, 7% CO_2, balance N_2) or a dry reforming mixture with CH_3Cl added (6% CH_4, 7% CO_2, 50ppm CH_3Cl, balance N_2) for 3 or 10 hours at either 400°C or 700°C, as shown in Table 4.4. During each segment, the effluent gas species were monitored. After the experiments, the samples were removed from the reactor for characterization.

Table 4.4: Experiment protocol for 4% Rh/γAl2O3 powder samples before characterization

Name	DR Conditions	[CH_3Cl]	Temp °C	Time
400°C 10hr	6% CH_4, 7% CO_2	0	400	10 hours
400°C w/Cl 10hr	6% CH_4, 7% CO_2	50ppm	400	10 hours
700°C 3hr	6% CH_4, 7% CO_2	0	700	3 hours
700°C w/Cl 3hr	6% CH_4, 7% CO_2	50ppm	700	3 hours
700°C 10hr	6% CH_4, 7% CO_2	0	700	10 hours
700°C w/Cl 10hr	6% CH_4, 7% CO_2	50ppm	700	10 hours

4.2.1 XPS

4.2.1.1 Binding Energy Assignments

X-ray photoelectron spectroscopy was used in an attempt to determine how and where CH_3Cl was decomposing on the catalyst. It was determined that the chlorinated species remaining on the catalyst was chloride, and important trends with temperature were observed, but whether the chloride was associated with rhodium or alumina remains ambiguous. Table 4.5 shows the orbital scans investigated and the peak binding energies determined for the elements shown, Al, Cl, O, and Rh in particular for each of the catalyst samples. Table 4.6 shows relevant known binding energies from the NIST XPS database[112] and literature[113, 114]. Finally, Table 4.7 shows the assignments given to the elemental scans using known binding energies and the surface composition of the catalyst sample in atom percent. Because there is some ambiguity in the Rh and chloride results, the binding energy assignments will be discussed in detail.

The Al2p and O1s orbital scan results were straight-forward. The peak binding energy for the Al2p orbital was in the range of 74.2-74.4 for all samples, corresponding to the Al_2O_3 state. The

O1s orbital peak binding energies were in the range of 531.2-531.4, also corresponding to the Al_2O_3 state.

There were two chemical species of rhodium present, referred to by subscripts "A" and "B." $Rh3d5,_A$ resulted in binding energy peaks in the range of 307.8-308.3, which according to Table 4.6 may correspond to reduced elemental rhodium, Rh, or to rhodium oxide, Rh_2O_3. In general the binding energies are more characteristic of Rh_2O_3, but the borderline cases, DR400C10hr WCl and DR700C10hr NoCl, are illustrated thusly in Table 4.7. The $Rh3d5,_B$ gave binding energy peaks in the range of 309.4-309.8 which may correspond to Rh_2O_3, Rh in a strong support interaction with the alumina, or rhodium chloride; $RhCl_3$. This ambiguity makes it difficult to determine in the chlorinated samples whether the Rh is associated with the chloride or only the aluminum oxide support. Again, the borderline cases, DR400C10hr WCl, DR700C3hr WCl, and DR700C10hr NoCl are shown in Table 4.7.

The Cl2p scan resulted in binding energy peaks ranging from 198.6 to 199.0. Many chlorides lie in this range of binding energy, such as NaCl, KCl, K_2PtCl_4, and $RhCl_3$. Even alumina chloride species can lie in this range of binding energies. Bennour et al treated thin films of alumina oxide with NaCl and found that Cl2p binding energies in the 198.4-198.6 range could be assigned to chloride ions bound to alumina in a hydroxide environment (near OH groups) and binding energies in the 199.1-199.5 range could be assigned to chloride ions bound to alumina in an oxide environment (less hydroxylation). Because binding energies for $RhCl_3$ and Al-Cl are so similar, it is difficult to make a definitive assignment.

Table 4.5: Peak binding energies determined for Al, C, Cl, O, and Rh for each of the catalyst samples

Binding Energy Table						
XPS Peak	DR 400C 10hr No Cl	DR 400C 10hr WCl	DR 700C 3hr No Cl	DR 700C 3hr WCl	DR 700C 10hr No Cl	DR 700C 10hr WCl
$Al2p_{,A}$	74.3	74.4	74.2	74.3	74.2	74.3
$C1s_{,A}$	284.7	284.8	284.6	284.8	284.7	284.8
$C1s_{,B}$	286.1	286.4	285.9	286.4	286.2	286.2
$C1s_{,C}$	288.4	288.8	288.2	288.4	288.4	288.4
$Cl2p_{,A}$	NA	199.0	NA	198.6	NA	198.7
$O1s_{,A}$	531.3	531.4	531.3	531.4	531.2	531.3
$Rh3d5_{,A}$	308.3	307.8	308.2	308.1	307.9	308.0
$Rh3d5_{,B}$	309.8	309.8	309.7	309.8	309.4	309.6

Table 4.6:Known binding energies from NIST database and literature values. References numbers refer to entries in the NIST database

Known Binding Energies from NIST and Literature				
	B.E. eV	Chemistry	Name	Reference
Rh3d5	307.3	Rh	Elemental Rh	29163
	308.2	Rh2O3	Rh oxide	28997
	308.7	Rh2O3	Rh oxide	28988
	308.9	Rh2O3	Rh oxide	28986
	309.4	Rh2O3	Rh oxide	28996
	309.6	Rh4(CO)12/AlOx	Rh-Aluminum oxide	2066
	309.6	Rh6(CO)16/AlOx	Rh-Aluminum oxide	2067
	310.1	RhCl3	Rh Chloride	28343
Cl2p	198.0, 198.4	Al-Cl	"Al hydroxi-chloride"	[114]
	198.3	Al-Cl	"stable Al-Cl complex"	[113]
	198.6	RhCl3	rhodium chloride	24119
	198.8	RhCl3	rhodium chloride	24121
	199.1	Al-Cl	"Al oxi-chloride"	[114]
	199.3	RhCl3	rhodium chloride	24117
Al2p	74.3	Al2O3	Aluminum Oxide	43499
O1s	531.3	Al2O3	Aluminum Oxide	22136

Table 4.7: Atom percent of surface species and assignments given using binding energies in Table 4.5 and 4.6

Surface Composition Table (Atom Percent)							
XPS Peak	Assignment	DR 400C 10hr No Cl	DR 400C 10hr WCl	DR 700C 3hr No Cl	DR 700C 3hr WCl	DR 700C 10hr No Cl	DR 700C 10hr WCl
$Al2p_{,A}$	Al2O3	36.34	36.46	34.98	35.51	35.96	35.76
$C1s_{,A}$	C_X	5.85	6.46	5.71	6.10	6.55	5.98
$C1s_{,B}$	C_X	2.01	1.38	2.54	1.43	2.00	1.37
$C1s_{,C}$	C_X	1.73	1.12	1.98	1.62	1.38	1.62
$Cl2p_{,A}$	X-Chloride	0.00	0.72	0.00	0.41	0.00	0.37
$O1s_{,A}$	Al_2O_3	53.50	53.07	54.18	54.30	53.43	54.19

$Rh3d5_{,A}$	Rh	0.00	0.17	0.00	0.00	0.33	0.00
	Rh_2O_3	0.10		0.23	0.30		0.35
$Rh3d5_{,B}$	Rh_2O_3	0.00	0.00	0.00	0.00	0.35	0.00
	Rh/AlO_X	0.57	0.61	0.37	0.33		0.37
	$RhCl_3$	0.00		0.00		0.00	0.00
Ratio	Rh/Al	0.018	0.021	0.017	0.018	0.019	0.020

4.2.1.2 Discussion

In order to gain more insight into the chemistry of rhodium and chloride on the catalyst samples, the binding energy assignments and atom percent table will be explored in more detail. There is a clear trend that more chloride is deposited on the surface, either on alumina or rhodium, at 400°C compared to 700°C. This is consistent with results from the flow through reactor that suggested that chloride poisoning decreases at higher temperatures. The chloride results also show that at the 700°C 3 hour and 10 hour samples, the surface chloride concentration was about the same, 0.41 to 0.37 atom %, respectively. This indicates that chloride deposition comes to equilibrium on the surface quickly and does not saturate over time. This is also consistent with flow through reactor results that show that the change due to CH_3Cl introduction, especially the change in water-gas shift activity, occurs rapidly.

When comparing the chlorinated samples to their respective non-chlorinated samples, if the chloride were binding to the rhodium, the Rh binding energy on the chlorinated samples would be slightly different. However, at 400°C, the $Rh3d5_{,B}$ binding energies are the same for the chlorinated and non chlorinated sample. It is this chemistry that would be assigned to either Rh_2O_3, Rh/AlO_X, or $RhCl_3$. At 700°C the binding energies for $Rh3d5_{,B}$ between the chlorinated and non-chlorinated samples are not identical, but are very close. Therefore the CH_3Cl does not cause a significant shift in the $Rh3d5_{,B}$ binding energies so it is unlikely that the chloride is associating strongly with the Rh. However, at 400°C, the $Rh3d5_{,A}$ binding energies, which

correspond to either elemental rhodium or Rh_2O_3 are different for the chlorinated and non chlorinated sample. This difference is greater at 400°C than at 700°C which may be correlated to the higher degree of chlorination at 400°C. This difference would correspond to a shift from oxidized rhodium to reduced rhodium with exposure to CH_3Cl at 400°C. While this may be a real effect, there is not enough data to indicate a trend.

The Cl2p binding energy at 400°C is higher than at 700°C. This could be an effect of temperature or degree of chlorination. According to one study, when chloride is associated with alumina, lower Cl2p binding energies correspond to chloride in a more hydroxylated environment, meaning there are more adjacent OH groups[114]. This would indicate that there are more hydroxyl groups at 700°C, meaning that the surface is more basic at 700°C compared to 400°C. This is consistent with acidity and basicity characterizations, discussed subsequently in Chapters 4.2.2 and 4.2.4, which show that a Rh/γAl2O3 catalyst exposed to a dry reforming feed either with or without CH_3Cl has a higher acidity and lower basicity at 400°C compared to 700°C.

Finally, the ratio of Rh/Al shown in Table 4.7, was calculated by dividing the atom percent of total rhodium species by the Al species. In every case, the Rh/Al ratio is higher for the sample exposed to CH_3Cl compared to the sample exposed to dry reforming alone. The difference is 0.003 at 400°C and 0.001 for both of the samples at 700°C. This difference could be correlated to the amount of chloride deposition. The changes in the Rh/Al ratios are relatively small, and therefore the result is on the border of significance, but it could suggest that exposure to CH_3Cl, or deposition of chloride, increases the surface area of rhodium. This would be consistent with

results from the flow-through reactor that showed that at 400°C with low concentrations of CH_3Cl or 50ppm HCl exposure during dry reforming, the CH_4 reforming activity actually improved. However this is not consistent with the fact that there is no evidence that chloride species are depositing on or interacting with the rhodium particles. In conclusion, more detailed characterizations, perhaps TEM, are necessary to observe the effect of chlorinated species on the size and availability of rhodium particles.

Despite the uncertainty resulting from the multiplicity of possible binding energy assignments, it is clear that chloride deposition decreases with increasing temperature. It seems unlikely that the chloride is bound to the rhodium because at 400°C, when chlorination is the highest, the $Rh3d5_{,B}$ binding energy that would correspond to either Rh_2O_3, Rh/AlO_X, or $RhCl_3$, is unaffected. Therefore the chemistry of the chloride on the surface is not definitive, but the XPS data combined with literature results suggest that the chloride is associated with the alumina and not the rhodium metal.

4.2.2 Acidity Characterization

The six Rh/γAl2O3 samples exposed to a dry reforming mixture with and without CH_3Cl for 3 or 10 hours at 400°C or 700°C, shown in Table 4.4, as well as un-reacted samples of Rh/γAl2O3 and γAl_2O_3, were tested for the sum of Lewis and Brönsted acidity by ammonia temperature programmed desorption. The alumina support contains a mixture of Lewis acid sites, Brönsted acid sites, basic oxygen anions, and hydroxyl groups than are usually basic but in some configurations can exhibit Brönsted acidity. For a thorough discussion of the sources of acidity on a Rh/Al_2O_3 surface, see Chapter 2.4.1. The number of acid sites is measured in mmol (mole*10^3) of NH_3 adsorbed at 20°C/gram of catalyst and the temperature at which the NH_3 is

desorbed is a measure of the strength of the acid site; higher NH_3 desorption temperatures indicate stronger acid sites. Both of these measures of acidity are considered here. Figure 4.15 shows the number of acid sites on un-reacted Rh/γAl2O3, γAl_2O_3, and the samples reacted for 10 hours. The Rh/γAl2O3 and the alumina sample were calcined at 725°C in air.

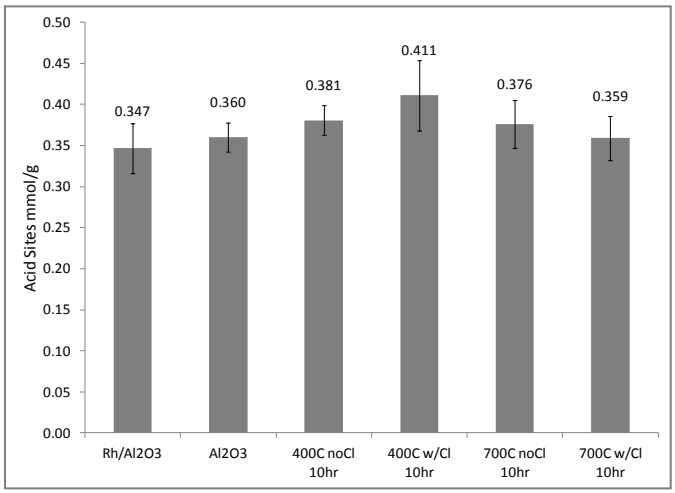

Figure 4.15: Acidity in mmole/g measured using NH_3 TPD of fresh and reacted 4% Rh/γAl2O3 powder samples

Figure 4.15 shows that γAl_2O_3 and Rh/γAl2O3 have approximately the same number of acid sites, with Rh/γAl2O3 slightly lower. This is because the acidity on a Rh/γAl2O3 catalyst results from the Lewis and Brönsted sites on the alumina surface. In the Rh/γAl2O3 catalyst the Rh displaces a portion of those acid sites and results in a slightly lower surface acidity. The number of Lewis + Brönsted acid sites on γAl_2O_3 determined with NH_3 adsorption in other studies ranges from 0.65 to 0.69 mmol/g [46, 83] and on 5% Rh/γAl2O3 the number of acid sites has been reported to be 0.47 mmol/g[84]. Therefore the result here that Rh/γAl2O3 has slightly fewer acid sites is generally consistent with literature, but the absolute values are less than reported in literature. This could result from the fact that NH_3 adsorption is calculated from the weight loss of the catalyst in the temperature range of 200-300°C when the rate of weight loss was the greatest, attributed to NH_3 removal from the catalyst. However, some NH_3 could be desorbing at a slower rate at lower and higher temperatures, and is not accounted for in this calculation.

Therefore the acidity measurements shown here could be considered relative values but perhaps not absolute values. Furthermore, the temperature peaks of NH_3 weight loss will also be discussed which provides more insight into the nature of the acid sites. For a detailed description of the data analysis routine, see the appendix section A.1.7.

According to Figure 4.15, there is little difference in the number of acid sites on the samples reacted at 400°C and 700°C, except for the case of 400°C reacted with CH_3Cl. This sample had a higher number of acid sites. At 700°C there was no statistical difference between the sample reacted with and without CH_3Cl. Therefore, the effect of CH_3Cl on the acidity of the support may be greater at low temperatures than high. This is consistent with flow-through reactor results that showed that the poisoning effect of CH_3Cl on reverse water-gas shift activity was highest at low temperatures, and the XPS result that chloride deposition is higher at 400°C than at 700°C. In addition to the loss of acid sites, CH_3Cl exposure also affects the strength of those acid sites present, presented in Figure 4.16.

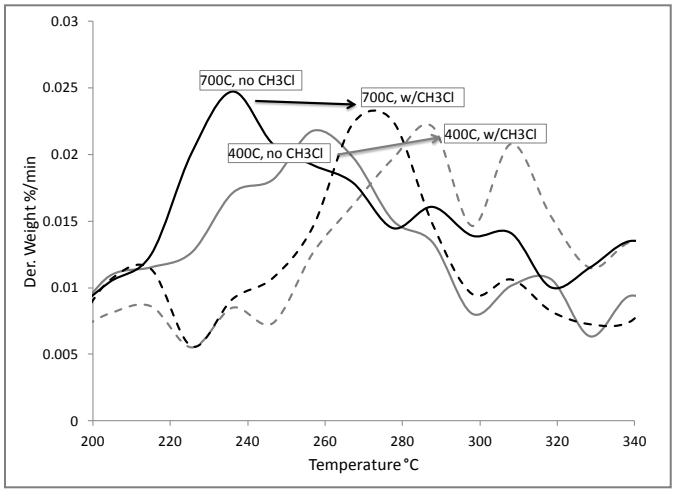

Figure 4.16: Absolute value of the derivative of weight change of Rh/γAl2O3 catalyst samples in %/min during NH_3 desorption step

Figure 4.16 shows the absolute value of the derivative of the weight change of the catalyst during NH_3 desorption as a function of temperature. The peaks shown in the figure indicate the temperature of the highest rate of NH_3 desorption. NH_3 that was desorbed at a higher temperature was likely associated with stronger acid sites on the catalyst. Therefore according to this plot, at the same reaction temperature, exposure to CH_3Cl increases the strength of acid sites on the catalyst. Furthermore, at the same degree of CH_3Cl exposure, samples reacted at 400°C have slightly stronger acid sites than samples reacted at 700°C.

The NH_3 desorption temperature peak data for all six samples is condensed into the following bar graph, Figure 4.17, for ease of reading. The most obvious result is that the samples reacted with CH_3Cl exhibit higher acid strength than those used in dry reforming alone. The acid strength for the samples reacted at 700°C without CH_3Cl for 3 and 10 hours have the same acid strength, because in both cases the maximum NH_3 desorption rate occurred at 236°C, indicating that acid strength does not change over time during dry reforming alone. However the acid strength for the samples reacted at 700°C with CH_3Cl does increase over time. For the sample reacted with CH_3Cl at 700°C for 3 hours the NH_3 desorbed at 257°C while for the sample reacted with CH_3Cl at 700°C for 10 hours the NH_3 desorbed at 277°C, suggesting that chlorination of the sample may increase with time. This is not consistent with flow through reactor and XPS results that indicate that chloride deposits and is removed rapidly. Finally, for both reaction with and without CH_3Cl, the sample at 400°C exhibited higher acidity than those reacted at 700°C.

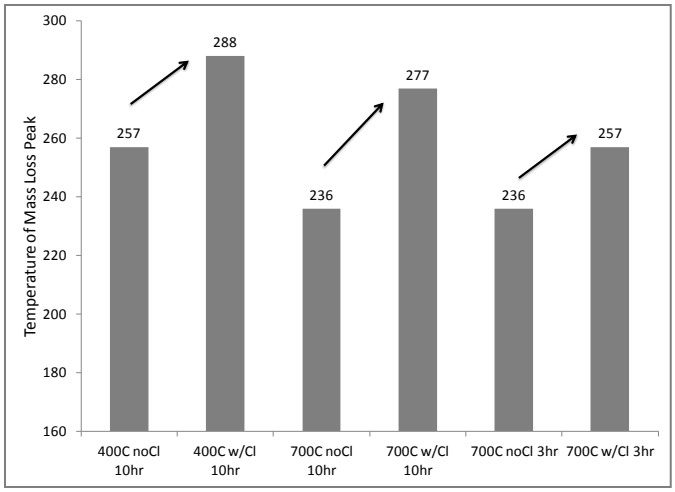

Figure 4.17: Temperature at maximum rate of weight loss of Rh/γAl2O3 catalyst samples during NH_3 desorption step

The result that irrespective of CH_3Cl exposure, samples reacted at 400°C have a higher acid strength than samples reacted at 700°C is consistent with literature and the reaction conditions of these samples. Both samples were previously used for the dry reforming of a 1:1 CH_4:CO_2 mixture, which also resulted in some H_2O production from the reverse water-gas shift reaction. The reverse water-gas shift reaction is endothermic and is therefore favored at higher temperatures. Therefore the sample produced at 700°C was exposed to more H_2O than the one produced at 400°C. As discussed previously, the alumina surface contains Lewis and Brönsted acid sites, and basic hydroxyl sites. In the presence of H_2O, some Lewis acid sites react to form Brönsted acid base pairs, which are more weakly acidic. Therefore it is likely that the sample produced at 400°C has a higher proportion of Lewis acid sites to Brönsted sites, and therefore the overall acidity is higher. The sample produced at 700°C with a greater H_2O concentration likely has a higher proportion of weaker Brönsted acid sites to Lewis acid sites, and therefore a lower overall acidity.

The result that exposure to CH_3Cl increases acid strength of the catalyst acid sites is completely consistent with literature. XPS results showed that exposure to CH_3Cl leaves chloride on the surface, likely on the alumina. Chlorination of alumina replaces basic surface hydroxyl groups and polarizes the O-H bonds of the remaining hydroxyl groups, leading to higher Brönsted acidity. This is one reason why the naphtha reforming process exposes the catalyst to HCl or CCl_4; because the chloride increases the acidity of the catalyst which maintains the activity of the isomerization reactions. The increase in acid strength with CH_3Cl is highest for the sample reacted at 700°C for 10 hours, followed by the sample reacted at 400°C for 10 hours. This is contrary to the results in Figure 4.15 showing that the effect of CH_3Cl on number of acid sites is highest at 400°C. However, it is clear that CH_3Cl increases the strength of acid sites at both 400°C and 700°C, but only at 400°C the number of acid sites is significantly affected.

In summary, the acidity characterization revealed that catalyst samples exposed to CH_3Cl at both 400°C and 700°C had an increase in the strength of acid sites, and at 400°C the number of acid sites also increased. Because stronger acid sites can be correlated to more hydrogen mobility on the surface[88], increased acidity may improve CH_4 reforming activity, and supports that explanation for the improved dry reforming activity seen with small concentrations of CH_3Cl and 50ppm concentration of HCl.

4.2.3 CO Chemisorption

The six Rh/γAl2O3 samples exposed to a dry reforming mixture with and without CH_3Cl for 3 or 10 hours at 400°C or 700°C as well as un-reacted samples of Rh/γAl2O3 were tested for dispersion, or available Rh metal area, by CO chemisorption. It is assumed that CO chemisorbs

to Rh, and not significantly to Al_2O_3, at a 1:1 mole ratio, and is therefore a measure of the available metal area.

Dispersion is calculated using the following formulae (Equations 4.7-4.11):

$$Dispersion = \frac{moles\ Rh\ on\ surface}{total\ moles\ Rh\ in\ catalyst\ sample} \quad 4.7$$

$$Moles\ Rh\ on\ surface = moles\ CO\ adsorbed = \frac{mass\ CO\ adsorbed\ (g)}{MW\ CO\ (\frac{g}{mole})} \quad 4.8$$

$$mass\ CO\ adsorbed(g) = catalyst\ weight\ gain\ during\ CO\ adsorption\ step\ (g) \quad 4.9$$

$$Total\ moles\ Rh\ in\ catalyst\ sample = \frac{Total\ weight\ Rh\ in\ catalyst\ sample\ (g)}{MW\ Rh\ (\frac{g}{mole})} \quad 4.10$$

$$Total\ weight\ Rh\ in\ catalyst\ sample\ (g) = \%\ Rh\ in\ Al_2O_3\ * Weight\ catalyst\ sample\ (g) \quad 4.11$$

Figure 4.18 shows the results of the CO chemisorption experiments and calculations for each catalyst sample. The dispersion of un-reacted 4% Rh/γAl2O3 is 40%, which is in the same range as other reported dispersions of precious metals on alumina catalysts[13]. All of the reacted samples had a lower dispersion than the un-reacted Rh/γAl2O3 (all calcined at 725°C in air), indicating that reaction decreases the available metal area. This could occur by sintering or site blocking by deposited compounds such as carbon. Extensive sintering is unlikely because the catalyst has already been calcined at 725°C in air, but some sintering may still occur in the reaction environment. Site blocking could occur by carbon deposition. If carbon deposition were occurring, one would expect the dispersion of the catalyst used for dry reforming at 700°C would be less than that at 400°C, because carbon deposition is favored at higher temperatures. However this trend is not seen. In fact, for the sample used for dry reforming at 700°C for 10 hours, the dispersion is slightly higher than the samples used for 400°C for 10 hours and 700°C for 3 hours. This effect is barely significant, but it does suggest that extensive carbon deposition

does not occur on the samples used for dry reforming at either 400°C or 700°C within 10 hours of reaction time.

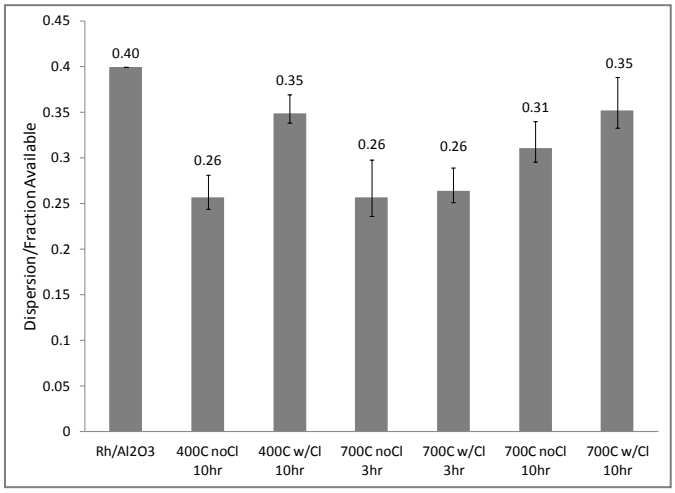

Figure 4.18: Dispersion fraction measured using CO chemisorption of fresh and reacted 4% Rh/γAl2O3 powder samples

The sample reacted at 400°C with exposure to CH_3Cl had a significantly higher Rh dispersion than the samples used for dry reforming alone at 400°C. The samples reacted at 700°C for 3 hours with and without CH_3Cl have approximately the same amount of dispersion. The sample reacted at 700°C for 10 hours with exposure to CH_3Cl had a slightly higher dispersion than one reacted at 700°C for 10 hours for dry reforming alone.

These results indicate that CH_3Cl may have a positive effect on rhodium dispersion. This effect is higher at 400°C than at 700°C, and at 700°C increasing reaction time increases the effect of CH_3Cl on dispersion. This effect of CH_3Cl on dispersion and the impact of temperature was also shown in the XPS results. In the XPS results, the samples exposed to CH_3Cl had higher Rh/Al ratios than those not exposed to CH_3Cl, and the impact of CH_3Cl was most pronounced at 400°C compared to 700°C. However, the chloride deposition may also change the interaction of CO with the surface which may artificially alter dispersion values. There may be a real trend that the

introduction of CH_3Cl to a dry reforming feed increases the available area of the rhodium. In the absence of other poisoning or promotion effects, this should cause an increase in dry reforming activity. To confirm this, however, further spectroscopic techniques such as TEM should be conducted to confirm the effect of CH_3Cl on rhodium particle size and surface area.

4.2.4 Basicity Characterization

The six Rh/γAl2O3 samples exposed to a dry reforming mixture with and without CH_3Cl for 3 or 10 hours at 400°C or 700°C as well as un-reacted samples of Rh/γAl2O3 and γAl_2O_3, were tested for basic sites by CO_2 adsorption. Because CO_2 is an acidic molecule the amount that irreversibly adsorbs to a sample at low temperature after CO_2 is removed from the gas phase is a measure of the amount of basic sites. On the alumina surface, CO_2 primarily adsorbs to surface hydroxyl groups to form bicarbonate[46, 115] but can also react with basic oxygen anions [115]. However CO_2, also adsorbs on the Rh metal at room temperature[116] and so the values obtained for basicity should be corrected for Rh dispersion.

The amount of CO_2 adsorbed to the catalyst in mmol/g was calculated using Equation 4.12.

$$CO_2 adsorbed\ \left(\frac{mmole}{g}\right) = \frac{CO_2\ mass\ adsorbed\ (g)}{MW\ CO_2\left(\frac{g}{mole}\right) * Catalyst\ mass\ (g)} * 1000 \qquad 4.12$$

The results of this calculation are shown in Figure 4.19. The specific CO_2 adsorption is much higher on the Rh/γAl2O3 sample compared to the Al_2O_3 sample due to the additional CO_2 adsorption on the rhodium. To calculate the amount of CO_2 adsorbed on the Al_2O_3 alone, this additional CO_2 adsorbed to rhodium must be subtracted from the Rh/γAl2O3 samples. As shown in the CO chemisorption section, the available rhodium metal area varies on each sample.

Therefore the different amounts of CO_2 adsorption based on the different catalyst dispersions must be accounted for.

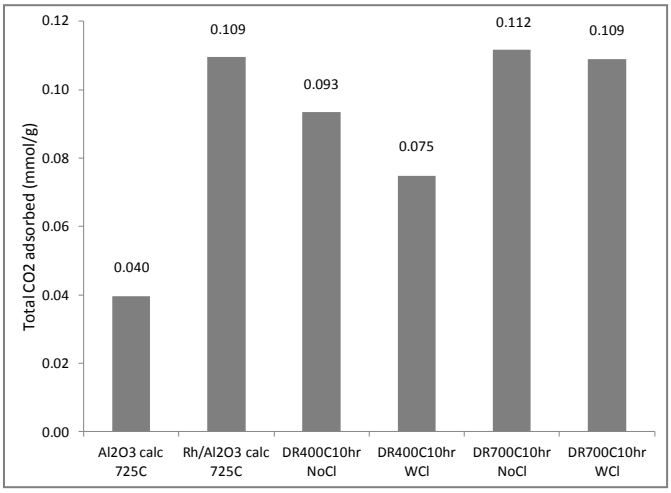

Figure 4.19: CO_2 adsorption in mmol/g measured using CO_2 chemisorption of fresh and reacted 4% Rh/γAl2O3 powder samples, not corrected for dispersion

The formulae (Equations 4.13 and 4.14) used to correct for CO_2 adsorption on rhodium are:

$$Rh\ CO_2 adsorption(g, unreacted\ sample) = \frac{Rh}{Al_2O_3} CO_2 adsorption(g, unreacted\ sample) - Al_2O_3\ CO_2 adsorption(g) \quad 4.13$$

$$\frac{Dispersion\ of\ Reacted\ Catalylst\ Sample}{Dispersion\ of\ Unreacted\ Rh/Al_2O_3} * Rh\ CO_2 adsorption(g, unreacted\ sample) = Al_2O_3\ CO_2 adsorption(g, reacted\ sample) \quad 4.14$$

The corrected values for basicity in mmol/g are shown in Figure 4.20. The unreacted Al_2O_3 and reacted Rh/γAl2O3 have approximately the same number of basic sites because that was the condition set in the correction calculations, 0.04 mmol/g. In other published work the amount of basic sites on γAl_2O_3 has been measured using CO_2 adsorption and found to be in the range of 0.09-0.21 mmol/g[46]. The values obtained here are lower than this range, and should be understood as relative values of catalyst basicity. The Rh/γAl2O3 sample used for dry reforming

at 700°C developed more basicity than the sample used for dry reforming at 400°C. The Rh/γAl2O3 sample used for dry reforming at 400°C with CH_3Cl had much less basicity than the same sample without CH_3Cl exposure. The sample reacted at 700°C with CH_3Cl also had fewer basic sites than the sample reacted without CH_3Cl.

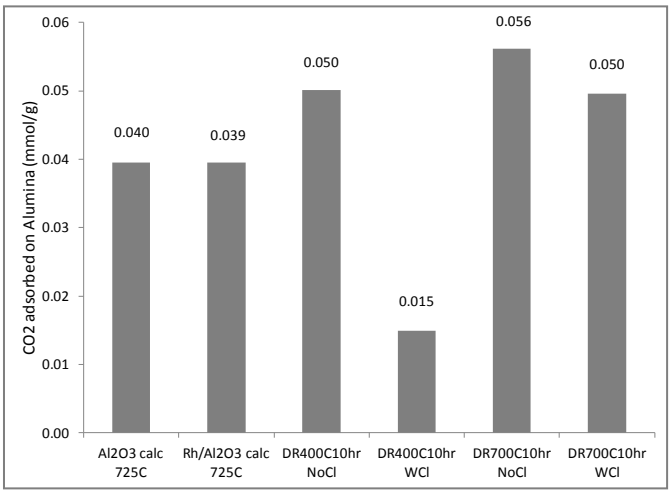

Figure 4.20: CO_2 adsorption in mmol/g on alumina support measured using CO_2 chemisorption of fresh and reacted 4% Rh/γAl2O3 powder samples, corrected for dispersion

This basicity data is consistent with the acidity data. The acidity data showed that for the dry reformed samples without CH_3Cl, those reacted at 700°C had lower acidity than those reacted at 400°C. The basicity result shows that the sample reacted at 700°C has more basicity than the one reacted at 400°C. The acidity data also showed that CH_3Cl increased the acidity of the catalyst samples at both 400°C and 700°C, with a greater effect in the number of acid sites at 400°C. The basicity data shows that exposure to CH_3Cl decreases the basicity of the catalyst sample at both 400°C and 700°C, but especially at 400°C.

The basicity result is another confirmation that CH_3Cl exposure increases the acidity, or decreases the basicity, of the Rh/γAl2O3. It is also another confirmation that the chloride replaces basic

hydroxyl groups on the alumina surface, as suggested by many previous studies on the chlorination of alumina[81, 85-88], which therefore increases the surface acidity.

4.2.5 Dry Reforming with CH_3Cl in TGA

TGA experiments were performed to measure the weight change of the 4% Rh/γAl2O3 catalyst as a result of a CH_3Cl pulse. These pulse tests were conducted by exposing the 4% Rh/γAl2O3 catalyst to the dry reforming mixture (6% CH_4, 7% CO_2, balance N_2) and heating to the desired reaction temperature. This experiment was performed at 400°C, 500°C, 600°C, and 700°C. Once the weight stabilized, 200 ppm of CH_3Cl was pulsed on for 15 minutes and then turned off. This resulted in a weight gain, interpreted as chloride adsorbing on the catalyst, which varied with temperature. After the pulse, there was a slight weight loss that varied with temperature. The weight gained and lost as a result of CH_3Cl adsorption and the calculation of the net weight gain is shown in Figure 4.22 and 4.23 as a function of temperature. A schematic of this experiment is shown in Figure 4.21.

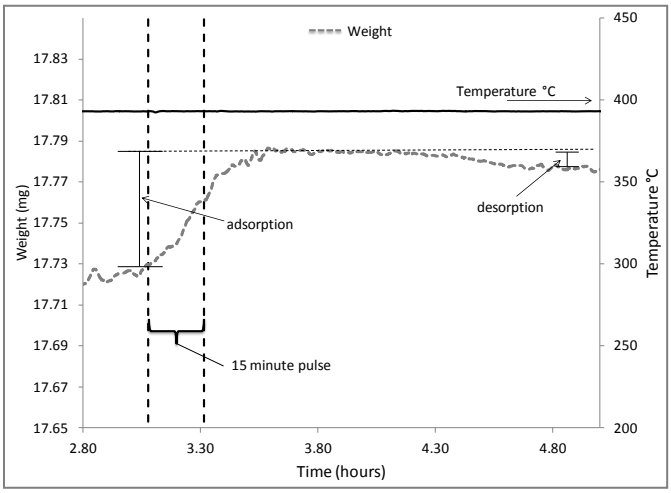

Figure 4.21: Typical TGA CH3Cl pulse experiment to observe adsorption and desorption on catalyst

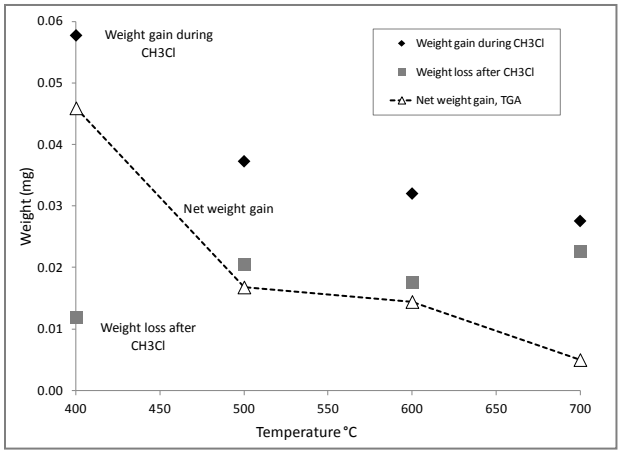

Figure 4.22: Rh/γAl2O3 powder catalyst weight in mg as a function of temperature during and after 200ppm CH_3Cl exposure in a feed of 6% CH_4, 7% CO_2, balance N_2

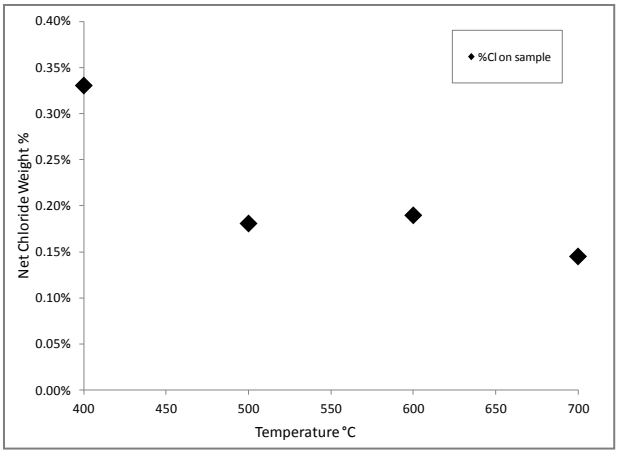

Figure 4.23: Net chloride weight % on the Rh/γAl2O3 powder catalyst as a function of temperature after 200ppm CH_3Cl exposure in a feed of 6% CH_4, 7% CO_2, balance N_2, calculated from net weight gain in Figure 4.22

Figure 4.22 shows the weight of the catalyst (mg) as a function of temperature during and after CH_3Cl exposure. As temperature increased, the weight gain of the catalyst during the CH_3Cl pulse decreased and after the CH_3Cl was turned off the weight increased. Therefore the net weight gain of the catalyst decreased, almost reaching zero for 700°C. In light of the XPS tests, the species that absorbs causing a weight gain is likely chloride, and XPS tests concur with this TGA result that chloride deposition is higher at lower temperatures. Carbon deposition may also cause a weight gain on the catalyst surface, but carbon deposition is not expected thermodynamically at these conditions. Therefore it is assumed that the depositing species is chloride and not carbon. Figure 4.23 shows the calculation of chloride weight percent deposited on the catalyst after the CH_3Cl exposure using the net weight gain presented in Figure 4.22. The trend of chloride adsorption seen in both the XPS results and the TGA results agree; chloride deposition decreases at higher temperatures. However they are not directly comparable because the XPS results were produced on samples exposed to 50ppm CH_3Cl in a flow-through reactor, while Figures 4.22 and 4.23 were produced in a TGA using 200ppm CH_3Cl. The flow-through

reactor has a much higher mass transport rate than the TGA due to the higher flow rate and geometry of the reactor that allows for better contact between the gas phase and the solid catalyst. Therefore while the trend in chloride deposition observed in the TGA is valuable, it cannot be quantifiably compared to the chloride weight percent measuring using XPS for flow-through reactor samples.

4.2.6 BET Surface Area Measurements

The six Rh/γAl2O3 samples exposed to a dry reforming mixture with and without CH_3Cl for 3 or 10 hours at 400°C or 700°C, as well as un-reacted samples of Rh/γAl2O3 and γAl_2O_3, were tested for BET surface area. BET measurements of these samples are shown in Figure 4.24.

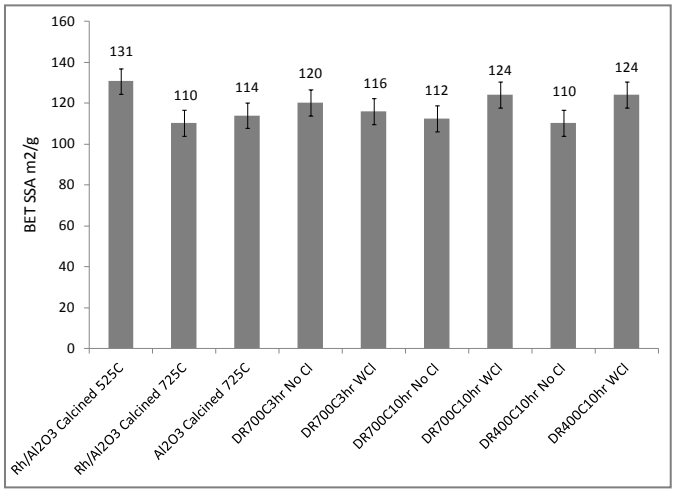

Figure 4.24: BET specific surface area in m^2/g of fresh and reacted 4% Rh/γAl2O3 powder samples and an A_2O_3 sample

Rh/γAl2O3 calcined at 725°C has less surface area than Rh/γAl2O3 calcined at 525°C due to support sintering. All of the γAl_2O_3 and Rh/γAl2O3, whether reacted or un-reacted, had the same surface area within the margin of error. This indicates that undergoing reaction over time or exposure to CH_3Cl did not significantly affect the surface area of the catalyst sample, and therefore sintering or pore blocking during reaction is not a likely deactivation mechanism.

Chapter 5 : Models and Mechanism

5.1 Alumina Chlorination Model

As previously mentioned in the literature review in Chapter 2.4, models have been developed on γAl_2O_3 and $Pt/\gamma Al_2O_3$ to understand the relationship between gas phase chlorine, in the form of HCl, and the degree of chlorination of the alumina surface. Castro et al.'s model [85, 87] assumes that chlorination occurs by the net reaction shown in Figure 5.1.

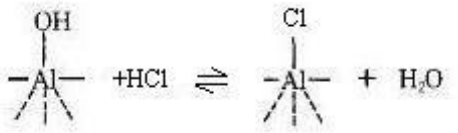

Figure 5.1: Alumina chlorination reaction

The expression for the chloride equilibrium concentration on the alumina surface is presented in Equation 5.1 [85, 87].

$$[Cl^*] = \frac{KL(1/R)}{1+K(1/R)} \qquad 5.1$$

Before HCl is introduced, L is only the number of hydroxyl groups, and can be thought of as the chloride retention capacity. Both K and L are only a function of temperature. The values of K and L were determined by experiment by Castro et al using various mixtures of H_2O and HCl on γAl_2O_3 a $Pt/\gamma Al_2O_3$ catalyst[87]. This model was proven to be valid for both Al_2O_3 and $0.38\%Pt/\gamma Al_2O_3$ catalysts because the amount of chloride associated with metal after a reduction step using H_2 was zero. Therefore H_2 is reactive toward surface chloride, removing it as HCl, but H_2O is needed to remove the chloride from the alumina surface. This means that the chlorination of the alumina is only a function of the temperature and the H_2O/HCl ratio.

This model was applied to various flow-through reactor conditions discussed previously in section 4.1 to assess the validity of the model on the 4% Rh/γAl2O3 catalyst. Experimental results presented in section 4.1.1 showed that as temperature increased, the effect of CH_3Cl on the change in product selectivity decreased. This change in selectivity in the dry reforming experiments was due to a poisoning of the reverse water-gas shift reaction, and can be represented by a change in the H_2/CO ratio of the products. Figure 5.2 shows experimental data on the effect of temperature on the change in H_2/CO ratio for the case of 50 ppm CH_3Cl introduction on the primary y axis. On the secondary y axis the figure shows the equilibrium constant of the reaction shown in Figure 5.1 as a function of temperature.

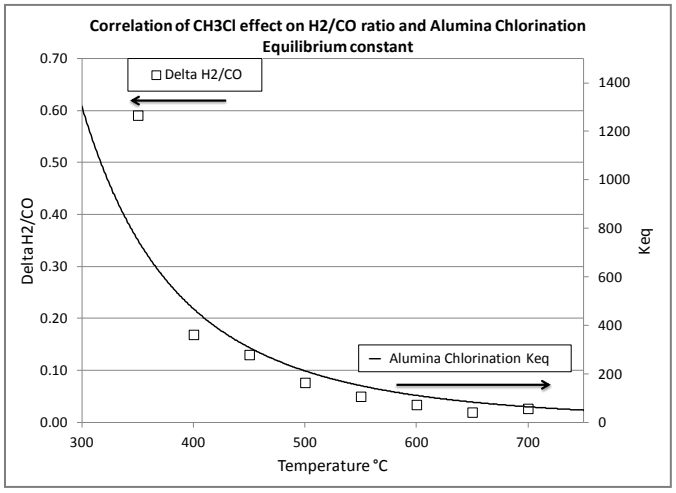

Figure 5.2: Change in H_2/CO ratio as a function of temperature as a result of 50ppm CH_3Cl exposure in a feed of 5% CH_4 and 6% CO_2 in a balance of N_2. Keq, equilibrium constant of alumina chlorination reaction, as a function of temperature calculated using Castro model

As temperature increases, the equilibrium constant decreases, resulting in more alumina hydroxyl groups and gas phase HCl, as opposed to chlorinated alumina and H_2O. In other words, at high temperatures, the chlorination of the alumina support is not favored. Because chlorination replaces alumina hydroxyl groups that are responsible for the activity of both the

forward and reverse water-gas shift reaction as discussed in section 2.3, less chlorination will result in less reverse water-gas shift poisoning, and therefore a smaller change in the H_2/CO ratio when CH_3Cl is introduced into the dry reforming feed. This provides an explanation for why the change in product selectivity, illustrated by the H_2/CO ratio, decreases as temperature increases. The correlation between the change in H_2/CO ratio and the equilibrium constant of the alumina chlorination reaction (Figure 5.1) is excellent, suggesting that this model predicts the chlorination trend as a function of temperature well for the Rh/γAl2O3 catalyst.

The model can also be used to calculate the weight percent of chloride on the alumina surface as a function of HCl, H_2O, and temperature. Assuming CH_3Cl is converted to HCl on the catalyst, or deposits chloride in the same way as HCl on the alumina surface, chloride weight percent for various concentrations of CH_3Cl can be calculated and correlated to the poisoning of the Rh/γAl2O3 catalyst. Figure 5.3 shows the change in H_2/CO ratio due to CH_3Cl introduction at various concentrations from experimental data. The secondary y axis shows the chloride weight percent on the alumina as calculated by the model.

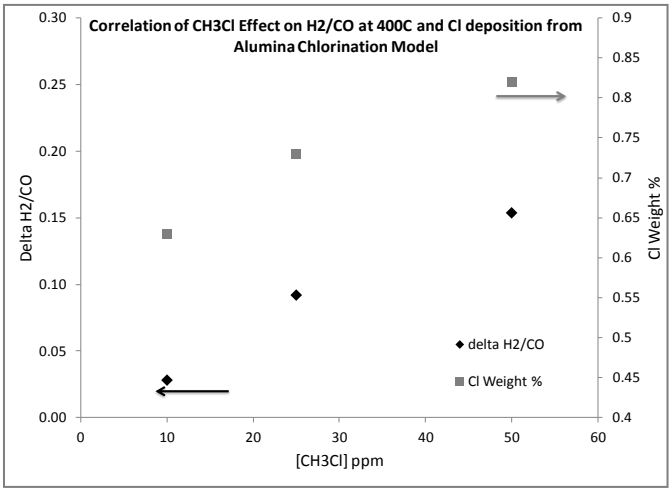

Figure 5.3: Change in H_2/CO ratio as a function of CH_3Cl concentration at 400°C in a feed of 5% CH_4 and 6% CO_2 in a balance of N_2. Chloride weight percent as a function of CH_3Cl concentration calculated using Castro model

Figure 5.3 shows that as the CH_3Cl concentration increases, the change in H_2/CO ratio of the reforming products increases. The calculated chloride weight percent also increases in an identical trend compared to the change in H_2/CO ratio. This is another indication that the model is a close description of the Rh/γAl2O3 catalyst and is useful for predicting relative changes in product selectivity due to changes in CH_3Cl concentration and temperature. However, when the weight percent of chloride calculated by the model is compared to the XPS results of chloride on the surface after exposure to CH_3Cl, shown in Table 5.1 and Figure 5.4, the agreement is qualitative but not quantitative. The relationship between chloride weight percent and temperature (i.e. the slope) is exactly the same in both the model and experimental results, as shown by the following figure, but they are offset by a constant value.

Table 5.1: Chloride Weight Percent on 4%Rh/γAl2O3 exposed to 50ppm CH_3Cl in a dry reforming feed

Temperature	Model Results	XPS Results
400°C	0.82%	1.25%
700°C	0.19%	0.65%

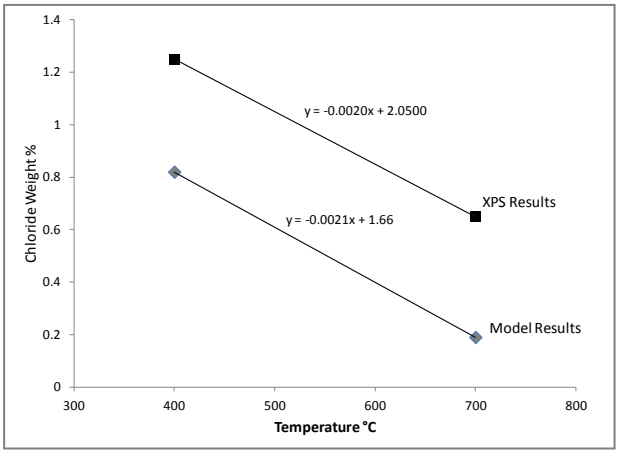

Figure 5.4: Chloride weight percent as a function of temperature on the 4% Rh/γAl2O3 catalyst exposed of 50ppm CH_3Cl in a feed of 5% CH_4 and 6% CO_2 in a balance of N_2 for 10 hours calculated from experimental XPS results and chloride weight percent calculated using the Castro model

There are a number of factors that could cause the quantitative discrepancy between the model developed by Castro et al. and the experimental data presented here. The K and L values in the Castro model were developed on a 0.38%Pt/γAl_2O_3 catalyst calcined at 650°C in air with a BET surface area of 165 m^2/gram. The experimental data presented here was produced on a 4%

$Rh/\gamma Al_2O_3$ catalyst calcined at 725°C in air with a BET surface area of 110 m^2/gram. The difference in metal is not likely to make a large difference in the results because in the Castro experiments the amount of platinum was small and not expected to interfere with the equilibrium chloride concentration on the alumina support. In the experimental results the catalyst was in a reducing atmosphere, due to the H_2 produced from the dry reforming reaction, which is expected to remove any chloride from the rhodium metal. Another factor that is different in this work compared to the work of Castro et al. is that the Castro model was developed using HCl as the chlorinating agent, whereas in this work CH_3Cl is the chlorinating agent. However, because experiments comparing 50ppm HCl to 50ppm CH_3Cl resulted in the same change in reverse water-gas shift activity, it is expected that the degree of alumina chlorination from these two compounds will be the same. Therefore in both catalysts the chloride is primarily interacting with the alumina support in the same way. This means that the properties of the alumina support are expected to have the greatest effect on the values of K and L.

L is the total number of hydroxyl groups and chloride groups on the alumina surface, and therefore does not change with chlorination. L can be affected by the calcination conditions because a high calcination temperature can produce defect sites on the alumina that are very acidic and result in more hydroxyl groups when the catalyst is exposed to H_2O[81]. During operation of the catalyst, as temperature increases L decreases due to dehydroxylation of the surface. Therefore, the value of L at room temperature in the presence of H_2O is a function of the calcination conditions as well as other features of the support, such as surface area and impurities that may increase or decrease the acidity of the alumina, but the rate of dehydroxylation is only a function of temperature. This means that the rate of dehydroxylation

should generally be the same on all gamma alumina surfaces, but the initial value of hydroxyl groups will be different depending on the type of alumina. This is the most likely explanation for the fact that when comparing the model to experimental results, the trend with temperature is the same, but the values are offset by a constant amount. K is the equilibrium constant of the reaction between alumina, H_2O, and HCl, and according to Castro et al. has a linear relationship with L. Therefore a higher L value would also result in a higher K value at each temperature, also resulting in the same trend with temperature but a constant offset.

It is possible that the Al_2O_3 support used in this experimental work had more hydroxyl groups, or a higher L value, compared to the Al_2O_3 support used in Castro's work because the one used in this work was calcined at a higher temperature; 725°C compared to 650°C. There could also be many other differences but the details are not disclosed, as the alumina used in the Castro work was a commercial Cyanamid Ketjen CK-300 alumina. In a later paper Castro et al. examined different commercial alumina samples that all exhibited different L values that varied by as much as 48%, although they were all calcined in air at the same temperature, 650°C. They claimed that the acidity of the alumina before chlorination has an effect on the degree of chlorination which may allow for an estimation of L based on the acidity of the Rh/γAl2O3 catalyst.

Figure 5.5, adapted from Castro et al.[85], shows the correlation of L calculated at 500°C with acid sites measured with n-Butylamine adsorption in molecules/cm^2. In general, as the acidity of the alumina supports increase, the L value, or chloride retention capacity, increases. This makes sense theoretically because the chloride anion from an acidic molecule such as HCl would react

with an acidic surface site, such as a Brönsted acid, to deposit on the alumina. Therefore as the acidity of a support increases, the chloride retention capacity increases.

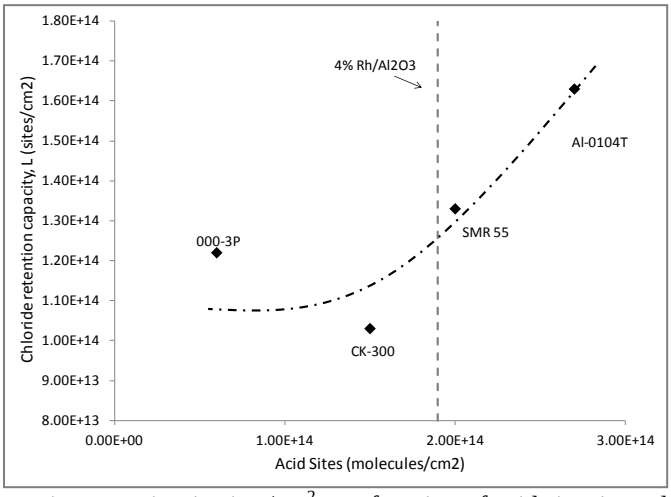

Figure 5.5: L, or chloride retention capacity, in sites/cm^2 as a function of acid sites in molecules/cm^2 measured using n-Butylamine adsorption, adapted from Castro et al.

Using the correlation relationship between acidity and chloride retention capacity, or L, in Figure 5.5 the value of L can be estimated for the 4% Rh/γAl2O3 catalyst, which according NH_3 TPD tests has an acidity of 1.90E14 molecules/cm^2, noted in Figure 5.5. It is assumed that the L value for 4% Rh/γAl2O3 is equal to the SMR55 alumina, which has almost the same acidity. Therefore the L value in sites/cm^2 is 1.33E14, at 500°C. Using this L value, the functions for L and K with temperature can be adjusted to more closely match the 4% Rh/γAl2O3 catalyst.

The formulas for L and K as a function of temperature are shown below in Equations 5.2-5.4. In equation 5.2 the slope of the linear function of L, -3.08E11 is kept the same in order to maintain the relationship between L and temperature. The intercept, 2.68E14 is adjusted so that L is equal to 1.33E14 at 500°C. The rest of the line is extrapolated. K is then recalculated using the linear relationship between K and L, Equation 5.4, so the new K value also has the same slope, or dependence on T, but a different magnitude to adjust for the different OH concentration.

$$L\left(\frac{sites}{cm^2}\right) = -3.08E11 * T(°C) + 2.68E14 \qquad 5.2$$

$$log\ K_{eq} = 1814 * \frac{1}{T(K)} - 0.0364 \qquad 5.3$$

$$K = 6E - 12 * L - 448.53 \qquad 5.4$$

Figure 5.6 shows the chloride weight percent as a function of temperature according to the experimental XPS results, the original model by Castro et al., and the modified model produced using a higher value for L that is expected to be more representative of the Rh/γAl2O3 surface. The modified model is a closer approximation to experimental data, but still not an exact quantitative match.

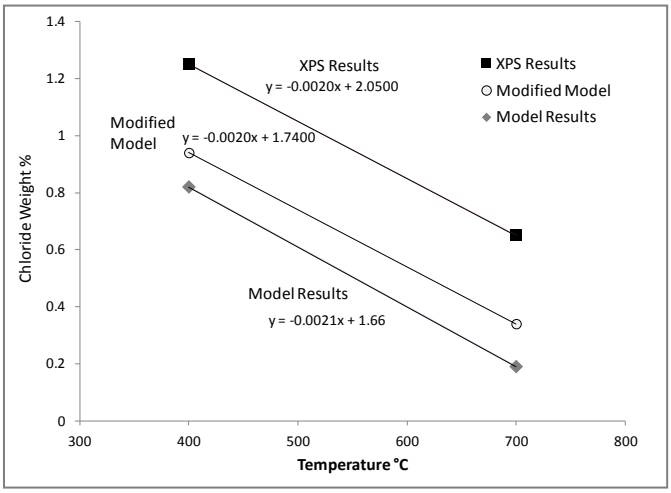

Figure 5.6: Chloride weight percent as a function of temperature for experimental XPS results and Castro model results, previously shown in Figure 5.4, and the modified Castro model to account for the higher chloride retention capacity of the 4% Rh/γAl2O3 catalyst

In order for the model to exactly predict the experimental results, the initial L value, which can be approximated as the y intercept of the linear function of L with temperature, would have to be higher. According to the Castro model, the initial L value on Pt/Al_2O_3 was 2.68E14 sites/cm^2. In the modified model using the measured acidity of the 4% Rh/γAl2O3 catalyst, the chloride retention capacity is 2.87E14 sites/cm^2. To adjust the model to match the XPS value for the 4%

Rh/γAl2O3 catalyst at 400°C, the initial L value would have to be set to 3.25E14, 21% larger than the value calculated by Castro et al for Pt/Al_2O_3. An initial L value 21% larger than the Castro model physically implies that the 4% Rh/γAl2O3 catalyst calcined at 725°C had 21% more acid sites after calcination in air compared to the 0.38% Pt/Al_2O_3 calcined at 650°C. This is a reasonable difference even amongst alumina samples calcined at the same temperature due to variations in preparation technique and impurities[46, 85, 117]. Considering the difference in calcination temperature, the difference is certainly accounted for. According to one study, increasing the calcination temperature of γAl_2O_3 from 600°C to 750°C more than doubled the surface acidity[47].

The alumina chlorination model developed by Castro et al. is a good description of the effect of temperature and H_2O/HCl gas ratio on chloride deposition on alumina. However, it was developed for a particular alumina with a certain hydroxyl group concentration. The model was modified here using data from the acidity characterization of 4% $Rh/\gamma Al_2O_3$ to include a larger chloride retention capacity, or L value, which allowed for a better quantitative match between the alumina chlorination model and experimental results.

5.2 Simulated Effect of O_2, H_2O, and CO_2 co-feeding

Flow-through reactor tests and catalyst characterizations showed that CH_3Cl introduction leads to chloride deposition on the alumina surface that poisons sites necessary for the forward and reverse water-gas shift reaction. The forward water-gas shift reaction is shown in Equation 5.5.

Water-Gas Shift $H_2O + CO \leftrightarrow CO_2 + H_2$ ΔH=-42 kJ mol^{-1} 5.5

The water-gas shift reaction poisoning practically manifests as a change in H_2/CO ratio of the syngas. When the forward water-gas shift reaction is poisoned, H_2O and CO increases while H_2 and CO_2 decrease, leading to a decrease in the H_2/CO ratio. When the reverse water-gas shift reaction is poisoned, CO_2 and H_2 increase while H_2O and CO decrease, leading to an increase in the H_2/CO ratio. When chloride poisons the alumina surface, active sites for both the forward and reverse water-gas shift reactions are poisoned. However in a H_2O or CO rich feed gas at which the forward water-gas shift reaction is kinetically favored, the active sites are primarily being used for the forward water-gas shift reaction, and therefore the rate of the forward water-gas shift reaction will decrease. The opposite scenario will occur with a CO_2 or H_2 rich feed gas, in which the active sites will be primarily used for the reverse water-gas shift reaction, and therefore the chloride poisoning will decrease the rate of the reverse water-gas shift reaction.

A CO_2 rich feed gas is typical of CH_4/CO_2 mixtures used for dry reforming, and in these cases experimental work previously discussed has shown that chloride introduction increases the H_2/CO ratio. When O_2 is added to the CH_4/CO_2 mixture, in the case of auto-thermal reforming, steam is produced from the combustion of CH_4, and the higher H_2O concentration leads to a poisoning of the forward water-gas shift reaction and a decrease in the H_2/CO ratio. Also, in literature it has been noted that during steam chlorocarbon reforming, in which the H_2O concentration is high, the forward water-gas shift reaction is poisoned. Therefore the relative ratio of CO_2, H_2O, and likely H_2 and CO, all play a role in the direction of water-gas shift poisoning.

In auto-thermal reforming, oxygen is added to the CH_4/CO_2 mixture to combust with CH_4 to produce H_2O, CO_2, and heat. Therefore the amount of oxygen added determines the amount of H_2O present in the product feed. Very small concentrations of oxygen will produce small amounts of H_2O compared to the CO_2 concentration, and therefore the reverse water-gas shift reaction would likely be poisoned, resulting in an increase in the H_2/CO ratio of the product gas. A high concentration of oxygen will produce a high concentration of H_2O which would likely result in forward water-gas shift poisoning, resulting in a decrease in the H_2/CO ratio of the product. To quantify this tradeoff, a calculation was performed to determine the changes in product selectivity due to chloride poisoning as a function of O_2 introduction. In addition to O_2, the theoretical effects of H_2O and CO_2 co-feeding were also determined.

The calculation was performed using experimental data, the alumina chlorination model discussed in Chapter 5.1, and equilibrium calculations. Experimental data was used to determine the relationship between the change in product selectivity as a result of CH_3Cl introduction and the number of OH, or hydroxyl groups, present on the surface. It is convenient to express the changes in product selectivity as a function of OH surface concentration because using the alumina chlorination model, the OH surface concentration on the 4% $Rh/\gamma Al_2O_3$ catalyst can be calculated for any product feed given the H_2O/XCl ratio (where XCl may be HCl or CH_3Cl) and the temperature. This allows for an extension of experimental data to other reactant mixtures. At a given temperature, the percent change in product species H_2, CO, H_2O, CO_2, and CH_4 determined by experiment were linear functions with OH because the primary change in product selectivity is due to chloride poisoning of the OH groups necessary for the water-gas shift reaction. Therefore at 400°C and 700°C, experimental data was used to determine the linear

function of the change in product selectivity due CH_3Cl introduction versus the catalyst surface OH concentration, calculated using the Castro model.

Equilibrium calculations were performed to calculate the expected equilibrium concentrations of product species based on the inlet temperature and various reactant concentrations without chlorocarbon introduction. Using the reaction temperature, the equilibrium H_2O concentration in the product gas, and the simulated concentration of CH_3Cl poison, the ratio of H_2O/CH_3Cl could be calculated, after which the chloride weight percent and surface OH concentration could be calculated using the alumina chlorination model. The chloride retention capacity of the 4% Rh/γAl2O3 catalyst was assumed to be 3.25E14 sites/cm^2 to match the chloride poisoning observed with the XPS data.

Using the surface OH concentration, the change in product selectivity from the equilibrium concentrations as a result of CH_3Cl poisoning could be calculated. Because experimental data showed that chloride deposition poisoned the water-gas shift reaction, causing the reactions to move farther from equilibrium, equilibrium calculations alone cannot account for the change in selectivity of the product species due to the introduction of a chlorocarbon. For this reason, this method of using experimental trends to modify equilibrium calculations was used.

The model results for the effect of O_2 introduction and 50 ppm CH_3Cl exposure are shown in Figure 5.8. Chloride weight percent, calculated using the alumina chlorination model, is shown on the primary y axis. The calculation of the change in H_2/CO ratio caused by the CH_3Cl introduction and OH poisoning is shown on the secondary y axis. Both the chloride weight

percent and the change in H_2/CO ratio is shown as a function of O_2 concentration at 400°C and 700°C.

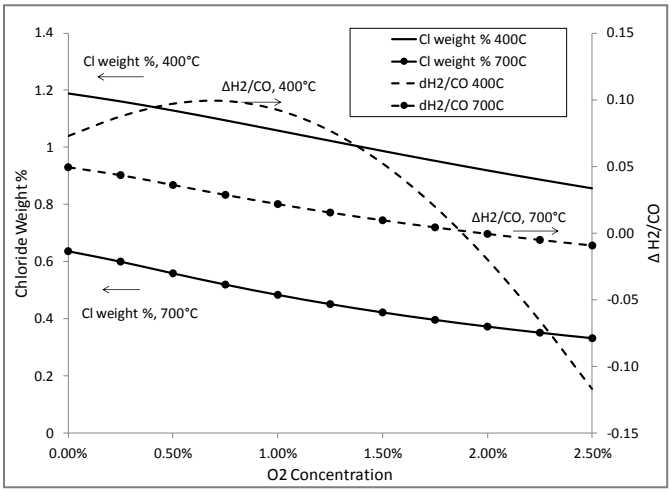

Figure 5.7: Chloride weight percent, calculated with the modified Castro model, and change in H_2/CO ratio, calculated using trends observed in experimental data, as a function of O_2 concentration at 400°C and 700°C

According to the model, at no oxygen addition, or dry reforming, when 50 ppm CH_3Cl is introduced at 400°C, the H_2/CO ratio increases by 0.07 and the chloride deposition is 1.2%. At 700°C, the H_2/CO ratio increases by 0.05 and the chloride deposition is 0.64 weight percent. As O_2 introduction increases, CH_4 combustion and partial oxidation occur on the catalyst, producing H_2O which has the ability to remove chloride from the alumina surface. Therefore the chloride weight percent on the catalyst decreases as O_2 concentration increases at both temperatures. At 400°C, as O_2 concentration increases, the change in H_2/CO ratio first increases to 0.10, then decreases to -0.12. According to the water-gas shift reaction (Equation 5.5), an increase in the H_2/CO ratio as a result of chloride deposition indicates that the reverse water-gas shift reaction is poisoned, while a decrease in the H_2/CO ratio indicates that the forward water-gas shift reaction is poisoned.

Therefore, at 400°C both the forward and reverse water-gas shift reaction can be poisoned depending on the O_2 concentration. As previously discussed in Chapter 3.2, O_2 introduction into a CH_4/CO_2 mixture results in CH_4 combustion that produces additional CO_2 and H_2O. At low O_2 concentrations the CO_2 and H_2O produced is small, and the H_2/CO ratio is closer to 1 at 400°C. At high O_2 concentrations, the CO_2 and H_2O production is larger, and the H_2/CO ratio is larger due to the occurrence of the forward water-gas shift reaction which is thermodynamically favored at low temperatures. Therefore at low O_2 concentrations the CO_2 concentration is sufficiently large that reverse water-gas shift reaction is poisoned, but as O_2 concentration increases, H_2O production increases, eventually causing a shift to forward water-gas shift reaction poisoning and a decrease in the H_2/CO ratio.

At 700°C, the change in H_2/CO ratio is positive in almost every case, indicating an increase in the H_2/CO ratio, at almost every O_2 concentration. This is due to the high temperature which favors the reverse water-gas shift reaction. The change in H_2/CO ratio is smaller at every O_2 concentration because the chloride poisoning is less at higher temperatures, as indicated by the chloride weight percent calculation.

Figure 5.9 shows the model results for the effect of H_2O introduction and 50 ppm CH_3Cl exposure to a 5% CH_4, 5% CO_2 gas mixture. Chloride weight percent, calculated using the alumina chlorination model, is shown on the primary y axis. The calculation of change in H_2/CO ratio caused by the CH_3Cl introduction and OH poisoning is shown on the secondary y axis. Both the chloride weight percent and the change in H_2/CO ratio is shown as a function of H_2O concentration at 400°C and 700°C. Figure 5.10 shows the same data and conditions in figure 5.9,

except that chloride weight percent and change in H_2/CO ratio is shown as a function of CO_2/CH_4 ratio in order to illustrate the effect of CO_2 co-feeding.

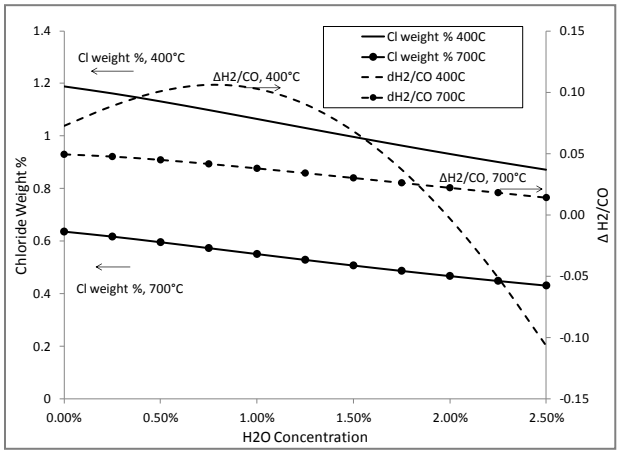

Figure 5.8: Chloride weight percent, calculated with the modified Castro model, and change in H_2/CO ratio, calculated using trends observed in experimental data, as a function of H_2O concentration at 400°C and 700°C

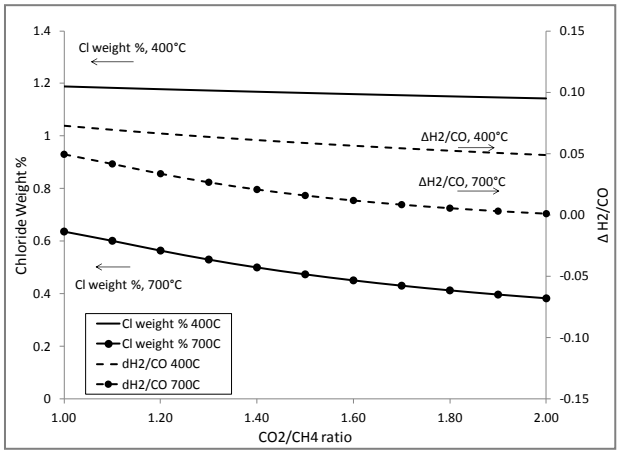

Figure 5.9: Chloride weight percent, calculated with the modified Castro model, and change in H_2/CO ratio, calculated using trends observed in experimental data, as a function of CO_2/CH_4 ratio at 400°C and 700°C

The trends in chloride weight percent and change in H_2/CO ratio as a function of H_2O concentration, shown in Figure 5.9, are almost exactly the same as with O_2 concentration in Figure 5.8. This shows that the primary function of O_2 introduction into the dry reforming reaction in terms of chloride poisoning is the production of H_2O. Co-feeding H_2O directly therefore has a similar result as O_2 introduction. Co-feeding CO_2 has a minimal effect on the chloride deposition at 400°C. At 700°C, chloride deposition decreases with increasing CO_2 because the higher temperature favors the reverse water-gas shift reaction. Therefore in this case the CO_2 and H_2 are converted to H_2O and CO, and the H_2O assists with the chloride removal from the alumina support. This also explains the trends seen in the change in H_2/CO ratio at both temperatures. At 400°C the change in H_2/CO is small because there is no change in the amount of chloride deposition. At 700°C the H_2/CO ratio decreases slightly with increasing CO_2

concentration because the chloride is being removed from the surface, decreasing the degree of reverse water-gas shift poisoning.

This model allowed for an extension of the experimental conditions to cases with O_2, H_2O, and additional CO_2 co-feeding. As expected, O_2 and H_2O introduction are beneficial for the catalyst, because both provide H_2O that removes chloride from the alumina support. O_2 introduction has the additional benefit of producing heat from the combustion with CH_4 which decreases the rate of chlorination. O_2 will also remove surface carbon, maintaining the activity of the catalyst. CO_2 is only effective for the removal of chloride at high temperatures when H_2O is produced from the reverse water-gas shift reaction. At 400°C the concentration of O_2 and H_2O introduced determines the direction of water-gas shift poisoning, causing an increase in the H_2/CO ratio at low temperature and a decrease at high temperatures. If the catalytic reactor is operated at low temperatures, the chloride poisoning can be taken advantage of to increase the H_2/CO ratio of the syngas. However, for maximum syngas production and CH_4 conversion, the catalytic reactor will more likely be operated at high temperatures, where chloride deposition is low, and therefore the change in H_2/CO ratio as a result of CH_3Cl introduction will be low.

5.2 Mechanism Postulation

The conversion and product distribution data combined with the catalyst characterization and alumina chlorination model support a mechanism by which CH_3Cl decomposes on the surface, depositing chloride on the alumina support and CH_3* groups on the rhodium metal. The chloride replaces primarily basic support hydroxyl groups, which increases the acidity of the surface and poisons the reverse water gas shift reaction.

The CH_3Cl may react on the surface by a step-wise dechlorination and dehydrogenation, shown in Equations 5.6-5.10, similar to the proposed mechanism for CH_4 reforming that proceeds via a step-wise dehydrogenation. The bond dissociation energy of a CH_3-H bond is 439 kJ/mole while that of a CH_3-Cl bond is 350 kJ/mole[107], so it is likely that the C-Cl bond will break before the C-H bonds. The initial breaking of the C-Cl bond as a rate limiting step in hydrodechlorination is observed in other work[102, 104-106] and could be plausible here. This is one reason why CH_4 conversion decreases slightly when CH_3Cl is on-stream; the CH_4 and CH_3Cl compete for sites and CH_3Cl preferentially reacts. This stepwise dehydrogenation produces H* that later forms H_2 in Equation 5.11, and surface C* that is oxidized to CO in a later step.

$$CH_3Cl + 2^* \rightarrow CH_3^* + Cl^* \qquad 5.6$$

$$CH_4 + 2^* \rightarrow CH_3^* + H^* \qquad 5.7$$

$$CH_3^* + ^* \rightarrow CH_2^* + H^* \qquad 5.8$$

$$CH_2^* + ^* \rightarrow CH^* + H^* \qquad 5.9$$

$$CH^* + ^* \rightarrow C^* + H^* \qquad 5.10$$

$$2H^* <-> H_2 + 2^* \qquad 5.11$$

If CH_3Cl reforming is analogous to CH_4 reforming, then steps 5.6-5.10 occur on the metal, while the role of the support is to activate CO_2 and transport hydrogen and oxygen species to and from the metal[38]. Therefore according to Equation 5.6, the chloride is first deposited on the rhodium metal, and then must move to the alumina support, since literature, XPS, CO_2 adsorption studies, and TGA reforming studies all support the theory that chloride deposits on the alumina support. Therefore the mechanism by which chloride moves from the rhodium metal to the support must be proposed. The chloride may spill over from the metal to the support, similar to the way H* moves from the metal to the support, or chloride may react with hydrogen to form HCl which then reacts with the alumina support.

First the spill-over mechanism will be explored. In order for the chloride to move from the metal to the support via spill-over, there must be sufficient OH groups around the perimeter of the rhodium to react with the chloride to produce aluminum chloride and H_2O. The number of OH groups can be calculated using the following formula (Equation 5.12):

$$I_o = \alpha * X_m * D^2 \qquad 5.12$$

Where I_o is the specific perimeter of the rhodium in units of m/g catalyst, α is the perimeter of one particle of rhodium in units of m/g catalyst, X_m is the metal loading in %, and D is the dispersion of the metal in %. α is assumed to be 8.8E5 m/g, assuming hemispherical particles of rhodium[42], X_m is 4%, and D is 33% according to CO chemisorption. This gives an I_o of 3.83E9 m/g catalyst. Assuming the distance between OH groups is 2Å[71], the concentration of OH groups around the periphery of the rhodium particles is 31.8 µmol/g. The amount of chloride deposited while dry reforming 5% CH_4, 6% CO_2, and 50 ppm CH_3Cl in a balance of N_2 at 400°C, the condition discussed frequently here, is 1.25 wt%, or 352 µmol/g. Therefore the

amount of chloride deposited on the alumina surface from the CH_3Cl is an order of magnitude greater than the number of OH groups around the periphery of the rhodium particles, so the chloride must not rely only on spill-over from the metal to the support to reach the alumina support.

For the chloride to form HCl, it must react with H* which is abundant on the metal due to reactions 5.7-5.10. The reaction between Cl* and H* is fast because it is often reported in literature that H_2 reduction of chlorinated metal species is an effective method for removing the metal chloride[85, 89]. The gas phase HCl is then mobile and may react with the alumina support to deposit chloride and hydrogen atoms. Flow-through reactor experiments showed that the effect of HCl on Rh/γAl2O3 was similar to the effect of CH_3Cl. Therefore HCl does clearly interact with the alumina surface and it is possible that HCl is the species responsible for the poisoning of the alumina.

Based on these calculations and flow-through reactor experiments, the most likely scenario is the reaction of Cl* and H* on the metal to form HCl* which may then desorb to form HCl. Gas phase HCl may then react with the alumina support to deposit chloride and hydrogen on the alumina. These steps result in the reactions shown in Equations 5.13-5.15. Reaction 5.15 is not an elementary step but the net reaction previously proposed in the chlorination of alumina[47, 85, 87, 88]

$$Cl^* + H^* \leftrightarrow HCl^* \qquad 5.13$$

$$HCl^* \leftrightarrow HCl + * \qquad 5.14$$

$$HCl^* + OH^* \leftrightarrow Cl^* + H_2O^* \qquad 5.15$$

In the micro-kinetic mechanism by Maestri et al.[35], the surface carbon originating from the CH_4 in Equation 5.10 is oxidized by surface OH* that may originate from gas phase CO_2 or H_2O in Equations 5.16-5.18. Because the oxidation of carbon relies on hydroxyl groups, this may be another explanation why CH_3Cl introduction slightly decreased CH_4 conversion; because carbon buildup on the metal originating from the additional CH_3Cl blocks reforming sites and decreases CH_4 conversion. That effect combined with the CH_3Cl/CH_4 species competition may explain the loss in CH_4 reforming activity. Another plausible explanation is the loss of hydrogen mobility and CO_2 support affinity at high levels of support chlorination which would decrease both CH_4 and CO_2 conversion.

$$C^* + OH \leftrightarrow CO^* + H^* \qquad 5.16$$

$$OH^* + H^* \leftrightarrow H_2O^* \qquad 5.17$$

$$H^* + CO_2^* \leftrightarrow CO^* + OH^* \qquad 5.18$$

The OH* groups are also crucial intermediates in the water-gas shift reaction, illustrated here with Equations 5.17 and 5.18. As written, the sum of Equations 5.17 and 5.18 is the reverse water-gas shift reaction. In the reverse water-gas shift reaction, OH is needed to combine with H* to produce H_2O while in the forward water-gas shift, OH* is needed to combine with CO* to make CO_2 and H*. The dependence of the forward and reverse water-gas shift reactions on alumina hydroxyl groups is one explanation for why the replacement of OH* groups by chloride via Equation 5.15 poisons the water-gas shift reactions.

Evidence from experimental work, catalyst characterization, the alumina chlorination model, and previous literature allowed for the modification of the dry reforming micro-kinetic mechanism,

largely based on the mechanism by Maestri et al., for CH_3Cl reforming reactions. This mechanism provides an explanation for the change in water-gas shift selectivity seen in both CO_2 rich and H_2O rich feeds, and the change in dry reforming activity due to the introduction of CH_3Cl. Future experimental and computational work to determine the activation energies and reaction rates of the elementary steps in reactions 5.13-5.15 would allow for the incorporation of the chlorocarbon reactions into pre-existing micro-kinetic models, which could provide another diagnostic tool to determine the effect of chlorocarbons on the dry, steam, and auto-thermal reforming of CH_4.

Chapter 6 : Conclusions

Biogas is a mixture of methane and carbon dioxide produced from the anaerobic microbial digestion of biomass, such as in landfills, waste water treatment plants, and anaerobic digestion of biomass and animal manure on farms. The CH_4 produced from these processes is approximately 18 billion cubic meters per year, which is currently valued at $2.5 billion per year. However, most of this fuel is wasted and not used for energy because the high CO_2 content of the biogas decreases the heating value and flame stability of the gas mixture which leads to increased emissions when combusted. Both dry and auto-thermal reforming allow for the complete conversion of inexpensive, local biogas into syngas which can be used as a combustion enhancer, a feedstock for the production of liquid fuels, or to provide H_2 for fuel cells. Converting the biogas into syngas therefore provides more opportunities to completely utilize the energy contained therein.

Dry reforming using a $Rh/\gamma Al_2O_3$ catalyst converts the CH_4 and CO_2 in biogas to H_2 and CO without deactivation due to carbon formation when the CH_4/CO_2 ratio of the biogas is one or lower. The dry reforming reaction is subject to carbon forming side reactions, and therefore at CH_4/CO_2 ratios higher than one, catalytic carbon formation is a concern. If carbon does form on the catalyst, blocking active sites for reforming, the catalyst can be regenerated in air to remove carbon and recover the activity of the catalyst. Carbon formation can also be minimized by performing the reaction with additional O_2 or air which provides additional oxidant and removes the potential for carbon formation, even for methane rich biogas mixtures. Excess CO_2 can also reduce the carbon formation potential, but it is half as effective as O_2.

O_2 or air addition into the dry reforming reaction is also useful because the addition of air produces H_2O and CO_2 from the combustion of CH_4 and H_2 and CO from the partial oxidation of CH_4. The additional H_2O produced reacts in the water gas shift reaction, which is active at low temperatures, and results in a higher H_2/CO ratio of the product gas. Therefore at low reactor temperatures, at approximately 400°C, the H_2/CO ratio of the syngas can be tuned depending on the amount of O_2 introduced. With enough air addition, the reactor can be operated auto-thermally, called auto-thermal reforming (ATR), in which the heat from the CH_4 combustion supplies all of the heat needed for the endothermic reforming reactions. This is an especially useful technique when the CH_4/CO_2 ratio of the biogas is higher than one.

The water-gas shift reaction always accompanies the dry and auto-thermal reforming reactions, either in the forward or reverse direction, which affects the H_2/CO ratio of the syngas. In both directions the water gas shift mechanism is affected by the basicity of the alumina, specifically relying on the hydroxyl groups to oxidize CO in the forward direction and activate CO_2 in the reverse direction. Therefore any changes to the support acidity or basicity can affect the activity of the water-gas shift reactions.

In any catalytic reforming system, gas compounds may be present with the potential to poison the catalyst, reducing activity and selectivity to desired products. In the case of biogas, CH_3Cl and other chlorocarbons are potential catalyst poisons that have not been extensively researched for their effect on a catalyst during the dry reforming reaction. Other relevant fields, such as chlorocarbon steam reforming, hydrodechlorination, and naphtha reforming have been studied and provide insight into the effect of CH_3Cl on the dry reforming reaction. In general,

chlorocarbons and HCl can react with both the alumina support and precious metal of the catalyst, but in reducing atmospheres where H_2 is present, chloride on the precious metal is easily removed. This reduction process is used in catalyst preparation to remove chloride from the metal sites of catalysts prepared using chlorinated precursors. Therefore chlorination of the catalyst primarily occurs on the alumina support.

Chloride reacts with the alumina support by replacing basic hydroxyl (OH) groups and polarizing the remaining neighboring hydroxyl groups, increasing the acidity of the alumina support. This was confirmed with NH_3 temperature programmed desorption and CO_2 adsorption. The amount of chloride deposition is sensitive to the concentration of the chlorinating compound (CH_3Cl or HCl), H_2O, and temperature. Chloride can be removed from the alumina by reaction with H_2O, which restores alumina hydroxyl groups. Chlorination is less thermodynamically favored at high temperatures and therefore chloride deposition decreases as temperature increases, confirmed with XPS and TGA reaction experiments.

Chloride deposition affects the product selectivity of the dry reforming reaction by replacing hydroxyl groups on the alumina support, thereby affecting the rate of the forward and reverse water-gas shift reactions. In CO_2 rich environments the reverse water gas shift reaction is poisoned, resulting in an increase of H_2/CO ratio while in H_2O rich environments the forward water gas shift reaction is poisoned, resulting in a decrease of the H_2/CO ratio. The poisoning of the water gas shift reaction and the resulting change in product selectivity is completely reversible once CH_3Cl is removed from the feed.

Chloride deposition also reversibly poisons the dry reforming activity largely for the same reason that it poisons the reverse water-gas shift reaction; because it decreases the concentration of basic hydroxyl groups on the surface which will reduce the degree of CO_2 activation on the support and reduce the hydrogen and oxygen mobility, which will cause a decrease in the dry reforming reaction rate. Both the activity and selectivity changes caused by CH_3Cl are a function of the concentration of CH_3Cl, and are less prominent at high temperatures where the alumina chlorination is not as favored. Competition of CH_3Cl with CH_4 for reforming sites is another but less significant cause of dry reforming activity loss.

Introduction of HCl instead of CH_3Cl under the same reaction conditions causes the same changes in selectivity as CH_3Cl, indicating that HCl may be the chlorination agent. If CH_3Cl reforming behaves similar to CH_4 reforming, CH_3Cl will decompose on the metal to produce CH_3* and Cl*, which will be reduced by neighboring H*, also present on the metal, to produce HCl. The HCl is more mobile than the surface chloride and will more easily react with alumina hydroxyl groups to chlorinate the alumina support.

Because the acid-base pairs on the alumina are attacked by HCl to deposit chloride, a support with less acidity or fewer acid-base pairs would not be as vulnerable to chloride poisoning. A ZrO_2 support which has fewer acidic and basic sites has been shown in other work to resist chloride poisoning during the steam reforming of CH_3Cl. For specific chlorocarbon reforming applications in which chloride deposition is not desired, catalyst formulations with less acidity may be advantageous.

CH_3Cl exposure may also increase rhodium dispersion on the Al_2O_3 support, suggested by some flow-through reactor experiments, CO chemisorption and XPS. The redispersion of the rhodium causes a slight increase in the dry reforming activity in some cases, such as with the introduction of HCl at 50 ppm, CH_3Cl at 10-25ppm, and with 50 ppm CH_3Cl introduction during ATR, but not with 50 ppm CH_3Cl introduction during dry reforming. Another explanation for the changes in dry reforming activity could be due to chlorination of the alumina support which affects the affinity of CO_2 for the support and the mobility of hydrogen, both of which affect the dry reforming activity. Therefore the effect of chloride species on redispersion of rhodium is inconclusive and should be studied further using other characterization techniques such as TEM.

O_2 and H_2O co-feeding are useful for minimizing surface chlorination and changes in activity and selectivity due to CH_3Cl introduction. O_2 is beneficial because it produces H_2O from the CH_4 combustion reaction, which also raises the temperature, both of which decrease chlorination. H_2O can also be co-fed directly to reduce the chloride deposition on the alumina and the resulting changes in dry reforming activity and selectivity to syngas.

In summary, the amount of chloro-carbon expected in a biogas mixture, between 10-50ppm, is not particularly harmful for the 4% Rh/γAl2O3 catalyst. The most noticeable effect of chloride deposition is a change in H_2/CO ratio of the syngas that is proportional to the amount of chloro-carbon in the feed. The effect is completely and quickly reversible after the chloro-carbon is removed from the feed. The effect can also be reduced by co-feeding air or H_2O, or by operating at high temperatures, in the range of 600°C-900°C to minimize chlorocarbon poisoning. Air introduction has the additional benefit of reducing the carbon formation potential on the catalyst,

and providing heat within the catalytic reactor for the endothermic reforming reactions. Therefore catalytic auto-thermal reforming is the most effective method for converting biogas into syngas so that the energy contained in the biogas can be fully utilized.

Appendix

A.1 Experimental Methods

A.1.1 Catalyst Preparation

A 4% $Rh/\gamma Al_2O_3$ catalyst was used for all of the experimental work presented here. Powder catalyst and a wash-coated cordierite monolith (400 cpsi), both obtained from BASF Catalysts, were used. The catalyst was prepared using a Rh nitrate, $Rh(NO_3)_3$, solution, so any chloride present on the catalyst originated from the reaction conditions and not the preparation technique. The monolith had a bulk density of 0.44 g/cm3 and wash coat loading of 1.2-1.6 g/in.^{3} The powder catalyst was prepared by ball milling the impregnated catalyst to an average particle size of 10 microns. The catalysts were calcined in air at 725°C.

A.1.2 Flow-through Reactor Testing

Flow through reactor experiments were performed in a quartz flow-through reactor at 1 atm pressure and temperatures between 200°C and 900°C. Gas hourly space velocities (GHSV) ranged from 8,000 hr^{-1} for performance tests to over 100,000 hr^{-1} for kinetic tests. For the catalyst powder tests, weight hourly space velocities (WHSV) were 1,050 hr^{-1} for all tests. UHP CH_4, CO_2 and N_2 (Techair) were used to simulate a landfill gas. A mixture of 1000ppm CH_3Cl in N_2 (Techair) was used to introduce CH_3Cl. The mass flow rate of each inlet gas into the reactor was controlled with mass flow controllers (Aalborg, GFC17). A schematic of the apparatus is shown in Figure A1.

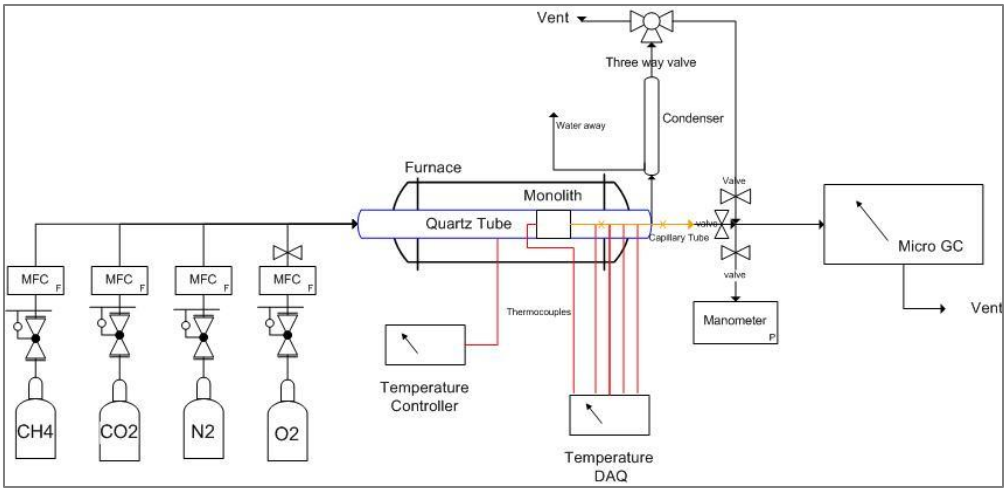

Figure A.1.1: Schematic of flow-through reactor apparatus

A tube furnace was controlled with a temperature controller (Omega, CN9000A Series) and K-type thermocouples (Omega, KMTIN Series) to achieve temperatures between 350°C and 900°C. Depending on the experiment, thermocouples were either placed at multiple points along a monolith or only at the inlet and outlet of the catalyst bed. The reactor was coupled to an on-line Agilent Micro GC (3000) instrument to measure the gas product composition. For long-term performance tests monoliths were used and operated at equilibrium for approximately 50 hours. Experiments in the kinetic regime were operated far from equilibrium for reaction times between 1 and 10 hours.

A.1.3 Capillary Sampling

A capillary sampling method was developed to obtain gas samples along the axis of a monolith. This technique is especially useful for reaction systems with very disparate reaction rates that will take place in different regions of the reactor bed. A capillary sampling technique provides data at multiple points along the axis of the monolith and therefore gives more insight into the reaction rates.

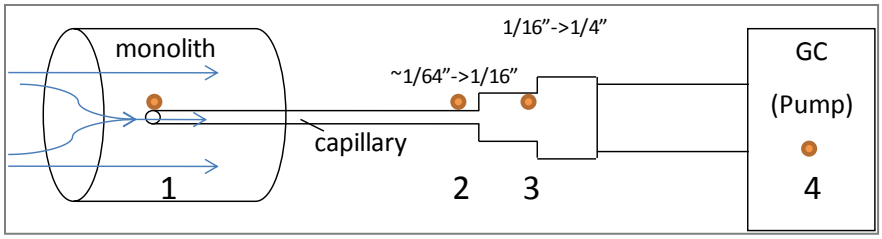

Figure A.1.2: Schematic of capillary sampling apparatus

A diagram of the capillary sampling apparatus is shown in Figure A.2. One end of a fused silica capillary is threaded through a stainless steel tube with an ID slightly larger than the OD of the capillary. This stainless steel tube is more rigid than the capillary and keeps it radially centered in the quartz reactor tube. The capillary is then threaded into a channel of the monolith so that the capillary but not the stainless steel sheath is in contact with the monolith. This is to prevent catalytic reactions with the stainless steel in the monolith. The outlet end of the capillary is attached to a micrometer to control the position of the capillary inlet in the monolith. After the micrometer, the outlet gas from the capillary is injected into the μGC for analysis. 1/16” UT fittings with silica O-rings are used to make the gas tight seal between the reactor and the capillary tube.

Calculations were performed to ensure that the pressure drop introduced by the capillary system was less than the pull of the GC pump. If this were not the case, an external pump would have been required to pull the sample through the capillary tube and into the GC. It was also a requirement that the linear velocity in the reactor be approximately the same as the linear velocity in the capillary tube, so that the pump did not pull too much sample and perhaps obtain a gas sample before the reaction had reached equilibrium. At these velocities the Mach number was subsonic (approximately 2E-10) and the Reynolds number is low (0.5) and therefore the flow can be assumed to be laminar. It was also assumed that the pressure at the capillary inlet is

atmospheric. The Bernoulli equation (Equation A.1), with terms for the friction along the capillary tube and entrance, was used to calculate the pressure drop along the tube.

$$\boldsymbol{P_1} + \frac{\boldsymbol{1}}{\boldsymbol{2}}\boldsymbol{\rho v_1^2} =$$

$$\boldsymbol{P_4} + \frac{\boldsymbol{1}}{\boldsymbol{2}}\boldsymbol{\rho v_4^2} + \boldsymbol{H_{minor,cap\ entrance}} + \boldsymbol{H_{minor,\frac{1}{32}to\frac{1}{16}}} + \boldsymbol{H_{minor,\frac{1}{16}to\frac{1}{4}}} + \boldsymbol{H_{major,friction\ along\ capillary}} \quad A.1$$

Where P_1=pressure in the reactor, assumed to be atmospheric
v_1=linear velocity in reactor=v_o
P_4=unknown
$H_{minor,\ capillary\ entrance,}$ evaluated at v_1
$H_{minor,\frac{1}{32}to\frac{1}{16}}$, evaluated at v_2
$H_{minor,\frac{1}{16}to\frac{1}{4}}$, evaluated at v_3
$H_{major,friction\ along\ capillary}$, evaluated at v_1, flow is laminar
$v_4=Q_{capillary}/A_4$
ρ was evaluated as a function of temperature

Because the velocity is so low, the most important contributors to the pressure drop are the entrance effects from the reactor into the capillary tube, and the friction along the capillary. For the experimental conditions discussed in this thesis, the pressure drop in the capillary tube was approximately 0.3 psi, well within the power of the GC pump.

A.1.4 TGA

Thermo gravimetric analysis was used to measure weight change in the catalyst as a result of changes in the gas and temperature atmosphere of the catalyst. Temperature programmed oxidation (TPO), ammonia temperature programmed desorption (TPD), CO chemisorptions, and CO_2 adsorption were all performed in a thermo gravimetric analyzer (Netzsch, STA 409 PC Luxx). The TGA was also used to measure the weight change of the catalyst as a result of exposure to dry reforming conditions with and without CH_3Cl at various temperatures. The details of each test are described in their respective experimental method and/or results sections.

A.1.5 BET

Specific surface area of the catalyst samples were measured using the BET method with a Quantachrome Nova 2200e. The BET method was developed by Stephen Brunauer, Paul Hugh Emmett, and Edward Teller in 1938[118]. It is extension of Langmuir adsorption in which molecules adsorb on a surface in layers. The BET equation is shown in Equation A.2:

$$\frac{1}{v[\left(\frac{p_o}{p}\right)-1]} = \frac{c-1}{v_m c}\left(\frac{p}{p_o}\right) + \frac{1}{v_m c} \qquad A.2$$

$$c = exp\left(\frac{E_1 - E_L}{RT}\right) \qquad A.3$$

Where v is the volume of adsorbed gas, in this case N_2 was used, p_o is the saturation pressure of N_2, p is the equilibrium pressure of N_2, v_m is the volume of gas adsorbed on the surface in a monolayer, and c is a constant. C is expressed in Equation A.3 where E_1 is the heat of adsorption of the first monolayer, E_L is the heat of adsorption for subsequent monolayers, R is the gas constant and T is the temperature at adsorption. Equation A.2 can be plotted as a straight line in the region of $0.05<p/p_o<0.35$ to determine v_m.

$$\text{SSA} = \frac{\text{v}_\text{m}\text{Ns}}{\text{Va}} \qquad \text{A.4}$$

Specific surface area of the surface is calculated using Equation A.4 by multiplying the monolayer volume of gas by N, avogadro's number, by s, the adsorption cross section of N_2, and dividing by V, the molar volume of N_2, and a, the mass of the adsorbent.

A.1.6 XPS

XPS analysis was carried out using a Thermo Fisher K Alpha XPS equipped with an Al Kα monochromatic source. Fresh and used powder catalyst sample was mounted on double sided

tape for analysis. The run conditions were as follows: pass energy=40 eV, vacuum conditions were 5E-8 torr or lower. Data was analyzed using Thermo Fisher Advantage software and Scofield sensitivity factors. Binding energies were referenced to C1s=285.0 eV.

A.1.7 Acidity Characterization

Low temperature adsorption and temperature programmed desorption of ammonia is used to measure the acidity of the catalyst surface and the relative strength of acid sites. When a gaseous base, in this case NH_3, is adsorbed to an acid site, a base adsorbed on a strong acid will be more strongly held and difficult to desorb than one adsorbed to a weak acid. Therefore temperature programmed desorption gives a measure of the temperatures required to desorb the gaseous base, which is a measure of acid strength. The total amount of base desorbed gives a measure of the total number of acid sites [46].

This characterization was performed in a thermo-gravimetric analyzer (Netzsch, STA 409 PC Luxx). In this protocol the catalyst is first dried in N_2 at 150°C for 1.5 hours. The catalyst temperature is then reduced to 100°C and then 1% NH_3 in Argon is flowed through the TGA for 10 minutes to allow adsorption of the NH_3 to the surface. The system is then flushed with N_2 and the temperature is increased from 100°C to 700°C at 10°C/min to desorb the NH_3. The derivative of the weight loss during the desorption step will show a peak (or multiple peaks) at which weight loss is the most rapid, attributed here to the removal of NH_3, shown in the following figure.

The number of acid sites is calculated using the weight loss of the catalyst during this weight change derivative peak, as shown in Figure A.3. Error bars on the resulting values originate from the fact that the baseline, or endpoints for the mass loss peak, can be drawn from more than

one set of points. For this reason the number of acid sites is a more uncertain measure of acidity than the temperature at which the derivative mass loss peak occurs. Therefore both the number of acid sites and the temperature at which the NH_3 is desorbed will be examined to understand the acidity of the surface.

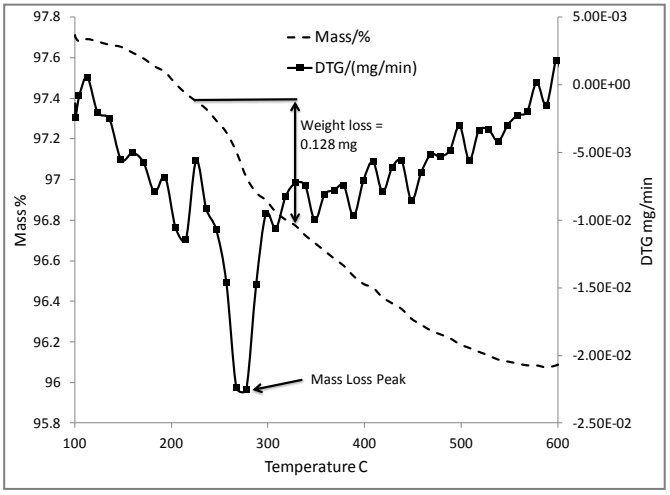

Figure A.1.3: Mass percent and mass derivative as a function of temperature during NH_3 TPD

The following formula is used to calculate the number of acid sites from this weight change. The number of acid sites is given in mmoles of NH_3 adsorbed per gram of catalyst.

$$Acid\ Sites\ (\frac{mmole}{g}) = \frac{Weight\ Loss\ (g) * \frac{1}{MW\ NH_3(\frac{g}{mole})}}{Catalyst\ Weight\ after\ pretreatment\ (g)} * \frac{1000 mmole}{mole} \qquad A.5$$

This NH_3 TPD method does not distinguish between Lewis and Brönsted acid sites. Therefore the acidity measured using this method is a sum of Lewis and Brönsted acidity. Infrared spectroscopic work on the adsorption of NH_3 on alumina and Rh/γAl2O3 suggest that NH_3 exists as coordinately bonded NH_3 to Lewis acid sites and as NH_4^+, resulting from a reaction with a Brönsted center [46, 119]. The relative intensity of their corresponding bands are a 4:1 ratio of Lewis to Brönsted acid sites [46]. This is not surprising considering Lewis acid sites are stronger and more likely to react with NH_3.

A.1.8 Basicity Characterization

Low temperature adsorption of CO_2 is used to measure the relative number of basic sites on the Rh/γAl2O3 samples exposed to various environments. Because CO_2 is an acidic molecule the

amount that irreversibly adsorbs to a sample at low temperature is a measure of the amount of basic sites. On the alumina surface, CO_2 primarily adsorbs to surface hydroxyl groups which account for the basicity on alumina[46]. It is assumed that there is a 1:1 ratio of CO_2:OH groups adsorbed. However CO_2 also adsorbs on the Rh metal at room temperature [116] so the values obtained for basicity should be viewed in light of the Rh dispersion and understood as relative values.

This characterization was performed in a thermo-gravimetric analyzer (Netzsch, STA 409 PC Luxx). In this protocol the catalyst is first dried in N_2 at 150°C for 1.0 hours. The catalyst temperature is then reduced to 30°C and then 50% CO_2 is introduced for 1 hour to allow adsorption of the CO_2 to the surface. The system is then flushed with N_2 for 1 hour to remove physisorbed CO_2. The weight gain of the catalyst is calculated from the weight before CO_2 adsorption to the weight 1 hour after the N_2 flushing step. The weight gain is assumed to be only from CO_2 adsorption.

A.1.9 Chemisorption

The dispersion, or surface availability of Rh sites is determined using CO chemisorption. It is assumed that CO chemisorbs to Rh, and not significantly to Al_2O_3, at a 1:1 ratio, and is therefore a measure of the available metal area. This characterization was performed in a thermo-gravimetric analyzer (Netzsch, STA 409 PC Luxx). In this protocol the catalyst is first dried in N_2 at 350°C for 1.0 hours and then reduced in 4% H_2 for 1 hour at 350°C. The catalyst temperature is then reduced to 30°C and then 5% CO is introduced for 1 hour to allow adsorption of the CO to the surface. The system is then flushed with N_2 for 1 hour to remove physisorbed CO and then the temperature is increased from 30°C to 700°C at 10°C/min to desorb the

remaining CO. The weight gain of the catalyst during CO adsorption was used to calculate the amount of CO adsorption.

A.2. Kinetic Study of Dry Reforming Using Capillary Sampling Technique

A capillary sampling technique, mimicking a differential reactor, was used to study the kinetics of CO_2 reforming of CH_4. In a differential reactor is it important that the conversion of the reactants, the temperature change, and the reactant concentration in the bed is very small. Therefore, the reactant concentration can be assumed as constant throughout the reactor, and the reaction rate can be considered spatially uniform throughout the bed. Samples taken at 1/4" increments showed that the reactant concentration and therefore the reaction rate was not uniform throughout the 2" monolith. However, by examining two locations along the monolith ¼" apart, we can look at a small slice of the monolith in which the conversion is small, and therefore the reactant concentrations are somewhat constant. In this small "slice" or increment, the temperature change is also small and is measured with a thermocouple moved along with the capillary.

The rate of reaction of dry reforming will take the form in Equation A.6 near equilibrium:

$$Rate = k_f (CH_4)^{\alpha} (CO_2)^{\beta} - k_r (H_2)^{\upsilon} (CO)^{\omega} \qquad A.6$$

Near equilibrium, the production of H_2 and CO inhibits the forward reaction since the reverse reaction rate becomes significant. Operating far from equilibrium, at low reactant conversions, reduces this effect, so that the rate expression takes the form of Equation A.7. Therefore the reverse reaction compared to the forward reaction can be neglected at low reactant conversion.

$$Rate = k_f (CH_4)^{\alpha} (CO_2)^{\beta} \qquad A.7$$

The parameter k_f is a function of the temperature and surface properties. It includes the pre-exponential factor and activation energy of the reaction, as shown in Equation A.8.

$$k_f = k_o \exp\left(\frac{-E_a}{RT}\right) \qquad A.8$$

Therefore, the complete rate expression is shown in Equation A.9.

$$Rate = k_o \exp\left(\frac{-E_a}{RT}\right)(CH_4)^{\alpha} (CO_2)^{\beta} \qquad A.9$$

To determine k_f, and therefore the activation energy, E_a, it is assumed that the reaction is first order in CH_4. One way to ensure this is to have the concentration of CO_2 as a flooding reactant so that any change in the concentration of CO_2 will be negligible. This is a simplifying assumption for now, but this will be checked later after the orders for CH_4 and CO_2 are determined. The first order assumption for CH_4 yields Equation A.10:

$$\frac{dCH_4}{dt} = -k_f (CH_4) \qquad A.9$$

Integrating this gives Equation A.11:

$$\ln \frac{[CH_4]_t}{[CH_4]_i} = -k_f * t \qquad A.10$$

Where t=1/GHSV. Conversion of CH_4, X, is given by Equation A.12 and A.13.

$$X = 1 - \frac{[CH_4]_t}{[CH_4]_i} \qquad A.12$$

$$\ln(1-X) = -k_f\left(\frac{1}{GHSV}\right) \qquad A.11$$

By determining conversion at varying space velocities and temperatures, k_f can be determined for a particular temperature. Table A.1 shows data from the dry reforming reaction at varying temperatures and space velocities produced by taking data at different locations along the monolith, resulting in different effective space velocities.

Table A.1: Conversion of CH_4 as a function of temperature and axial position, or space velocity (GHSV)

Temperature K	**673**	**823**	**973**
GHSV	X CH_4	X CH_4	X CH_4
238,776	1.1%	33.4%	64.7%
119,388	1.6%	33.4%	79.0%
79,592	1.5%	38.7%	90.3%
59,694	1.8%	41.4%	96.9%
47,755	2.5%	45.4%	98.5%
39,796	3.0%	50.0%	
34,111	3.6%	55.4%	

Ln (1-X) vs 1/GHSV was plotted to determine k_f for each temperature as shown below in Figure A.4.

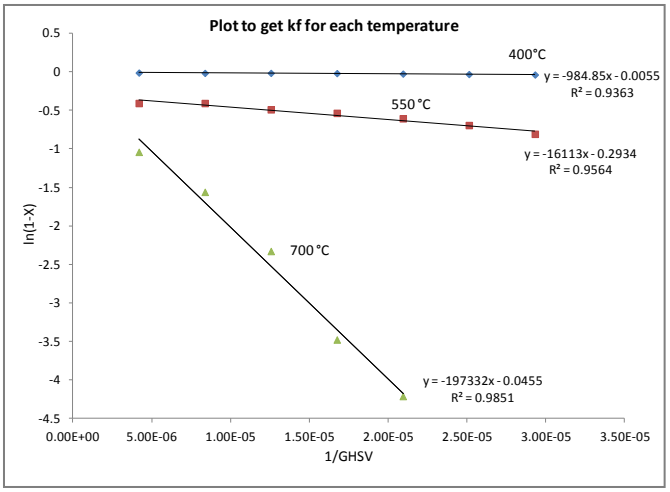

FigureA.1.4: ln(1-X) vs. 1/GHSV to determine kf at each reaction temperature

Using this data, activation energy and k_o can be found by plotting lnk vs 1/T, where Ea/R is the slope of the plot, shown in Figure A.5.

$$\ln k = \ln k_o - \left(\frac{E_a}{R}\right)\left(\frac{1}{T}\right) \qquad A.12$$

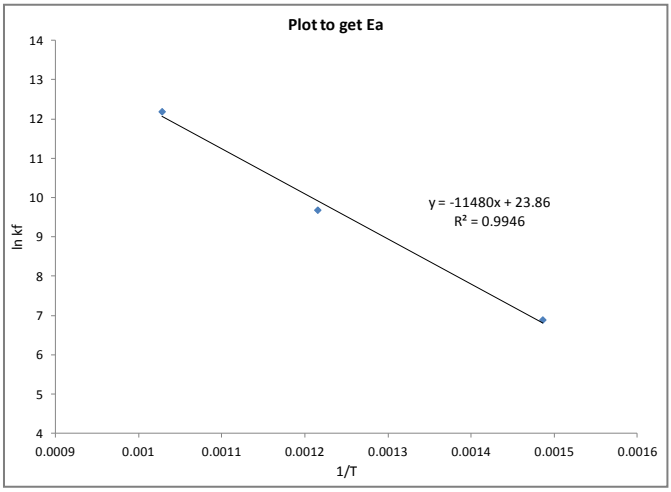

Figure A.1.5: ln k_f vs 1/T to determine the activation energy E_A of the dry reforming reaction using CH_4 conversion data

The slope of the curve is equal to -11480. Using R=8.314 J/K-mole, the activation energy is 95.44 kJ/mole.

To determine the reaction orders of CH_4 and CO_2, one reactant should remain constant while the other varies. It is important that when measuring the reaction order of one reactant, the other reactant should not affect the reaction, so that it is truly constant. One way to do this is to operate in excess of the "constant" reactant. Therefore Equation A.7 can be expressed as Equation A.15. Then the natural log of the reaction rate can be plotted vs natural log of the desired reactant to find the order.

$$\ln(rate) = C + \alpha \ln(CH_4) \qquad \textit{Where } C=k_f(CO_2) \qquad A.13$$

Rate is calculated as shown in Equation A.16 where W is the weight of the catalyst in grams and F is the reactant flow rate in moles/s.

$$R_i = \frac{F_i - F_f}{W} \qquad A.14$$

To determine the methane order, methane was varied from 2% to 9% of the flow and CO_2 remained in excess at 18% at a temperature of 550°C. In these experiments, the CO_2 conversion did not exceed 7%, so CO_2 concentration will be assumed to be constant. This process was repeated to find the CO_2 reaction order at CO_2 inlet concentrations of 10, 14, 18, and 22% while maintaining CH_4 concentrations at 9% of flow. It was impossible to run at highly excess CH_4 because this would lead to carbon formation which would deactivate the catalyst and not give clear information on the kinetic of the dry reforming reaction. Therefore CO_2 was kept in excess but varied to obtain an approximation of the CO_2 order. Using the size of the monolith, the catalyst loading, and the washcoat loading, the volume of catalyst in each monolith increment was calculated. Each 0.25” increment contained 0.012 grams of rhodium.

One interesting aspect of the capillary data is that the axial resolution showed that the reaction rate is much faster in the entrance region of the monolith compared to the downstream portion of the monolith, shown in Figure A.6.

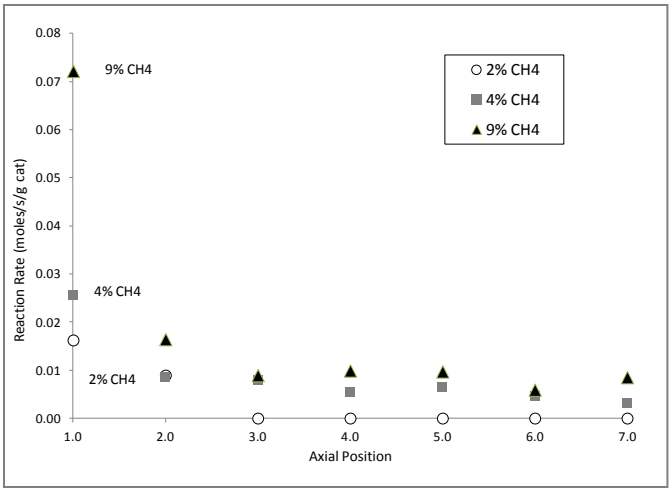

Figure A.1.6: Dry reforming reaction rate in moles/g/s as a function of axial position in the Rh/γAl2O3 monolith

This behavior is likely a combination of many factors. First is that the concentrations of the reactants are highest at the entrance to the monolith. Also, the temperature will be the highest at the entrance because the endothermic dry reforming reaction has not proceeded and decreases the temperature of the monolith. Finally, and most interestingly, the entrance region of the monolith is a turbulent region in which there is more mass transport from the gas phase to the surface, allowing for a faster reaction rate. Downstream in the monolith a laminar flow develops which decreases mass transfer as well as the reaction rate. This highlights a benefit of using capillary sampling for kinetic studies because it allows for samples to be taken right at the entrance to a monolith where turbulence and mass transfer is high. In this region it is more likely that the intrinsic kinetics can be discovered because mass transport limitations are not affecting the rate of the reaction.

Figure A.7 shows a plot of ln(rate) vs ln(CH4) at 550°C in the turbulent entrance region of the monolith and the laminar, downstream portion of the monolith. The slope of the line is the methane order. This shows that in the entrance region the methane order is 0.58, while in the laminar region it is 0.26. This indicates that in the entrance region the reaction rate is more

sensitive to CH_4 concentration, which may mean that the entrance region is more kinetically limited compared to the downstream portion of the monolith.

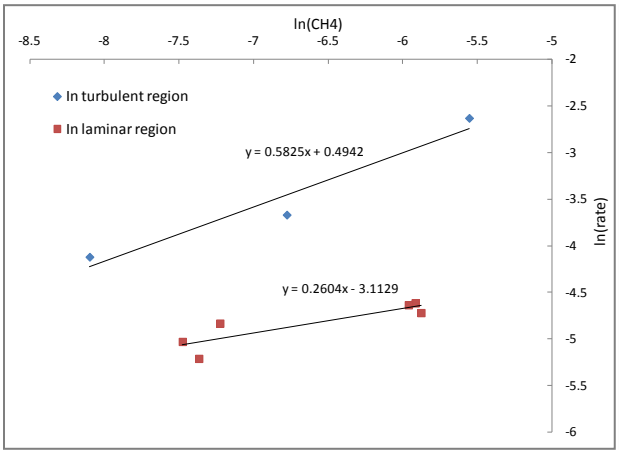

Figure A.1.7: ln(rate) vs ln(CH_4) at 550°C in the turbulent and laminar regimes of the monolith

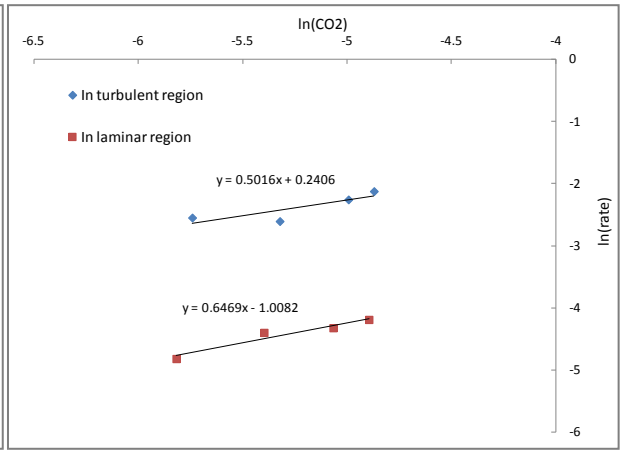

Figure A.1.8: ln(rate) vs ln(CO_2) at 550°C in the turbulent and laminar regimes of the monolith

Figure A.8 shows a plot of ln(rate) vs ln(CO_2) at 550°C in the turbulent entrance region of the monolith and the laminar, downstream portion of the monolith. The slope of the line is the CO_2 order. This shows that in the entrance region the CO_2 order is 0.50, while in the laminar region it is 0.65. This indicates that in the turbulent, more kinetically limited portion of the monolith, the reaction rate is not as sensitive to CO_2 concentration compared to the downstream portion of the monolith.

Table A.2 summarizes the findings for CH_4 and CO_2 reaction orders and activation energy.

Table A.2: Summary of Reaction Orders at 550°C and E_A

	CH_4	CO_2
Turbulent	0.58	0.50
Laminar	0.26	0.65
Activation energy, E_A=95.44 kJ/mole.		

References

[1] EPA, Landfill Methane Outreach Program, in, 2011.

[2] P. Simmons, N. Goldstein, S. Kaufman, N.J. Themelis, J. Thompson, The State of Garbage, BioCycle, 1 (2006) 26-43.

[3] N.J. Themelis, P.A. Ulloa, Methane generation in landfills, Renewable Energy, 32 (2007) 1243-1257.

[4] J. Controls, Turning Digester Gas into Energy, in: J.C. Inc. (Ed.), Milwaukee, WI, 2007.

[5] F.E.M. Program, FEMP Focus, in: O.o.E.E.a.R.E. U.S. Department of Energy (Ed.), Washington, D.C., 2005, pp. 5.

[6] AgSTAR, Market Opportunities for Biogas Recovery Systems, in: E.P. Agency (Ed.), 2010.

[7] K. Krich, D. Augenstein, J. Batmale, J. Benemann, B. Rutledge, D. Salour, Biomethane from Dairy Waste, in: U.S.D.o. Agriculture (Ed.), 2005.

[8] J.M. MacDonald, E.J. O'Donoghue, W.D. McBride, R.F. Nehring, C.L. Sandretto, R. Mosheim, Profits, Costs, and the Changing Structure of Dairy Farming, in: U.S.D.o.A.E.R. Service. (Ed.), 2007, pp. 41.

[9] U.S.E.I. Administration, Natural Gas Prices, Yearly Average, in, 2012.

[10] M.P. Kohn, J. Lee, M.L. Basinger, M.J. Castaldi, Performance of an Internal Combustion Engine Operating on Landfill Gas and the Effect of Syngas Addition, Industrial & Engineering Chemistry Research, 50 (2011) 3570-3579.

[11] G. Tchobanoglous, H. Theisen, S. Vigil, Integrated Solid Waste Management, 1993.

[12] EPA, Project Profile: Fresh Kills High Btu Project, in: Landfill Methane Outreach Program, 2010.

[13] R.J. Farrauto, C. Bartholomew, Fundamentals of Industrial Catalytic Processes, 2 ed., John Wiley & Sons; American Institute of Chemical Engineers, Portland, Oregon, 2006.

[14] F. Fischer, The Conversion of Coal into Oils, in: R. Lessing (Ed.), London, 1925, pp. 279.

[15] N. Whitmore, Landfill Gas Constituents, in: M. Castaldi (Ed.), 2004.

[16] J.T.G. Hamilton, W.C. McRoberts, F. Keppler, R.M. Kalin, D.B. Harper, Chloride methylation by plant pectin: An efficient environmentally significant process, Science, 301 (2003) 206-209.

[17] J. Bao, G.N. Krishnan, P. Jayaweera, J. Perez-Mariano, A. Sanjurjo, Effect of various coal contaminants on the performance of solid oxide fuel cells: Part I. Accelerated testing, Journal of Power Sources, 193 (2009) 607-616.

[18] W.C. Keene, M.A.K. Khalil, D.J. Erickson, A. McCulloch, T.E. Graedel, J.M. Lobert, M.L. Aucott, S.L. Gong, D.B. Harper, G. Kleiman, P. Midgley, R.M. Moore, C. Seuzaret, W.T. Sturges, C.M. Benkovitz, V. Koropalov, L.A. Barrie, Y.F. Li, Composite global emissions of reactive chlorine from anthropogenic and natural sources: Reactive Chlorine Emissions Inventory, Journal of Geophysical Research-Atmospheres, 104 (1999) 8429-8440.

[19] A. McCulloch, M.L. Aucott, C.M. Benkovitz, T.E. Graedel, G. Kleiman, P.M. Midgley, Y.F. Li, Global emissions of hydrogen chloride and chloromethane from coal combustion, incineration and industrial activities: Reactive Chlorine Emissions Inventory, Journal of Geophysical Research-Atmospheres, 104 (1999) 8391-8403.

[20] J. Rostrup-Nielsen, J. Sehested, J.K. Norskov, Hydrogen and synthesis gas by steam- and CO(2) reforming, in: B.C. Gates, H. Knozinger (Eds.) Advances in Catalysis, Vol 47, 2002, pp. 65-139.

[21] J. Rostrup-Nielsen, Promotion by poisoning, Catalyst Deactivation, 68 (1991) 85-101.

[22] J. Rostrup-Nielsen, EQUILIBRIA OF DECOMPOSITION REACTIONS OF CARBON-MONOXIDE AND METHANE OVER NICKEL CATALYSTS, Journal of Catalysis, 27 (1972) 343-&.

[23] J. Rostrup-Nielsen, J.H.B. Hansen, CO2-REFORMING OF METHANE OVER TRANSITION-METALS, Journal of Catalysis, 144 (1993) 38-49.

[24] J.R.H. Ross, Natural gas reforming and CO2 mitigation, Catalysis Today, 100 (2005) 151-158.

[25] A. Erdohelyi, J. Cserenyi, F. Solymosi, ACTIVATION OF CH4 AND ITS REACTION WITH CO2 OVER SUPPORTED RH CATALYSTS, Journal of Catalysis, 141 (1993) 287-299.

[26] J.M. Wei, E. Iglesia, Isotopic and kinetic assessment of the mechanism of methane reforming and decomposition reactions on supported iridium catalysts, Physical Chemistry Chemical Physics, 6 (2004) 3754-3759.

[27] J.M. Wei, E. Iglesia, Isotopic and kinetic assessment of the mechanism of reactions of CH4 with CO2 or H2O to form synthesis gas and carbon on nickel catalysts, Journal of Catalysis, 224 (2004) 370-383.

[28] J.M. Wei, E. Iglesia, Structural requirements and reaction pathways in methane activation and chemical conversion catalyzed by rhodium, Journal of Catalysis, 225 (2004) 116-127.

[29] J.M. Wei, E. Iglesia, Structural requirements and activation pathways in reactions of methane catalyzed by supported metals, Abstracts of Papers of the American Chemical Society, 227 (2004) U1072-U1072.

[30] D. Chen, R. Lodeng, A. Anundskas, O. Olsvik, A. Holmen, Deactivation during carbon dioxide reforming of methane over Ni catalyst: microkinetic analysis, Chemical Engineering Science, 56 (2001) 1371-1379.

[31] S.G. Wang, Y.W. Li, J.X. Lu, M.Y. He, H.J. Jiao, A detailed mechanism of thermal CO2 reforming of CH4, Journal of Molecular Structure-Theochem, 673 (2004) 181-189.

[32] A. Nandini, K.K. Pant, S.C. Dhingra, Kinetic study of the catalytic carbon dioxide reforming of methane to synthesis gas over Ni-K/CeO2-Al2O3 catalyst, Applied Catalysis a-General, 308 (2006) 119-127.

[33] Y.H. Cui, H.D. Zhang, H.Y. Xu, W.Z. Li, Kinetic study of the catalytic reforming of CH4 with CO2 to syngas over Ni/alpha-Al2O3 catalyst: The effect of temperature on the reforming mechanism, Applied Catalysis a-General, 318 (2007) 79-88.

[34] C.A.M. Abreu, D.A. Santos, J.A. Pacifico, N.M. Lima, Kinetic evaluation of methane-carbon dioxide reforming process based on the reaction steps, Industrial & Engineering Chemistry Research, 47 (2008) 4617-4622.

[35] M. Maestri, D.G. Vlachos, A. Beretta, G. Groppi, E. Rronconi, A C(1) Microkinetic Model for Methane Conversion to Syngas on Rh/Al(2)O(3), Aiche Journal, 55 (2009) 993-1008.

[36] I. Sarusi, K. Fodor, K. Baan, A. Oszko, G. Potari, A. Erdohelyi, CO(2) reforming of CH(4) on doped Rh/Al(2)O(3) catalysts, Catalysis Today, 171 (2011) 132-139.

[37] M. Nagai, K. Nakahira, Y. Ozawa, Y. Namiki, Y. Suzuki, CO2 reforming of methane on Rh/Al2O3 catalyst, Chemical Engineering Science, 62 (2007) 4998-5000.

[38] P. Ferreira-Aparicio, M. Fernandez-Garcia, A. Guerrero-Ruiz, I. Rodriguez-Ramos, Evaluation of the role of the metal-support interfacial centers in the dry reforming of methane on alumina-supported rhodium catalysts, Journal of Catalysis, 190 (2000) 296-308.

[39] S. Therdthianwong, A. Therdthianwong, C. SiangChin, S. Yonprapat, Synthesis gas production from dry reforming of methane over Ni/Al2O3 stabilized by ZrO2, International Journal of Hydrogen Energy, 33 (2008) 991-999.

[40] N. Laosiripojana, S. Assabumrungrat, Catalytic dry reforming of methane over high surface area ceria, Applied Catalysis B-Environmental, 60 (2005) 107-116.

[41] M. Rezaei, S.M. Alavi, S. Sahebdelfar, P. Bai, X.M. Liu, Z.F. Yan, CO2 reforming of CH4 over nanocrystalline zirconia-supported nickel catalysts, Applied Catalysis B-Environmental, 77 (2008) 346-354.

[42] D. Martin, D. Duprez, Mobility of surface species on oxides .2. Isotopic exchange of D-2 with H of SiO2, Al2O3, ZrO2, MgO, and CeO2: Activation by rhodium and effect of chlorine, Journal of Physical Chemistry B, 101 (1997) 4428-4436.

[43] D. Martin, D. Duprez, Mobility of surface species on oxides .1. Isotopic exchange O-18(2) with O-16 of SiO2, Al2O3, ZrO2, MgO, CeO2, and CeO2-Al2O3. Activation by noble metals. Correlation with oxide basicity, Journal of Physical Chemistry, 100 (1996) 9429-9438.

[44] X.E. Verykios, Mechanistic aspects of the reaction of CO2 reforming of methane over Rh/Al2O3 catalyst, Applied Catalysis a-General, 255 (2003) 101-111.

[45] M.C.J. Bradford, M.A. Vannice, CO2 reforming of CH4, Catalysis Reviews-Science and Engineering, 41 (1999) 1-42.

[46] K. Tanabe, M. Misono, Y. Ono, H. Hattori, New Solid Acids and Bases, Elsevier, Tokyo, 1989.

[47] E. Santacesaria, D. Gelosa, S. Carra, BASIC BEHAVIOR OF ALUMINA IN PRESENCE OF STRONG ACIDS, Industrial & Engineering Chemistry Product Research and Development, 16 (1977) 45-47.

[48] T. Inui, Rapid catalytic reforming of methane with CO2 and its application to other reactions, Appl. Organomet. Chem., 15 (2001) 87-94.

[49] P.M. Torniainen, X. Chu, L.D. Schmidt, COMPARISON OF MONOLITH-SUPPORTED METALS FOR THE DIRECT OXIDATION OF METHANE TO SYNGAS, Journal of Catalysis, 146 (1994) 1-10.

[50] D.A. Hickman, L.D. Schmidt, Steps in CH4 Oxidation on Pt and Rh Surfaces: High-Temperature Reactor Simulations, Aiche Journal, 39 (1993) 1164-1177.

[51] D.A. Hickman, E.A. Haupfear, L.D. Schmidt, SYNTHESIS GAS-FORMATION BY DIRECT OXIDATION OF METHANE OVER RH MONOLITHS, Catalysis Letters, 17 (1993) 223-237.

[52] D.A. Hickman, L.D. Schmidt, PRODUCTION OF SYNGAS BY DIRECT CATALYTIC-OXIDATION OF METHANE, Science, 259 (1993) 343-346.

[53] D.A. Hickman, L.D. Schmidt, SYNTHESIS GAS-FORMATION BY DIRECT OXIDATION OF METHANE OVER PT MONOLITHS, Journal of Catalysis, 138 (1992) 267-282.

[54] R. Horn, K.A. Williams, N.J. Degenstein, A. Bitsch-Larsen, D.D. Nogare, S.A. Tupy, L.D. Schmidt, Methane catalytic partial oxidation on autothermal Rh and Pt foam catalysts: Oxidation

and reforming zones, transport effects, and approach to thermodynamic equilibrium, Journal of Catalysis, 249 (2007) 380-393.

[55] R. Horn, K.A. Williams, N.J. Degenstein, L.D. Schmidt, Mechanism of H-2 and CO formation in the catalytic partial oxidation of CH4 on Rh probed by steady-state spatial profiles and spatially resolved transients, Chemical Engineering Science, 62 (2007) 1298-1307.

[56] R. Horn, K.A. Williams, N.J. Degenstein, L.D. Schmidt, Syngas by catalytic partial oxidation of methane on rhodium: Mechanistic conclusions from spatially resolved measurements and numerical simulations, Journal of Catalysis, 242 (2006) 92-102.

[57] S. Specchia, G. Negro, G. Saracco, V. Specchia, Fuel processor based on syngas production via short contact time catalytic partial oxidation reactors, Applied Catalysis B-Environmental, 70 (2007) 525-531.

[58] J.A.C. Ruiz, F.B. Passos, J.M.C. Bueno, E.F. Souza-Aguiar, L.V. Mattos, F.B. Noronha, Syngas production by autothermal reforming of methane on supported platinum catalysts, Applied Catalysis a-General, 334 (2008) 259-267.

[59] A. Donazzi, A. Beretta, G. Groppi, P. Forzatti, Catalytic partial oxidation of methane over a 4% Rh/alpha-Al2O3 catalyst Part I: Kinetic study in annular reactor, Journal of Catalysis, 255 (2008) 241-258.

[60] A. Donazzi, A. Beretta, G. Groppi, P. Forzatti, Catalytic partial oxidation of methane over a 4% Rh/alpha-Al2O3 catalyst Part II: Role Of CO2 reforming, Journal of Catalysis, 255 (2008) 259-268.

[61] M. Simeone, L. Salemme, C. Allouis, Reactor temperature profile during autothermal methane reforming on Rh/Al2O3 catalyst by IR imaging, International Journal of Hydrogen Energy, 33 (2008) 4798-4808.

[62] S. Rabe, T.B. Truong, F. Vogel, Low temperature catalytic partial oxidation of methane for gas-to-liquids applications, Applied Catalysis a-General, 292 (2005) 177-188.

[63] Y. Liu, F.Y. Huang, J.M. Li, W.Z. Weng, C.R. Luo, M.L. Wang, W.S. Xia, C.J. Huang, H.L. Wan, In situ Raman study on the partial oxidation of methane to synthesis gas over Rh/Al2O3 and Ru/Al2O3 catalysts, Journal of Catalysis, 256 (2008) 192-203.

[64] A. Donazzi, M. Maestri, A. Beretta, G. Groppi, E. Tronconi, P. Forzatti, Microkinetic analysis of CH(4) CPO tests with CO(2)-diluted feed streams, Applied Catalysis a-General, 391 (2011) 350-359.

[65] A. Donazzi, M. Maestri, B.C. Michael, A. Beretta, P. Forzatti, G. Groppi, E. Tronconi, L.D. Schmidt, D.G. Vlachos, Microkinetic modeling of spatially resolved autothermal CH(4) catalytic partial oxidation experiments over Rh-coated foams, Journal of Catalysis, 275 (2010) 270-279.

[66] M. Maestri, D.G. Vlachos, A. Beretta, P. Forzatti, G. Groppi, E. Tronconi, Dominant Reaction Pathways in the Catalytic Partial Oxidation of CH(4) on Rh, Topics in Catalysis, 52 (2009) 1983-1988.

[67] M. Maestri, D.G. Vlachos, A. Beretta, G. Groppi, E. Tronconi, Steam and dry reforming of methane on Rh: Microkinetic analysis and hierarchy of kinetic models, Journal of Catalysis, 259 (2008) 211-222.

[68] A.P.E. York, T.C. Xiao, M.L.H. Green, J.B. Claridge, Methane oxyforming for synthesis gas production, Catalysis Reviews-Science and Engineering, 49 (2007) 511-560.

[69] B.C. Michael, A. Donazzi, L.D. Schmidt, Effects of H(2)O and CO(2) addition in catalytic partial oxidation of methane on Rh, Journal of Catalysis, 265 (2009) 117-129.

[70] C. Ratnasamy, J.P. Wagner, Water Gas Shift Catalysis, Catalysis Reviews-Science and Engineering, 51 (2009) 325-440.

[71] G.G. Olympiou, C.M. Kalamaras, C.D. Zeinalipour-Yazdi, A.M. Efstathiou, Mechanistic aspects of the water-gas shift reaction on alumina-supported noble metal catalysts: In situ DRIFTS and SSITKA-mass spectrometry studies, Catalysis Today, 127 (2007) 304-318.

[72] D.C. Grenoble, M.M. Estadt, D.F. Ollis, THE CHEMISTRY AND CATALYSIS OF THE WATER GAS SHIFT REACTION .1. THE KINETICS OVER SUPPORTED METAL-CATALYSTS, Journal of Catalysis, 67 (1981) 90-102.

[73] A.B. Mhadeshwar, D.G. Vlachos, Is the water-gas shift reaction on Pt simple? Computer-aided microkinetic model reduction, lumped rate expression, and rate-determining step, Catalysis Today, 105 (2005) 162-172.

[74] F.C. Meunier, D. Tibiletti, A. Goguet, R. Burch, DRIFTS-MS-SSITKA study of the reverse water-gas shift reaction, Oil Gas Sci. Technol., 61 (2006) 497-502.

[75] R. Burch, Gold catalysts for pure hydrogen production in the water-gas shift reaction: activity, structure and reaction mechanism, Physical Chemistry Chemical Physics, 8 (2006) 5483-5500.

[76] M.M. Schubert, H.A. Gasteiger, R.J. Behm, Surface formates as side products in the selective CO oxidation on Pt/gamma-Al2O3, Journal of Catalysis, 172 (1997) 256-258.

[77] J.J. Benitez, R. Alvero, M.J. Capitan, I. Carrizosa, J.A. Odriozola, DRIFTS STUDY OF ADSORBED FORMATE SPECIES IN THE CARBON-DIOXIDE AND HYDROGEN REACTION OVER RHODIUM CATALYSTS, Applied Catalysis, 71 (1991) 219-231.

[78] C. Morterra, G. Magnacca, A case study: Surface chemistry and surface structure of catalytic aluminas, as studied by vibrational spectroscopy of adsorbed species, Catalysis Today, 27 (1996) 497-532.

[79] H. Knozinger, P. Ratnasamy, CATALYTIC ALUMINAS - SURFACE MODELS AND CHARACTERIZATION OF SURFACE SITES, Catalysis Reviews-Science and Engineering, 17 (1978) 31-70.

[80] F. Habashi, Bayer's Process for Alumina Production: A Historical Perspective, Bull. Hist. Chem, 17/18 (1995).

[81] J.B. Peri, A Model for the Surface of Gamma Alumina, Journal of Physical Chemistry, 69 (1965) 220-230.

[82] G. Sposito, The Environmental Chemistry of Aluminum, 2 ed., Lewis Publishers, Boca Raton, Florida, 1995.

[83] S.-M. Kim, Synthesis and characterization of a highly active alumina catalyst for methanol dehydration to dimethyl ether, Applied Catalysis, 348 (2008) 113-120.

[84] P. Maki-Arvela, Liquid phase hydrogenation of citral: suppression of side reactions, Applied Catalysis, 237 (2002) 181-200.

[85] A.A. Castro, O.A. Scelza, G.T. Baronetti, M.A. Fritzler, J.M. Parera, CHLORINE ADJUSTMENT IN AL2O3 AND NAPHTHA REFORMING CATALYSTS, Applied Catalysis, 6 (1983) 347-353.

[86] M. Digne, P. Raybaud, P. Sautet, D. Guillaume, H. Toulhoat, Atomic scale insights on chlorinated gamma-alumina surfaces, Journal of the American Chemical Society, 130 (2008) 11030-11039.

[87] A.A. Castro, O.A. Scelza, E.R. Benvenuto, G.T. Baronetti, J.M. Parera, Regulation of the chlorine content on PtAl2O3 catalyst, Journal of Catalysis, 69 (1981) 222-226.

[88] J.C. Musso, J.M. Parera, ADSORPTION AND SPILLOVER OF HYDROGEN ON AL2O3 AND PT/AL2O3, Applied Catalysis, 30 (1987) 81-90.

[89] L. Lloyd, Handbook of Industrial Catalysis, Springer, New York, 2011.

[90] G. Ertl, H. Knozinger, J. Weitkamp, Preparation of Solid Catalysts, Wiley-VCH, Weinheim, Germany, 1999.

[91] S.M. Aboul-Fotouh, A.K. Aboul-Gheit, Hydroconversion of cyclohexene using platinum-containing catalysts promoted with other noble metals and chlorine or fluorine, Applied Catalysis a-General, 208 (2001) 55-61.

[92] D. Simone, T. Kennelly, N. Brungard, R.J. Farrauto, Reversible poisoning of palladium catalysts for methane oxidation, Applied Catalysis, 70 (1991) 87-100.

[93] F.J. Gracia, J.T. Miller, A.J. Kropf, E.E. Wolf, Kinetics, FTIR, and controlled atmosphere EXAFS study of the effect of chlorine on Pt-supported catalysts during oxidation reactions, Journal of Catalysis, 209 (2002) 341-354.

[94] K. Intarajang, J.T. Richardson, Catalytic steam reforming of chlorocarbons: catalyst comparisons, Applied Catalysis B-Environmental, 22 (1999) 27-34.

[95] J.D. Ortego, J.T. Richardson, M.V. Twigg, Catalytic steam reforming of chlorocarbons: Methyl chloride, Applied Catalysis B-Environmental, 12 (1997) 339-355.

[96] J.T. Richardson, J.D. Ortego, N. Coute, M.V. Twigg, Chloride poisoning of water-gas shift activity in nickel catalysts during steam reforming, Catalysis Letters, 41 (1996) 17-20.

[97] N. Coute, J.D. Ortego, J.T. Richardson, M.V. Twigg, Catalytic steam reforming of chlorocarbons: trichloroethane, trichloroethylene and perchloroethylene, Applied Catalysis B-Environmental, 19 (1998) 175-187.

[98] N. Coute, J.T. Richardson, Steam reforming of chlorocarbons: chlorinated aromatics, Applied Catalysis B-Environmental, 26 (2000) 217-226.

[99] T.E. McMinn, F.C. Moates, J.T. Richardson, Catalytic steam reforming of chlorocarbons: catalyst deactivation, Applied Catalysis B-Environmental, 31 (2001) 93-105.

[100] M. Shafiei, J.T. Richardson, Dechlorination of chlorinated hydrocarbons by catalytic steam reforming, Applied Catalysis B-Environmental, 54 (2004) 251-259.

[101] N. Coute, J.T. Richardson, Catalytic steam reforming of chlorocarbons: polychlorinated biphenyls (PCBs), Applied Catalysis B-Environmental, 26 (2000) 265-273.

[102] B. Coq, G. Ferrat, F. Figueras, CONVERSION OF CHLOROBENZENE OVER PALLADIUM AND RHODIUM CATALYSTS OF WIDELY VARYING DISPERSION, Journal of Catalysis, 101 (1986) 434-445.

[103] Y. Hashimoto, A. Ayame, Low-temperature hydrodechlorination of chlorobenzenes on platinum-supported alumina catalysts, Applied Catalysis a-General, 250 (2003) 247-254.

[104] Y. Hashimoto, Y. Uemichi, A. Ayame, Low-temperature hydrodechlorination mechanism of chlorobenzenes over platinum-supported and palladium-supported alumina catalysts, Applied Catalysis a-General, 287 (2005) 89-97.

[105] N. Chen, R.M. Rioux, L. Barbosa, F.H. Ribeiro, Kinetic and Theoretical Study of the Hydrodechlorination of CH(4-x)Cl(x) (x=1-4) Compounds on Palladium, Langmuir, 26 (2010) 16615-16624.

[106] P. Choudhury, J.K. Johnson, Methyl Chloride Reactions on Lithiated Carbon Nanotubes: Lithium as Both Reactant and Catalyst, Journal of Physical Chemistry C, 115 (2011) 11694-11700.

[107] CRC Handbook of Chemistry and Physics, in: W.M. Haynes, D.R. Lide (Eds.), 2012.

[108] J.B. Peri, Infrared studies of Pt and Pt□Re reforming catalysts, Journal of Catalysis, 52 (1978) 144-156.

[109] F.C. Moates, T.E. McMinn, J.T. Richardson, Radial reactor for trichloroethylene steam reforming, Aiche Journal, 45 (1999) 2411-2418.

[110] N. Whitmore, Greenhouse Gas Catalytic Reforming to Syngas, in: Department of Earth and Environmental Engineering (HKSM), Columbia University, New York, 2007.

[111] J.F. Munera, S. Irusta, L.M. Cornaglia, E.A. Lombardo, D.V. Cesar, M. Schmal, Kinetics and reaction pathway of the CO2 reforming of methane on Rh supported on lanthanum-based solid, Journal of Catalysis, 245 (2007) 25-34.

[112] C.D. Wagner, A.V. Naumkin, A. Kraut-Vass, J.W. Allison, C.J. Powell, J.R. Rumble Jr, NIST X-ray Photoelectron spectroscopy Database, in, 2007.

[113] H. Karhu, A. Kalantar, I.J. Vayrynen, T. Salmi, D.Y. Murzin, XPS analysis of chlorine residues in supported Pt and Pd catalysts with low metal loading, Applied Catalysis a-General, 247 (2003) 283-294.

[114] I. Bennour, V. Maurice, P. Marcus, X-ray photoelectron spectroscopy study of the interaction of ultra-thin alumina films on NiAl alloys with NaCl solutions, Surface and Interface Analysis, 42 (2010) 581-587.

[115] J.Y. Shen, R.D. Cortright, Y. Chen, J.A. Dumesic, MICROCALORIMETRIC AND INFRARED SPECTROSCOPIC STUDIES OF GAMMA-AL2O3 MODIFIED BY BASIC METAL-OXIDES, Journal of Physical Chemistry, 98 (1994) 8067-8073.

[116] T. Iizuka, Y. Tanaka, Dissociative adsorption of CO2 on supported rhodium catalyst: Comment on surface interaction between H2 and CO2 on Rh□Al2O3, Journal of Catalysis, 70 (1981) 449-450.

[117] M. Trueba, S.P. Trasatti, gamma-Alumina as a support for catalysts: A review of fundamental aspects, Eur. J. Inorg. Chem., (2005) 3393-3403.

[118] S. Brunauer, P.H. Emmett, E. Teller, Adsorption of gases in multimolecular layers, Journal of the American Chemical Society, 60 (1938) 309-319.

[119] D.K. Paul, C.D. Marten, J.T. Yates, Control of Rh-I(CO)(2) formation on Rh/Al2O3 catalysts by complexation of surface -OH groups using NH3, Langmuir, 15 (1999) 4508-4512.